The Scientific Institute for Advanced Training and Studies

Experimental and Theoretical NANOTECHNOLOGY

Vol. 1, No. 2, 2017

Yarub Al-Douri

Editor-in-Chief

e-ISSN: 2590-4132

Contact us

Experimental and Theoretical NANOTECHNOLOGY

Prof. Dr. Yarub Al-Douri; Founding Editor-in-Chief :editor.etn@siats.co.uk

http://etn.siats.co.uk

Experimental and Theoretical
NANOTECHNOLOGY
http://etn.siats.co.uk/

Experimental and Theoretical NANOTECHNOLOGY

VOL. 1, NO. 2, 2017

e-ISSN 2590-4132

2017

Experimental and Theoretical NANOTECHNOLOGY

Experimental and Theoretical NANOTECHNOLOGY is a multidisciplinary peer-reviewed international journal published four issues a year. It includes specialized research papers, short communications, reviews and selected conference papers in special issues on the characterization, synthesis, processing, structure and properties of different principles and applications of NANOTECHNOLOGY; with focus on advantageous achievements and applications for the specialists in engineering, chemistry, physics and materials science.

Experimental and Theoretical NANOTECHNOLOGY covers and publishes all aspects of fundamental and applied researches of experimental and theoretical nanoscale technology dealing with materials synthesis, processing, nanofabrication, NANO probes, spectroscopy, properties, biological systems, nanostructures, NANO electronics, Nano-optics, NANO-mechanics, NANO-devices, NANO biotechnology, nanomedicine, Nano toxicology within the scope of the journal. Experimental and Theoretical NANOTECHNOLOGY aims to acquire the recent and outstanding researches for the benefit of the human being.

Exp. Theo. NANOTECHNOLOGY 2 **(2017)** 49 – 68

Experimental and Theoretical
NANOTECHNOLOGY
http://etn.siats.co.uk/

Nano-ceramics Ti_3SiC_2 Max phase reinforced single walled carbon nanotubes by spark plasma sintering

Badis Bendjemil[1,2], Jamal Bougdira[3], Faming Zhang[4,5], Eberhard Burkel[4]

[1]*LASEA, Dept of Chemistry, University of Badji-Mokhtar, 23000 Annaba, Algeria*
[2]*University of 8 Mai 1945 Guelma, 24000 Guelma, Algeria*
[3,4]*Physics of New Materials, Institute of Physics, 18055 Rostock, Germany*
[4,5]*School of Materials Science and Engineering, Southeast University, 211189 Nanjing, China*
[5,3]*Institut Jean Lamour, UMR 7198 CNRS - Université de Lorraine Faculté des Sciences et Technologies BP 70239 F-54506 Vandoeuvre les NANCY cedex*
*) E-mail: Badis23@gmail.com

Received 27 May 2015; Revised 12 April 2016; Accepted 19 April 2016

Ceramics titanium silicon carbide Ti_3SiC_2 Max phase was rapidly synthesised and simultaneously consolidated by spark plasma sintering at which the extensive volume expansion occurred as a function of the temperature from ball milled SiC/Ti/C powders with Ti/SiC ratio of 3:1:2. The XRD patterns results were confirmed by FESEM observations and the EDAX analyses. The 3Ti+1.2SiC+0.8C nano-ceramics were processed from 3Ti+1.2SiC+0.8C/SWCNTs powders using spark plasma sintering (SPS) at temperatures of 1100, 1200 and 1300 °C with diting of SWCNTs from 0.0 to 1.0 wt% SWCNTs/Ti_3SiC_2 nanocomposite. The effects of SWCNTs addition on phases, microstructure and hardness of the nanocomposite were investigated. The best product contained 1.0 wt% CNTs/ Ti_3SiC_2/TiC which was sintered at 1300 °C, 60 MPa for 10 min The phase composition of the product could be tailored by adjusting the process parameters. The anisotropic hardness was observed in respect to the textured product.

Keywords: MAX phase; Ti_3SiC_2; SPS.
PACS: 73.30.+y; 73.40.Ns; 73.40.-c.

Introduction

The fabrication of the ternary Ti_3SiC_2 compound was carried out in a single step by PAS (Plasma Activated Sintering) starting from Ti, Si and graphite powders in a 3:1:2 molar ratio [1]. The synthesis/densification process was conducted under vacuum and consisted of two stages. During the first one, an electric pulsed current (10% on) of 100 A was applied for 99 s under a pressure of 34.5 MPa, while in the second stage, the current (non pulsed) was increased up to 1800–3500 A with an holding time in the range of 0–2 h and applied pressure in the range of 34.4–68.8 MPa. The maximum temperature values achieved were ranged from 1525 to 2500 °C. The optimal condition to give a nearly dense product characterized by density values of 4.53- 0.02 g/cm^3 very close to the reported theoretical value of 4.531 g/cm^3, and containing small amounts (2 mol%) of TiC as a second phase, was a temperature of 1525 °C maintained for 2 h as well as an applied pressure of 34.4 MPa. Dense samples synthesized in this study were examined by optical and electron microscopy. The maximum size in the elongated dimension of these grains is about 25 mm, which is smaller by a factor of four than the average grain size (100 mm) reported for samples produced by HIPing at 1600 °C for 4 h [1]. Numerous papers on the synthesis and characterization of Ti_3SiC_2-based materials by means of the PDS technique were published by a Japanese research group [2–11].

Specifically, this ternary compound was first synthesized by reacting a Ti, SiC, and TiC powder mixture in the 4:2:1 molar ratio [2]. PDS process was conducted under vacuum at the temperature range of 1250–1450 °C for 15–120 min with a heating rate of 50–60 8C/min and 50 MPa mechanical pressure. The purity and density of the obtained Ti_3SiC_2 product were higher than 92 vol.% and 99%, respectively, when the sintering temperature was higher than 1350 °C. At this latter value, the TiC content was almost constant in the sintering time interval of 15–120 min.

Regarding samples microstructure, it was found to be of three types, that is, fine, coarse and duplex grains, depending on the sintering temperature and time. Besides the already investigated Ti/SiC/TiC reactants, another powdered mixture, that is, Ti/$TiSi_2$/TiC with 1:1:4 or 1:1:3 molar ratio was tested to synthesize the Ti_3SiC_2 compound by PDS [3.].

The process was carried out in a temperature range of 1100–1325 °C for 0–60 min, 50–60 °C/min heating rate and 50 MPa pressure. It was found that the formation of Ti_3SiC_2 phase commenced at temperatures above 1200 °C. The obtained products consisted of the desired compound along with TiC as a second phase. In particular, when the sintering was conducted at a temperature near 1300 °C for 15 min, the maximum product purity for the 1:1:3 and 1:1:4 systems were about 93 and 95 wt.%, respectively. A good densification was achieved by the PDS technique, being the relative density of 1:1:3 and 1:1:4 samples higher than 99 and 98%, respectively, at sintering temperatures above 1250 °C. Moreover, a solid–liquid reaction mechanism between Ti–Si liquid phase and TiC particles was proposed to interpret the rapid formation of Ti_3SiC_2.

To synthesize Ti_3SiC_2 samples, three further mixtures, that is, Ti/Si/C, Ti/SiC/C, and Ti/Si/TiC, were also processed by PDS [5–7].

Powder mixtures of Ti/Si/C with stoichiometric (3:1:2) and off-stoichiometric (3:1.05:2, 3.1:1:2, 3:1.15:2, 5:2:3, and 3:1.5:2) ratios were pulse discharge sintered in vacuum in a temperature range of 1200–1500 °C for 15–60 min, 50–60 °C/min heating rate and 50 MPa pressure [7]. It was found that the fabrication of high purity products was possible only when starting from nonstoichiometric powders, being the best product obtained with stoichiometric powders characterized by a Ti_3SiC_2 content of only 65.2 wt.%. Conversely, when 5Ti/2Si/3C powders were sintered at 1300 °C for 15 min, the TiC content was reduced to about 6.4 wt.% and the corresponding relative density was approximately 99% of the theoretical value. When the 3Ti/SiC/C powder mixture was examined, it was found that the sintered material is characterized by a secondary TiC phase whose content is higher than 50 wt.% [7].

Finally, two Ti/Si/TiC powder mixtures with 1:1:2 and 2:2:3 molar ratios were subjected to PDS under the following operating conditions, that is, sintering temperature in the range 1200–1400 °C, dwell time 8–240 min, pressure of 50MPa, heating rate 50–60 °C/ min [6–9]. With the aim of minimizing the amount of TiC in final products, it was found that the optimum sintering temperature was in the range of 1250–1300 °C. Correspondingly, the highest Ti_3SiC_2 content was about 96–97 wt.% and higher than 99 wt.% for the cases of the 1:1:2 and 2:2:3 mixtures, respectively. In addition, when the PDS process was performed at sintering temperatures above 1275 °C, the relative density of the obtained 2:2:3 samples was higher than 99%. Moreover, it was also found <that the excess of Si in Ti/Si/TiC samples did not play a specific role in improving the purity of Ti_3SiC_2 [9]. The product consists of large plate-shaped grains and small equiaxed grains and no secondary phases were identified.

Thus, by summarizing the results above, the PDS (Pulse Discharge Sintering) method seems to represent a powerful tool for the fabrication of Ti_3SiC_2-based materials. Moreover, among the five different mixtures investigated by PDS, that one corresponding to 2Ti/2Si/3TiC led to the best Ti_3SiC_2 product under the optimal sintering conditions of 1300 °C/ 15 min/50 MPa=. Adapted from Sun et al. [7].

Coarse Ti particles (0.15 mm) were also successfully used for the synthesis of dense Ti_3SiC_2 by PDS when starting from 2Ti/2Si/3TiC powder mixtures [11]. In particular, a 99% dense product with 97.8 wt.% purity was synthesized at 1450 °C for 20 min under an applied pressure of 50 MPa. More recently, to investigate the effect of Al addition on the synthesis of dense Ti_3SiC_2 by PDS, powder mixtures of 3Ti/SiC/C/xAl (x = 0–0.2) were processed by the same group [12]. It was observed that small amount of Al addition favored both synthesis and consolidation of Ti_3SiC_2. In fact, an almost single-phase product was obtained if x = 0.15 or 0.2, when the sintering temperature of 1200 °C was held for 15 min.

The various Ti_3SiC_2 products obtained via PDS by the Japanese research group as described above have also been extensively characterized from the mechanical point of view in terms of deformation, fracture and cyclic fatigue propagation behavior, and the obtained results were reported elsewhere [10,13–15].

The rapid synthesis and consolidation of Ti_3SiC_2 were performed by SPS (Spark Plasma Sintering) from the starting powders of Ti/Si/TiC mixed in a stoichiometric ratio of 1:1:2 [16]. The investigation was carried out in vacuum on a SPS-1050 machine (12/2 on–off time ratio) in temperature range 1125–1400 °C, 100 °C/min heating rate, 20– 60 MPa pressure and 0–10 min holding time. Evidence of the Ti_3SiC_2 formation was observed at about 1200 °C, which is several hundreds degrees lower than the temperature of conventional reactive hot pressing. The optimal result was obtained at 1250 °C 60 MPa/10 min and corresponded to an almost fully densified product consisting of Ti_3SiC_2 with 2 wt.% TiC.

Another Japanese research group have investigated the synthesis/ densification of Ti_3SiC_2 taking advantage of the SPS apparatus [17–19]. Reactant powders used were made of TiC, Ti, carbon black. The effect of the Al addition on the synthesis process was investigated by SPS experiments which were performed at 80 °C/min heating rate, 30 MPa pressure, sintering temperature in the range 600–1400 °C for 0–30 min holding time. It was found that the appropriate addition of Al accelerated the formation of Ti_3SiC_2 and favored its grain growth. Specifically, a 97.8% dense and pure Ti_3SiC_2 product was obtained when the 3Ti/1Si/2C/0.2Al powder mixture was processed by SPS at 1150–1250 °C/30 MPa/10 min.

Also, the SPS products displayed a Vickers hardness of 4 GPa (at 1 N and 30 s). For the sake of comparison, the same powders were processed by HP (High Pressure) and similar products in terms of density and purity were obtained when sintering at higher temperatures and longer processing times, that is, 1300–1400 °C/30 MPa/2 h. More recently, the influence of Al addition to 3Ti/Si/2C powders on the fabrication of dense Ti_3SiC_2 by SPS was further examined [20]. A SPS-2040 model apparatus was used in vacuum under the condition of 50 MPa mechanical pressure, 100–200 °C/min heating rate, 1100–1350 °C temperature, and 2–36 min holding time. It was found that dense Ti_3SiC_2 materials (>98%) with TiC content less than 2 wt.% could be obtained from 3Ti/Si/2C/0.2Al mixtures at 1280 °C when the holding time was higher than 6 min. Product purity was improved by increasing the holding time but it was accompanied by an increase in grain size.

Carbon nanotubes (CNTs) received a great deal of attention due to their superior mechanical and physical properties. In particular, multi-walled carbon nanotubes (MWCNTs) are expected to be used in industrial applications as their price has steadily decreased [22]. CNTs have been considered as useful and attractive additives to organic materials [23, 24], bulky metal [25], metallic coating [26], bulky ceramic [27] and ceramic coating [28] in order to improve the wear resistance and lower friction of mechanical components.

According to the theoretical consideration, a friction coefficient between the walls of MWCNTs should be extremely low. That is, MWCNTs have a significant self lubricant property by nano-ball bearing effects [25]. It was reported [28] that the layered hexagonal MAX phases were thermodynamically stable nanolaminates displaying unusual and sometimes unique properties. Their layered nature suggests that they might have excellent promise as solid lubricant materials.

In our previous work, high-purity Ti_3SiC_2 powders were synthesized successfully by SPS of Ti/SiC/C at temperatures as low as 1400 °C [5–7]. Dense polycrystalline Ti_3SiC_2 of high purity was obtained by reactively hot isostatic pressing of Ti/SiC/C powders at 1300 °C, 60 MPa for 20 mn. Based on these results, in combination with the advantages of the SPS process, the purpose of this study is to obtain high-purity and dense Ti_3SiC_2 with a fine-grained structure at lower temperatures in a short time. The synthesis and densification behavior of Ti_3SiC_2 during the SPS were obtained. The reinforcement of Ti_3SiC_2 matrix nano-ceramics with additing of 1.0 wt% SWCNTs process, as well as the microstructure development, were studied. Several mechanical properties were also measured.

2. Experimental procedure

Commercially available powders of Ti (<45 mm, 99.7 purity, Sumitomo Sitix, Co. Ltd., Japan), SiC (<10 mm, 99.9 % purity, High Purity Chemicals Co. Ltd., Japan), C graphit (1.7 mm, 99.2 % purity, Nihon New Metals Co. Ltd., Japan) and SWCNTS with diameter of 1.2 nm were used as the raw materials (Fig. 1). The Ti, SiC, C and SWCNTs powders were mixed in a stoichiometric molar ratio of 1:1:2 in ethanol by SiC ball milling, and then dried in a vacuum. The mixtures were loosely compacted into a graphite die of 20 mm in diameter and sintered in the vacuum (1 Pa) at various temperatures (1100–1300 °C) using an SPS apparatus (Tycho SINTER, SPS-1050, Sumitomo Coal Mining Co. Ltd.,GERMANY) (Table 1, Fig.2). A constant heating rate of 100 °C/min was employed, while the applied pressure was 60 MPa. The on/off time ratio of the pulsed current was set to 12/2 in each run. The maximum current reached approximately 3000 A during sintering.

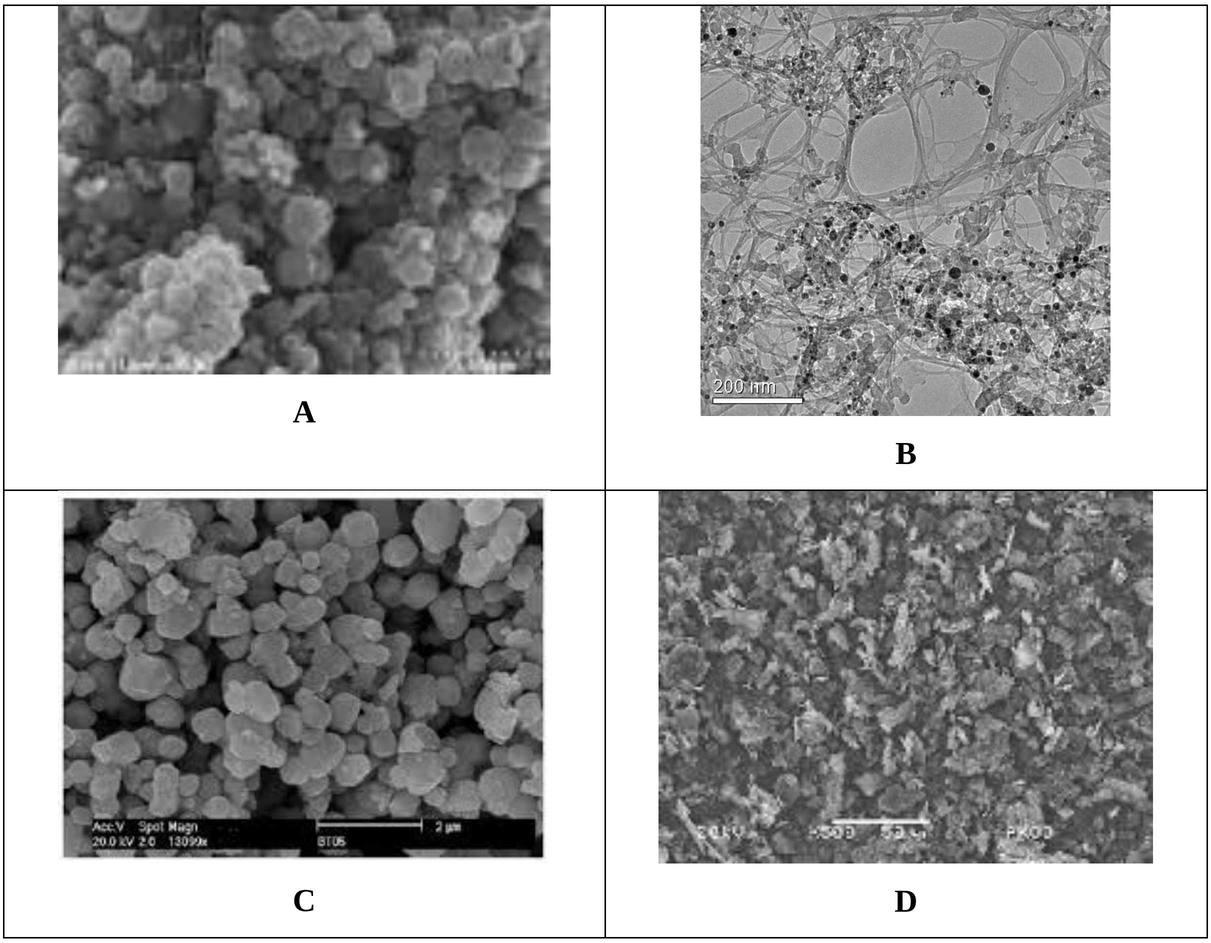

Figure. 1 Starting powders, **A.** SiC powder**, B.** Carbon nanotubes powder**, C.** Titanium powder **et D.** Carbon graphit powder

Table 1 Caracteristics of the sintred samples

Samples	**T (C)**	**Time of the cycle (mn)**	**Heating rate (C/min)**	**P (MPa)**	**Ar (Sccm)**	**3Ti+1.2SiC+0.8C with wt% SWCNTs d=1.2 nm**	**Current (A)**
TSC	1300	20	100	60	200	00	3000
TSC_1	1300	20	100	60	200	1.0	3000
TSC_2	1200	20	100	60	200	1.0	3000
TSC_3	1100	20	100	60	200	1.0	3000

(a)

Program 2642 BADMqAl-1500°

Segment 005 Pyro control

P Time 000:24:52 Rest T 000:26:47

A Time 000:11:43 Rest T 000:08:18

accel time=000 00 00

cursor time= 000 24 49

final time=001 01 58

(b)

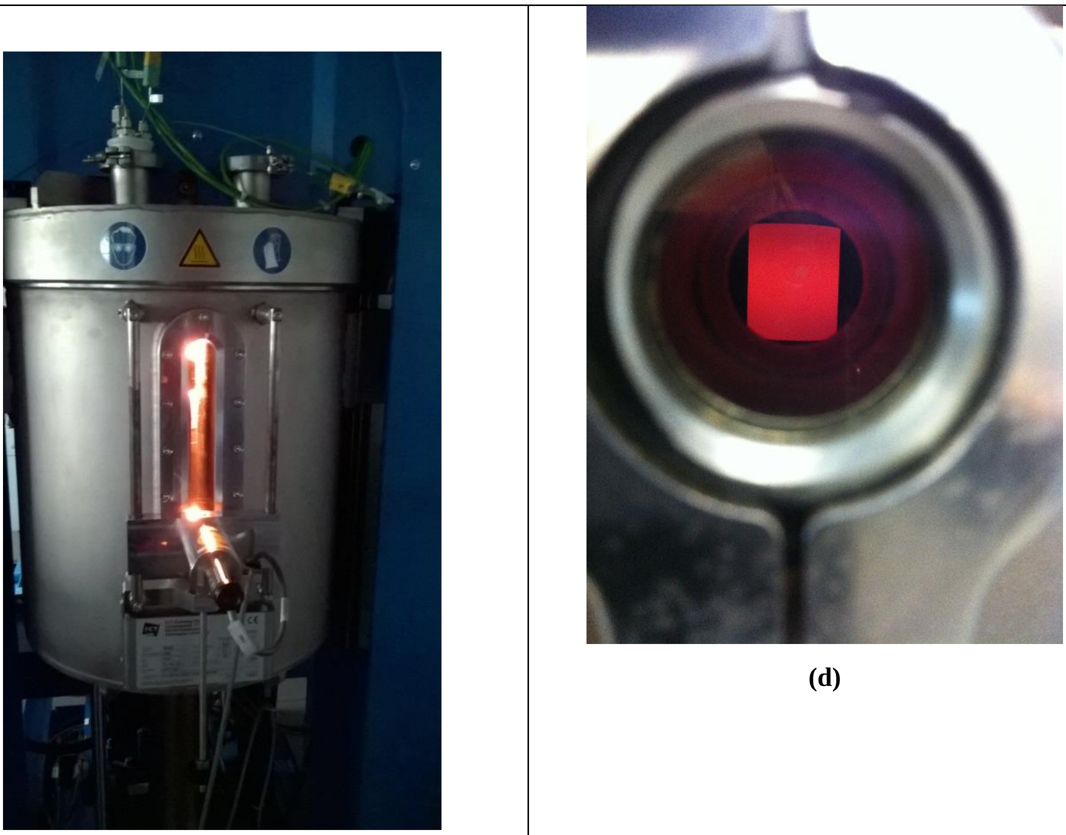

(c)

(d)

Figure. 2 : Tycho SINTER, SPS-1050, Sumitomo Coal Mining Co. Ltd., **Rostock, Germany**,

a- The researsher, **b-**Variation of he displacement, the displacement rate and the temperature in dependence of the heating time, **c- d-** The plasma produced by the current.

The soaking time at high temperatures was within 10 min. The upper ram of the SPS apparatus was fixed, while the displacement of the shifting lower press ram was recorded in order to analyze the synthesis and sintering behavior.

The sintered sample was polished and were evaluated by X-ray diffraction analysis using Cu K_α radiation. The microstructure of the sample was observed by FESEM. The product was cut along the cylindrical axis into two pieces. The microhardness at the top surface and the lateral surface were measured by a diamond Vickers hardness tester. The indentation loads, ranging from 10 to 500 N, were applied for 15 s for each measurement.

3. Results and discussion

3.1. XRD analysis of powders and sintered Ti_3SiC_2/SWCNTs nanocomposites

Figure 2A, B, C and D shows the XRD spectrum of the Ti_3SiC_2/TiC and the reinforced nanocomposite with 1.0 wt% SWCNTs at T= 1300, 1200 and 1100 °C, respectively. It can be seen that the main phase is the Ti_3SiC_2 phase, and precipitated TiC coexist in the sintred samples. XRD patterns of the Ti_3SiC_2, and the nanocomposites are shown in Fig. 2A. The phases were formed during the sintering process in all of the samples because it is a thermodynamically favorable phase at the sintering temperature compared to Ti_3SiC_2 phase [17]:

$$3Ti+1.2SiC+0.8C \rightarrow Ti_3SiC_2,\ \Delta G=-261\ \text{kJ/mol at 1023 K} \quad (1)$$

$$Ti + C \rightarrow TiC\ \ \Delta G=-261\ \text{kJ/mol at 1023 K} \quad (2)$$

XRD spectrum of the nanocomposite, which indicates that the reaction between the Ti powders and SWCNTs did happen during the sintering process. This reaction has been previously observed [24], and it is considered that disordered carbons on wall defects and the open ends of the SWCNTs serve as carbon sources for interfacial reaction. The sintered samples consisted mainly of Ti_3SiC_2 matrix, as major phases, and some secondary phases, such as TiC, appeared depending on the sintering temperature. X-ray diffraction patterns of sample (Ti_3SiC_2/TiC/1.0 wt% CNTs ceramic matrix nanocomposites sintered at 60 MPa pressure were enhanced because they are reinforced with the three phases, TiC and SWCNTs with higher intensity and is shown in Fig. 2B, C and D.

Fig. 2B shows the SWCNTs content at the sintering temperature of 1300 °C for 10 min at 60 MPa, which was reduced to 10 % when sintered at pressure because it reacted with Ti to produce Ti_3SiC_2, and TiC new reinforcement content slightly increased.

Fig. 2A shows the XRD spectrum the top surface. The strongest diffraction peak changed from (104) plane on both surfaces to that of (008) plane on the pulverized sample. The peak intensity of (104) plane on the lateral surface is higher than that on the top surface.

The sample was cut along the cylindrical axis into two pieces. X-ray diffraction analyses on the top and lateral surfaces were carried out. The pulverized sample was also analyzed by X-ray diffraction. These results suggest that Ti_3SiC_2 grains grew preferentially with the basal planes rotating towards the loading direction.

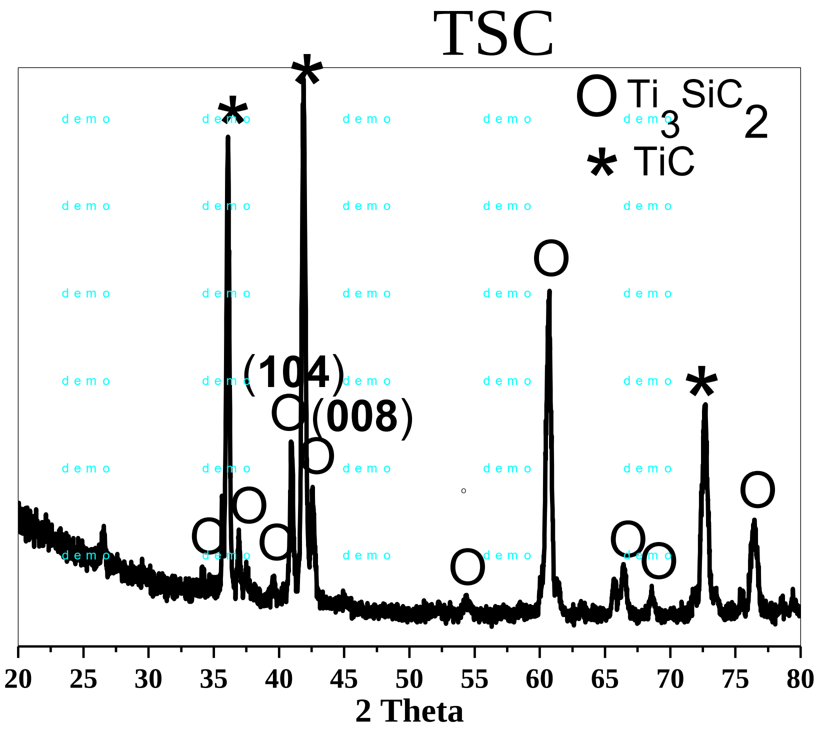
TSC
O Ti_3SiC_2
* TiC
(104)
(008)
20 25 30 35 40 45 50 55 60 65 70 75 80
2 Theta

Fig. 3A

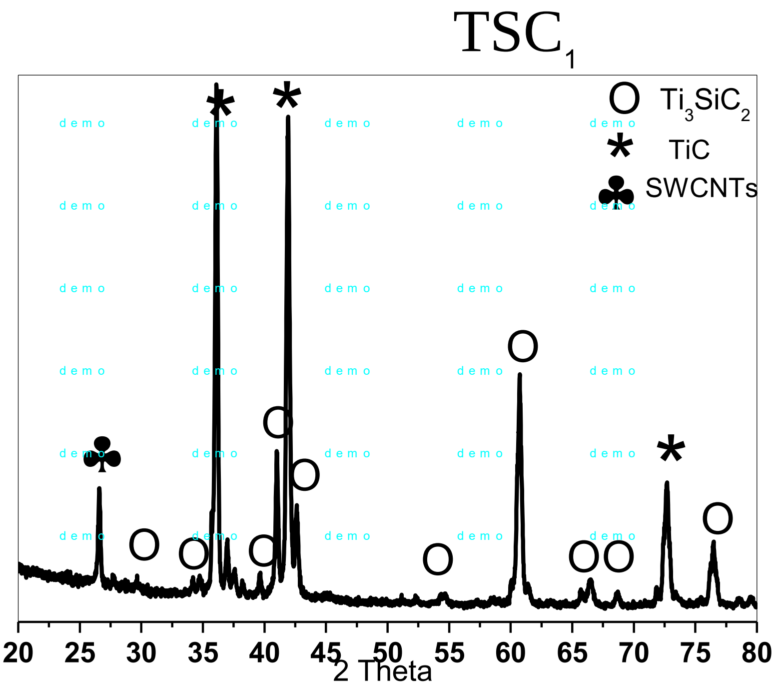
TSC_1
O Ti_3SiC_2
* TiC
♣ SWCNTs
20 25 30 35 40 45 50 55 60 65 70 75 80
2 Theta

Fig. 3B

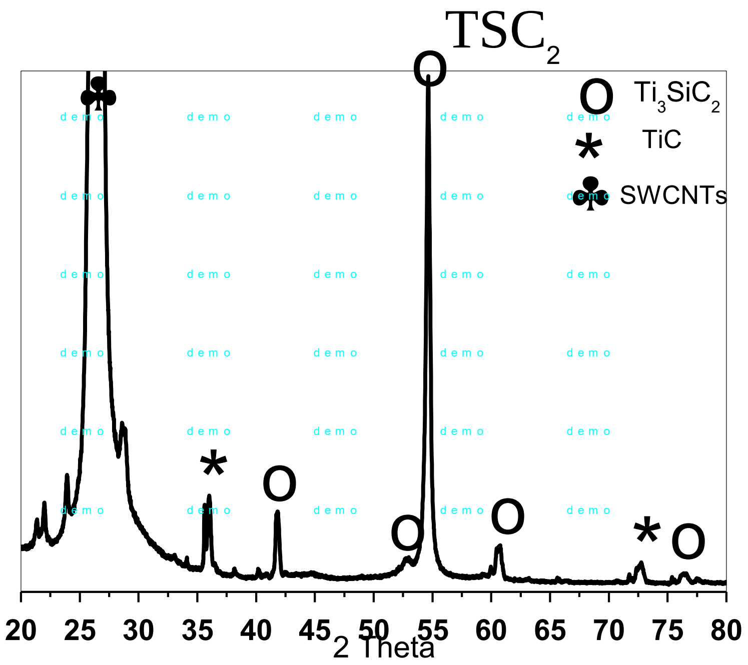

Fig. 3C

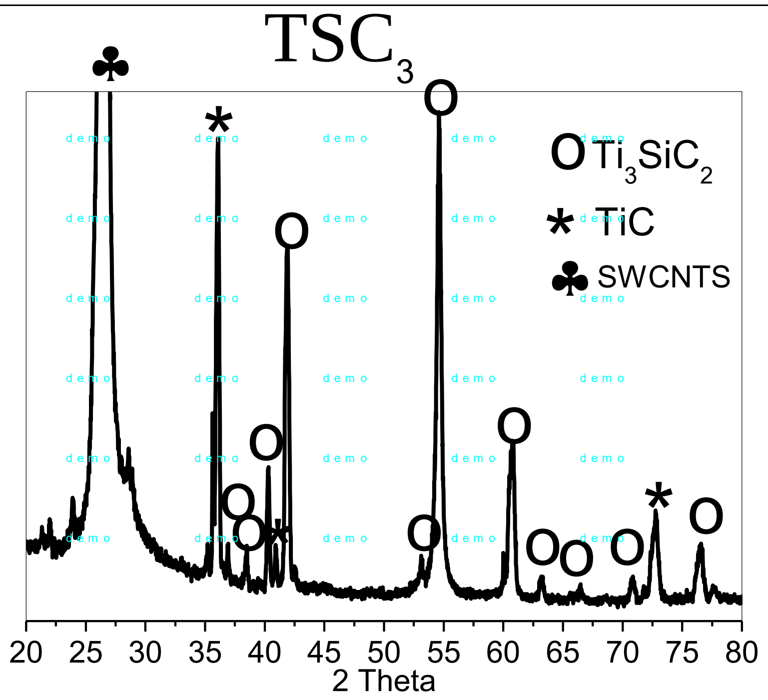

Fig. 3D

Figure. 3 X-ray diffraction spectrum on the top surface of the sintred samples using a 20-mm diameter die**, A.**TSC, **B.**TSC1**, C.**TSC2**, D.**TSC3.

3.2. FESEM microstructural observation of sintered Ti_3SiC_2/TiC/1.0 wt% CNTs nanocomposites

The formation of Ti_3SiC_2 seems to produce this volume expansion. Fig. 3 shows the fine grained structure of the top surface for the sample sintered at 1300, 1200 and 1100 °C, respectively at 60 MPa for 10 min after etching by an HF:HNO3 aqueous solution. The average grain size of Ti_3SiC_2 is below 10 µm. TiC (shown as a bright contrast is about 1–2 mm size, which is near the original TiC particle size in the as-received powders. Some closed pores inside the Ti_3SiC_2 grains can also be seen, which would be attributed to the short sintering time. The Ti_3SiC_2 typical grains have a thin plate-like form with a diameter of 10–30 mm and a thickness of 3–6 mm. These grain sizes are one order smaller than those of materials prepared by other methods.

FESEM analysis of the sintreed revelated the plate-like structure of the Ti_3SiC_2 materials is shown in the Fig.3 and shown several orientation of the grain with the plate-like structure, and gray contrast granular areas in between the bulk grains. Fig.3 is a higher magnefication view that shows the heavy nature of the plates formed probably due to the shock consolidation process.

The worn surfaces and wear debris are compared in Fig.4. The Microstructural and EDS analysis displays elemental analyses of the various regions of the sintered samples Ti_3SiC_2/TiC, and the Ti_3SiC_2/TiC/1.0 wt% CNTs nanocomposites in chemical composition (at.%) (Fig. 3). EDS spectra was used to determine the elemental composition of the different regions in the sample and are presented by the red specta. The FESEM micrographs in Fig. 3 shows a dark phase that corresponds to the Ti_3SiC_2 matrix Max phase, and TiC is represented by the agglomerat in cubique polycristal form in addition to unreacted SWCNTs, TiSi is not detected.

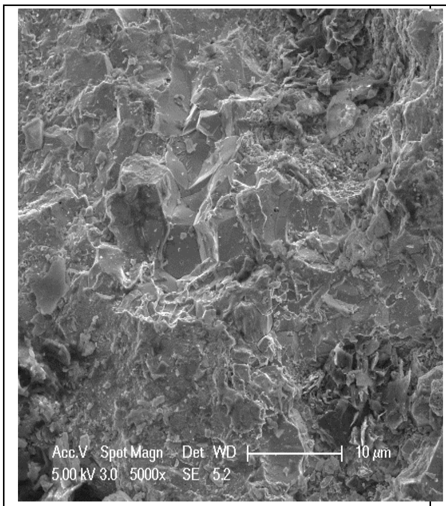

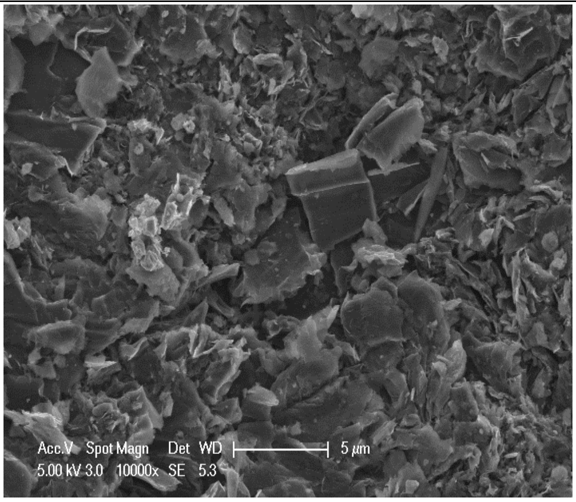

TSC **TSC**

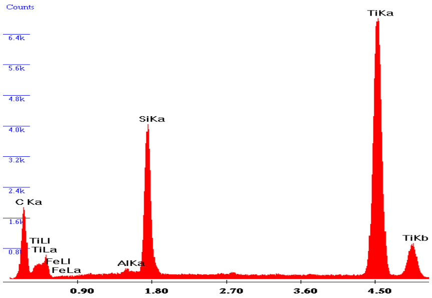

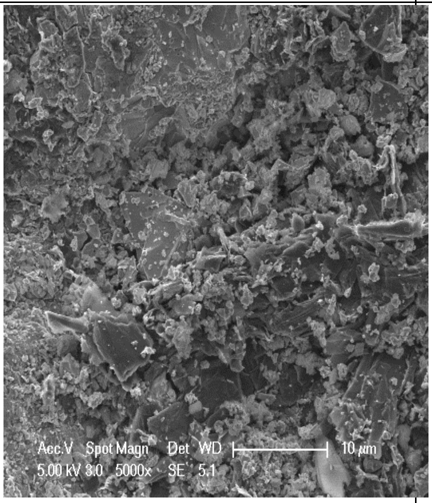

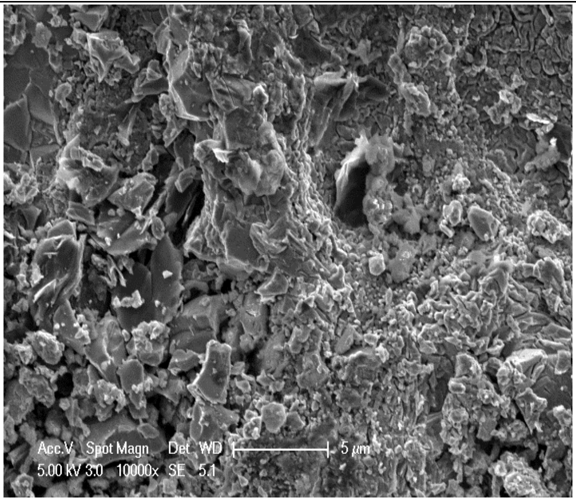

TSC$_1$ **TSC$_1$**

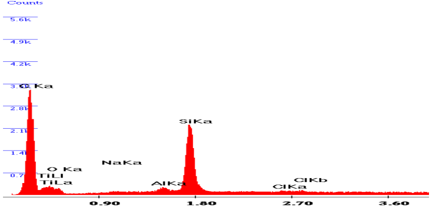

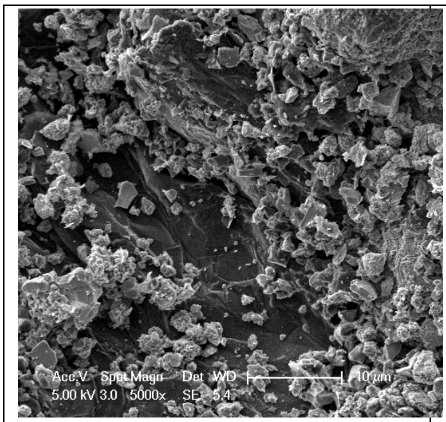
Acc.V Spot Magn Det WD 10 µm
5.00 kV 3.0 5000x SE 5.4

TSC$_2$

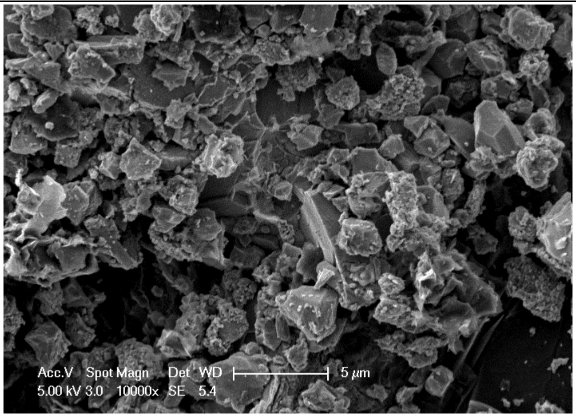
Acc.V Spot Magn Det WD 5 µm
5.00 kV 3.0 10000x SE 5.4

TSC$_2$

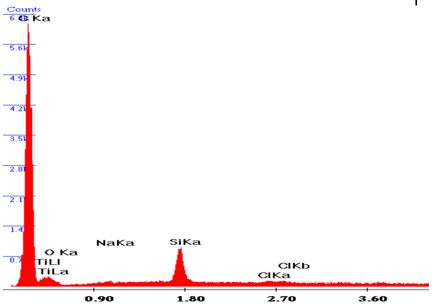
Counts
C Ka
5.6k
4.9k
4.2k
3.5k
2.8k
2.1k
1.4k
0.7k
O Ka
TiLl
TiLa
NaKa
SiKa
ClKb
ClKa
0.90
1.80
2.70
3.60

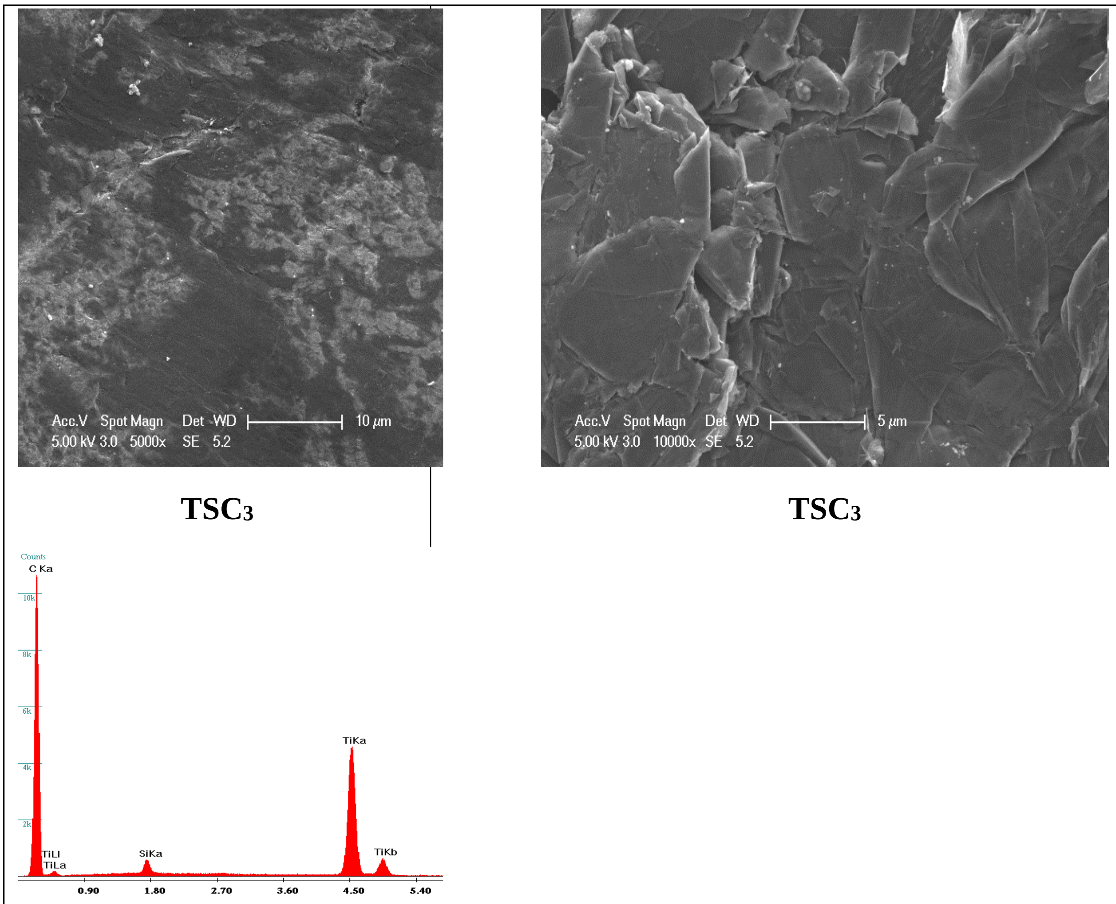

TSC3 **TSC3**

Figure. 4 FESEM micrograph of the polished and etched surface for the sintered samples using a 20-mm diameter die.

3.3. Microhardness

According to the above results, it can be concluded that the wickers hardness has been improved by adding SWCNTs and annhanced at a high temparature. Fig. 4 shows the hardness as a function of the applied indentation load for the same sample. At higher loads, the microhardness reaches a constant value of 4.0 GPa for Max phase matrix or unreinforced. The low hardness as indirect evidence of the purity of the as-synthesized Ti_3SiC_2. In the present study, the low hardness of the SPS synthesized sample containing 1.0 wt% SWCNTs at T= 1100 °C may be attributed to its low density (95% theoretical).

The hardness of the same sample exhibited an anisotropic behavior as shown in Fig. 4. On the top surface, the hardness, HV, decreased sharply at a load between 10 and 50 N and then decreased gradually at higher loads as already indicated in Fig. 4. On the lateral surface, the hardness, HV, showed less dependence on the indentation load and lower values than Hv at all load levels. Fig. 4 presents the variation of Vickers microhardness of Ti_3SiC_2/TiC/1.0 wt% CNTs nanocomposites with CNTs reinforcement content and temperature. The microhardness of the composites increased almost linearly with increasing temperature at the SWCNTs reinforcement content. The hardness of SWCNTs (28–30 GPa) is nearly 7–8 times the previously reported values of hardness of Ti_3SiC_2 (4 GPa). For the nearly single Max phase Ti_3SiC_2 (SPS) sintered in this investigation, the microhardness was found to be 5.94 GPa (measured with indentation load of 10 N), which is higher than the previously reported hardness values for monolithic [22]. While the higher hardness of the Ti_3SiC_2 sample could be due to a minor amount of SWCNTs phase in the Ti_3SiC_2 sample, it could also be due to indentation size effects. It was reported that the hardness decreases with increasing load and asymptot value of 2 GPa at higher loads. The microhardness in the range of about 2.5–3.5 GPa was found for lower loads (10 N). A slight increase in average hardness have been obtained from Max Ti_3SiC_2 matrix nanocomposites prepared by sintering Ti_3SiC_2/TiC/1.0 wt% CNTs nanocomposites reinforced with 1.0 wt% of SWCNTs with Ti and SiC elemental powders at T=1300 °C exhibited highest hardness of about 6.5–8.5 GPa (Fig.4A),. It is considered that in situ, TiC and the remaining SWCNTs act as reinforcements and plays the major role in the improvement.

The best product contained Ti_3SiC_2/TiC/1.0 wt% CNTs which was sintered at 1300 °C, 60 MPa for 10 min. The hardness of the product Ti_3SiC_2/TiC/1.0 wt% CNTs decresses with decreasing temperature (Fig.4B), with this, the electrodischarge among powders may lead to self-heating and purification of the particle surface, resulting in activation of the formation for Ti_3SiC_2, the platelet grains are parallel to the (001) plane and perpendicular to the c-axis of the Ti_3SiC_2 crystal structure. The platelet Ti_3SiC_2 grains tended to be parallel to the pressing direction. The corresponding FESEM micrographs around the indentation marks at the top and lateral surfaces show the lateral cracks extension from the indentation mark on the top surface, but not in the case of the lateral surface. It is suggested that on the lateral surface, the indentation load may act as a force to delaminate the platelet Ti_3SiC_2 in the weak Si bonding direction. Due to the energy dissipation in this process, a higher toughness and a lower hardness is exhibited on the lateral surface as a result of the anisotropy caused by the preferential grain growth.

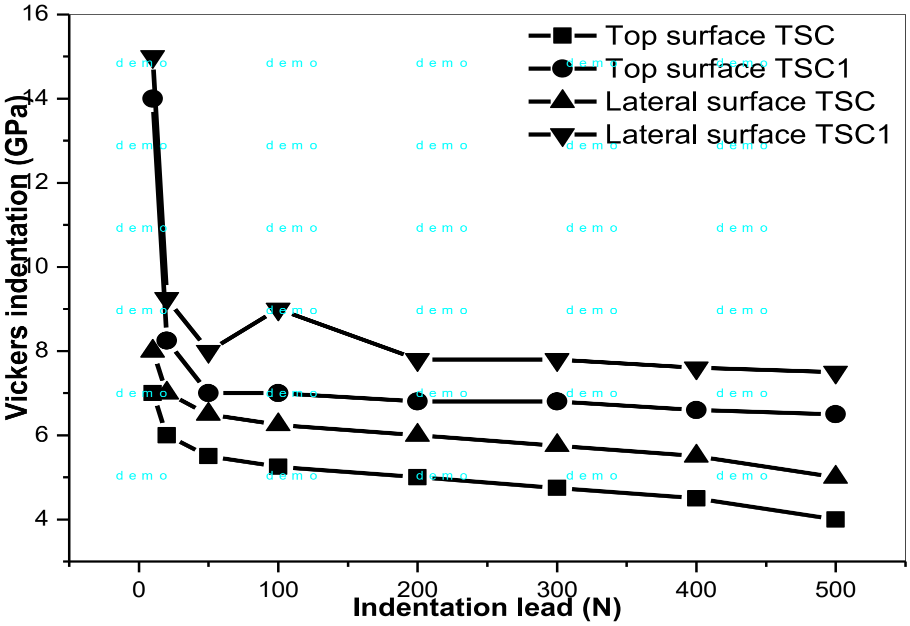

Figure. 5A

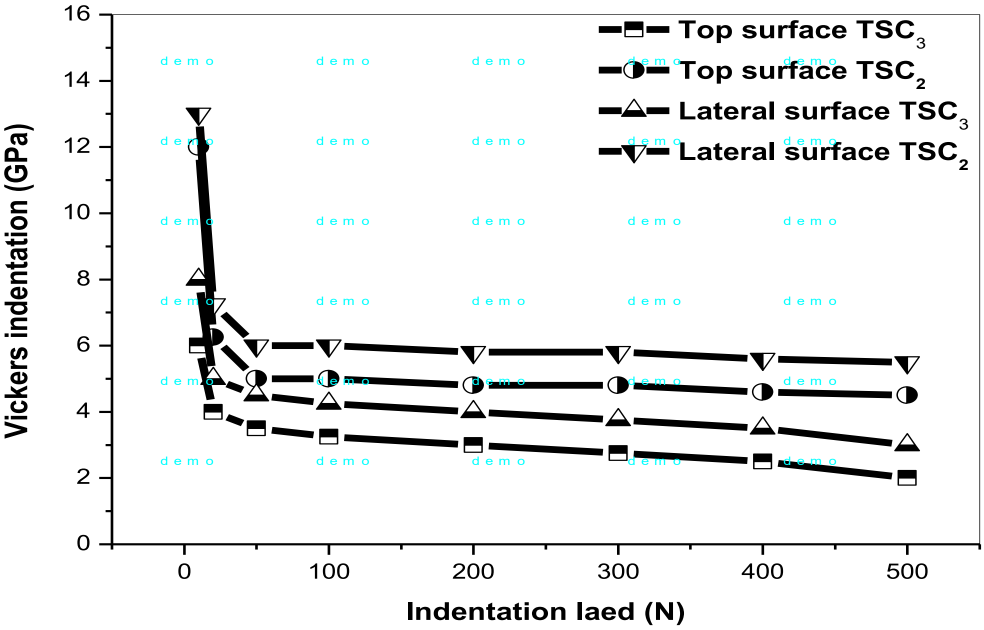

Figure. 5B

Figure. 5 ickers hardness of as-synthetized samples using a 20-mm diameter die as function of indentation load, measured along two directions, **A.** TSC and TSC_1, **B.** TSC_2 and TSC_3

3.4. Relative density

The variation of the relaties density of sintered Ti_3SiC_2/TiC and Ti_3SiC_2/TiC/1.0 wt% CNTs nanocomposites with SWCNTs reinforcement is shown in Fig.5. The theoritical density of the composite used for obtaining relative density was calculated using a rule of mixture, using the densities of two constituant hase ($\rho_{Ti3SiC2} =$ 4.53 g /cm^2 , $\rho_{TiiC} =$ 4.50 g /cm^2, $\rho_{SWCNTs} =$ 2.25 g/cm^2) with the given SPS processing paramaters, the Ti_3SiC_2/TiC sample exibited best densification with relative density greater than 99%, with the simlar processing parameters and variation of temperature Ti_3SiC_2/CNTs nanocomposites. The relative density decresed with incressing temperature at the reinforcement of 1.0 wt% SWCNTs . The Ti_3SiC_2/TiC/1.0 wt% CNTs nanocomposites at T=1300 °C exibited relative density of about 98%. Clearly, the densification of the Ti_3SiC_2/TiC/1.0 wt% CNTs decreases with decreasing temperature and reached the value of 96% at 1200°C and 94% at 1100°C. This seems to be the direct consequence of higher melting point of SWCNTs (T=3160 °C) compared to that of Ti_3SiC_2 (T= 3000 °C) and TiC (T= 3000 °C). XRD analysis indicated formation of new intermediate phase TiC from their action between Ti and C while the intensities of SWCNTs peaks remained unchanged. Depending on the final density to be achieved, the SPS operating condition were properly chosen, that is, 750 °C, 5 Mpa for 5 min, to obtain a relative density of 75 %, 800 °C, 25 Mpa for 5 min, for samples; 87 % dense, and 850 °C, 50 Mpa for 5 min, for zero porosity compacts. The 13% porosity sample exhibited a round microstructure with high ductility, while the 25% porous product displayed much lower stress flow as compared to that of the 13 % porosity [12]. Also, the easy sledding of their walls when attached by weak van der Waals force of coaleced MWCNTs can probably decrease the relative density. The density of the sintered samples was determined using the Archimedes water immersion method.

Figure.6: The mesureament of the relative density.

4. Conclusion

Simultaneous synthesis and densification of Max Ti_3SiC_2 was rapidly achieved by spark plasma sintering of Ti/SiC/C powder mixtures. Dense Max Ti_3SiC_2/TiC and Max Ti_3SiC_2/TiC/1.0 wt% CNTs nanocomposites with varying temperature and 1.0 wt% SWCNTs weight fraction were fabricated by SPS at 1300, 1200 and 1100 °C under a pressure of 60 MPa for 10 min in pure Ar atmosphere protection. Max phase Ti_3SiC_2/TiC/1.0 wt% CNTs at T= 1300°C had the highest Vicker's microhardness and relative density, which were HV 6.5 to 8.5 GPa and 98 %. Preferential grain growth of Ti_3SiC_2 along the crystallographic basal plane was detected by XRD analysis. Because these platelet grains tended to align perpendicular to the loading surface, an anisotropic hardness was obtained. This increased with the addition of SWCNTs. Although TiC was formed by reaction of SWCNTs and Ti, unreacted SWCNTs could be found. Mechanical properties of Ti_3SiC_2/TiC were enhanced by unreacted SWCNTs at high tempeerature.

Furthers studies will be performed with variation of the graphite die diameter, to control the TiC content in the Max phase matrix. By spark plasma sintering, the extensive volume expansion as a function of the pressure will occur.

Acknowledgements

We are grateful to Prof. Jaafar Ghambaja, (Institut Jean Lamour, University of Henri Point Carré, Nancy, France) for his help in FESEM and XRD investigations.

References

[1] A. Feng, T. Orling, Z.A. Munir, Mater. Res **14** (1999) 925
[2] Z.F. Zhang, Z.M. Sun, H. Hashimoto, T. Abe, Scripta Mater **5** (2001) 1461
[3] Z.F. Zhang, Z.M. Sun, H. Hashimoto, Adv. Eng. Mater **4** (2002) 864
[4] Z.F. Zhang, Z.M. Sun, H. Hashimoto, T. Abe, Mater. Res. Innov **5** (2002) 185
[5] Z.F. Zhang, Z.M. Sun, H. Hashimoto, T. Abe, J. Eur. Ceram. Soc **22** (2002) 2957
[6] Z.F. Zhang, Z.M. Sun, H. Hashimoto, Metall. Mater. Trans A **33** (2002) 3321
[7] Z.M. Sun, Z.F. Zhang, H. Hashimoto, T. Abe,; Mater. Trans **43** (2002) 428
[8] Z.F. Zhang, Z.M. Sun, H. Hashimoto, T. Abe,; J. Am. Ceram. Soc **86** (2003) 431
[9] Z.F. Zhang, Z.M. Sun, H. Hashimoto, T. Abe; J. Alloy Compd **352** (2003) 283
[10] Z.F. Zhang, Z.M. Sun, Mater. Sci. Eng A **408** (2005) 64

[11] Y. Zou, Z.M. Sun, H. Hashimoto, S. Tada,; Mater. Trans **47** (2006) 1910.

[12] Z.M. Sun, S. Yang, H. Hashimoto, J. Alloy Compd **439** (2007) 321

[13] Z.M. Sun, Z.F. Zhang, H. Hashimoto, T. Abe, Mater. Trans **43** (2002) 432

[14] ZF Zhang, ZM Sun, H Hashimoto, Mater. Lett. **57** (2003) 295

[15] H. Zhang, Z.G. Wang, Q.S. Zang, Z.F. Zhang, Z.M. Sun, Scripta Mate **49** (2003) 87

[16] N.F. Gao, J.T. Li, D. Zhang, Y. Miyamoto, J. Eur. Ceram. Soc **22** (2002) 2365

[17] J. Zhu, B. Mei,; J. Mater. Sci. Lett **22** (2003) 889

[18] J. Zhu, B. Mei, X. Xu, J. Liu, Scripta Mater **49** (2003) 693

[19] W. B. Zhou, B.C. Mei, J.Q. Zhu, Mater. Lett **59** (2005) 1547

[20] J. Zhang, L. Wang, W. Jiang, L. Chen, J. Alloy Compd **437** (2007) 203

[21] U. Anselmi-Tamburini, Y. Kodera, M. Gasch, C. Unuvar, Z.A. Munir, M. Ohyanagi, Journal of Materials Science **41** (2006) 3097

[22] T. Kuzumaki, K. Miyazawa, H. Ichinose, K. Ito, J. Mater. Res **13** (1998) 2445

[23] H. Kwon, M. Estili, K. Takagi, T. Miyazaki, A. Kawasaki, Carbon **47** (2009) 570

[24] W.A. Curtin, B.W. Sheldon, Today **7** (2004) 44

[25] G. Wei, Y. Jian, Q. Tai, Z. She-Ming, Journal of Inorganic Materials **25** (2010) 1081

[26] W.X. Chen, J.P. Tu, L.Y. Wang, H.Y. Gan, Z.D. Xu, X.B. Zhang, Carbon **41** (2003) 21527

[27] S.I. Cha, K.T. Kim, S.N. Arshad, C.B. Mo, S.H. Hong, Adv. Mater. **17** (2005) 1377

[28] D.H. Nam, S.I. Cha, B.K. Lim, H.M. Park, D.S. Han, S.H. Hong, Carbon **50** (2012) 2417

Exp. Theo. NANOTECHNOLOGY 2 **(2017)** 69 – 79

Experimental and Theoretical
NANOTECHNOLOGY
http://etn.siats.co.uk/

Effect of annealing temperature on the optical and electrical properties of Mg doped TiO_2 thin films

M. Devi[1], Manas R. Panigrahi[1,1]

[1]*Electroceramics lab, Department of Physics, KIIT University, Bhubaneswar-751024, India*
1)*E-mail: mrpanigrahifpy@kiit.ac.in*

Received 12 Oct. 2015; Revised 30 Jan. 2016; Accepted 13 Feb. 2016

In order to achieve high conductivity and transmittance of transparent conducting oxide (TCO), we attempted to fabricate Mg doped TiO_2 ($Mg_{0.01}Ti_{0.99}O_2$) thin films and characterized them for their structural and optical properties. The materials is prepared by modified sol-gel route. $Mg_{0.01}Ti_{0.99}O_2$ thin films have been deposited on glass substrate by doctor's blade technique. The structure of the films were confirmed to be tetragonal and particle size were estimated to be ≈11.1 nm from XRD analysis. The optical property study in the same range shows higher value of absorbance in comparison to the pure TiO_2 film after the wavelength 425 nm. The band gap is estimated to be much lower than pure TiO_2 (3.2 eV). So the study shows that doping a small amount of Mg can enhance the visible light absorption in the epitaxial thin film which can be a suitable material for use in solar cell to trap the solar-radiation.

Key words: Modified sol-gel route; Optical properties; Electrical properties.
PACS: 78.20.Ci; 81.20.Fw; 83.85.Hf.

1. Introduction

In this era of nanotechnology, nanomaterials have been the subject of enormous interest for the scientists and academicians. Due to their very small size, nano materials are known to have unique mechanical, thermal, biological, optical and chemical properties, and becoming a potential candidate for versatile industrial applications.

TiO_2 nanomaterials are one of the potential candidates for solar energy application due to TiO_2's unique optoelectronic and photochemical properties in general and especially, as a photovoltaic performer to convert solar radiations to efficient energy and thus receiving a great deal of attention for research. TiO_2 is a wide band-gap semiconducting materials and it is of much interest due to its various applications like water and air purification [1-3], nano-size TiO_2 as anode of dye sensitized solar-cell [4] . The large band gap (≈3.2 eV) restrict most of the solar spectrum unutilized. Thus several approaches are being adopted so that visible light active TiO_2 photocatalytic material can be produced. The efficiency of TiO_2 can be improved by morphological modifications or by incorporation of additional components in the TiO_2

structure. The morphological modification includes formation of small crystallite size. The visible light active TiO_2 has been produced by doping it with non-metals as well as metals [5-7]. To extend the optical absorption of TiO_2 to the visible region, various dopants have been added to the oxide to improve its solar efficiency [8-9]. To improve the quality as well as the physical and chemical properties of thin films, the addition of some metal ions as impurities is expected to play an important role in changing the charge carriers concentration of the metal oxide matrix, catalytic activity, the surface potential, the phase composition, the size of crystallites, and so on [10-11]. Doping a metal or nonmetal into TiO_2 could change the band edge or surface states of TiO_2 [12]. Usually the modification is done by doping transition metals. But the transition metal doping cause thermal instability to the anatase phase of TiO_2 [13]. In the process of doping if the metal does not incorporate into the TiO_2 frame work and remains on the surface it blocks the reaction site and thus it is the main demerit of metal doing into the TiO_2 matrix. The incorporation of transition metals in TiO_2 crystal lattice may result in the formation of new energy levels between valence band and conduction band [14]. Mg is an alkaline earth metallic material which is used to dope into TiO_2 anatase to improve photo activities [15]. There were several studies on alkaline earth metal doped TiO_2, out of which Mg is the most suitable one for doping into TiO_2 due to its atomic radius. Mg doped TiO_2 thin films were used as the cathode for solar cell application by Wang et al. [16] have found to have higher short circuit current density in comparison to that of undoped TiO_2, which is mainly due to the reduction in elecron-hole recombination rate. According to K. Manseki etal.[17] it is found that use of Mg doped TiO_2 nano particles increases the open circuit voltage of perovskite solar cell. The study of Mg doped TiO_2 nano particles by Md. A. Behnajadi etal.[18] showed a decrease in band gap energy and it was also found to enhance photo catalytic activity for degradation of acid red (AR-27**).** Accoding to T. Siva Rao etal.[19] Mg doped TiO_2 is found to reduce its band gap and hence its photo catalytic activity in visible light region in comparison to undoped TiO_2 increases.

Usually light of energy greater than the band-gap value of the material excites the electrons to jump from the valence band to the conduction band. The band-gap value of anatase TiO_2 is 3.2eV, so UV light is required to excite its electron from valence band to conduction band by creating a hole. But UV light only constitutes 5% of solar radiation so maximum part of solar radiation **remain** unused. Thus, it is attempted to produce visible light active TiO_2 nano thin films which will be able to use almost 40% of solar-radiation. In this paper, preparation of Mg doped TiO_2 thin film and its optical properties is studied by UV- Vis spectro photometer within a wavelength range 300-900nm. From X-ray diffraction it is **observed** that there is almost no change in the particle size between pure TiO_2 and Mg doped TiO_2 thin films but, the strongest peak is oriented towards the a-axis corresponding to (300) plane. The band-gap of the film is calculated by Tauc plot method which is found to be appreciably low i.e. 2.63eV**.** Usually, recombination is facilitated by impurity or defect. Prevention of recombination is usually done by doping with ions or hetrojunction coupling. So here we have doped the alkaline earth metal Mg to the TiO_2 thin film in the ratio (0.01 M :0.99 M).

2. Method of analysis

The crystal structure of the annealed film was investigated by X-ray diffraction (XRD, Shimandzu-6100) with CuKα radiation (λ=.1540nm). Optical transmittance spectra of the thin films were measured by UV-Vis spectrometer (Shimadzu-2540) in the wavelength range 300-900nm. The resistivity was measured by the Hall measurement.

3. Experimental procedure

Mg-doped TiO_2 ($Mg_xTi_{1-x}O_2$) thin film for x=0.01 have been prepared by the sol-gel method. Starting reagent materials were taken as MgO (99.99% pure Merck) and TiO_2 (99.99% pure Merck). DI water and Acetic acid were used as solvent. Stoichiometric proportionate powders of MgO and TiO_2 were mixed with suitable amount of acetic acid to form a uniform lump free paste. Then the DI water was added drop wise with continuous stirring at room temperature at 500 rpm until a homogeneous transparent sol is formed. Further with the adition of 0.1M HNO_3 refluxing was done at 180°C for 6-7 hrs at 1200 rpm to get the gel. Mg-doped thin films were deposited on the glass slide by doctor blade technique [20-21] and the films were annealed at temperatures like 300, 350 and 400 °C. Subsequently the annealed films were subjected to different types of characterization like, XRD, SEM and UV-VIS spectro photometer.

4. Results and discussion

The phase crystallinity and x-ray diffractogram of plain and Mg doped TiO_2 thin films are shown in Figure-1. There is no evidence of secondary phase in either case. All the x-ray micrographs matched with the anatase phase of nanocrystalline TiO_2. All the film planes are identified and leveled properly. For plain and Mg doped TiO_2 thin films the highest intensity occurs at the plane (102) and (300) respectively. The lattice parameters of TiO_2 thin film changes from a=b=5.358 Å, c= 9.541 Å to a=b=10.639Å, c=7.576 Å due to Mg doping when annealed at 300℃. But, for annealing temperature 350℃ and 400℃, the lattice parameters are, a=b=10.635Å, c=7.564 Å and a=b=10.632Å, c=7.562 Å, respectively**.** Here, it is seen that, magnesium modified titanium dioxide thin film is stretched more along the axis. But, with increasing annealing temperature the cell volume is decreasing slowly from 857.45 to 855.45 to 854.76 $Å^3$**.** This can be attributed to local lattice distortion induced by impurity site and shrinkage along the c--axis. The structure of TiO_2 anatase is described as a coordination of TiO_6 octahedrons in which there are double octahedron layers stacking alternatively along c-axis and having more empty spaces between layers than within layers. So, the crystal is more compressible along c-axis. C-axis is called as the soft axis of TiO_2 because the Young's modulus value in this direction is more than twice smaller than that along in plane direction **[**22]. When the impurity is added the size of the MgO_6 octahedron reduce causing the change in internal strain which in turn changes the value of bond length [23-24]. The particle size also changes from 11.416nm to 11.419nm by addition of Mg. The different estimated parameters as obtained from xrd analysis are presented in table-1.

Tables 1 Electronic parameters of TiO_2 and $Mg_{0.01}Ti_{0.99}O_2$ thin film**s** annealed at different temperatures.

Sample name	**Band-Gap in eV**	**Carrier Concentration in/cm3**	**Resistivity in Ohm.cm**	**Mobility in Cm^2/Vs**
TiO_2As is	2.82	$3.9x10^{13}$	$1.59x10^2$	1300
Mg-TiO_2As is	2.56	$9.6x10^{13}$	$1.438x10^3$	45.2

Mg-TiO2@300°C	1.85	1.325×10^{13}	2.677×10^{4}	17.6
Mg-TiO2 @350°C	1.64	2.714×10^{13}	4.63×10^{3}	57
Mg-TiO2@400°C	2.69	1.47×10^{14}	1.32×10^{4}	32.3

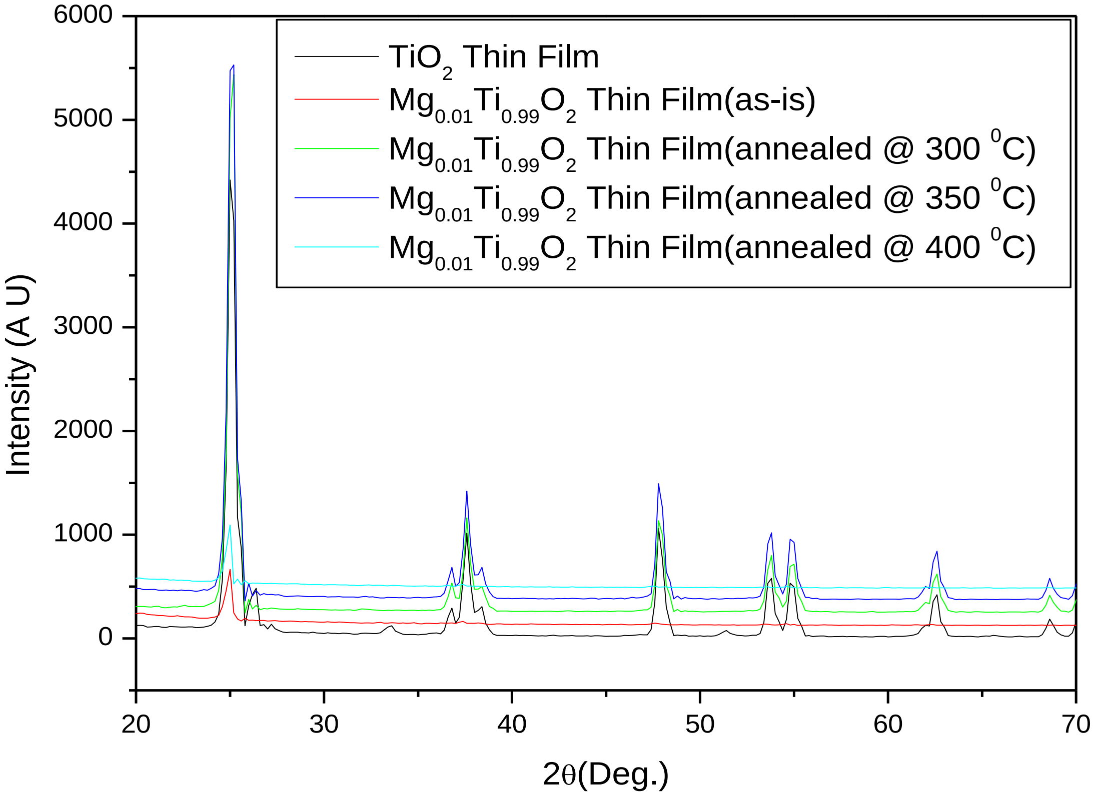

Figure 1 X-ray diffractogram of TiO_2 and $Mg_{0.01}Ti_{0.99}O_2$ thin film annealed at different temperatures.

The sharp decrease in the transmittance with most of the radiation absorbed for incident photons in the wavelength range 400–600 nm is associated with the fundamental absorption. It is evident from the spectra that the fundamental absorption edge shows a positive shift in the wavelength with increasing grain size, which indicates a shift in the optical band gap to lower energy. Further, the shift in the fundamental absorption edge is associated with a slight decrease in the transmittance above and below the absorption edge. However, the relative high spectral transmission above the fundamental absorption edge ($\lambda > 600$ nm) reveals that these oxide films, in general, are weakly absorbing in the spectral range of investigation. An increase in the scattering coefficient would decrease the optical transmittance in the UV region [25]. This feature clearly observed in the transmittance curves as shown in Fig. 2 supports the idea of scattering losses due to random distribution of grains.

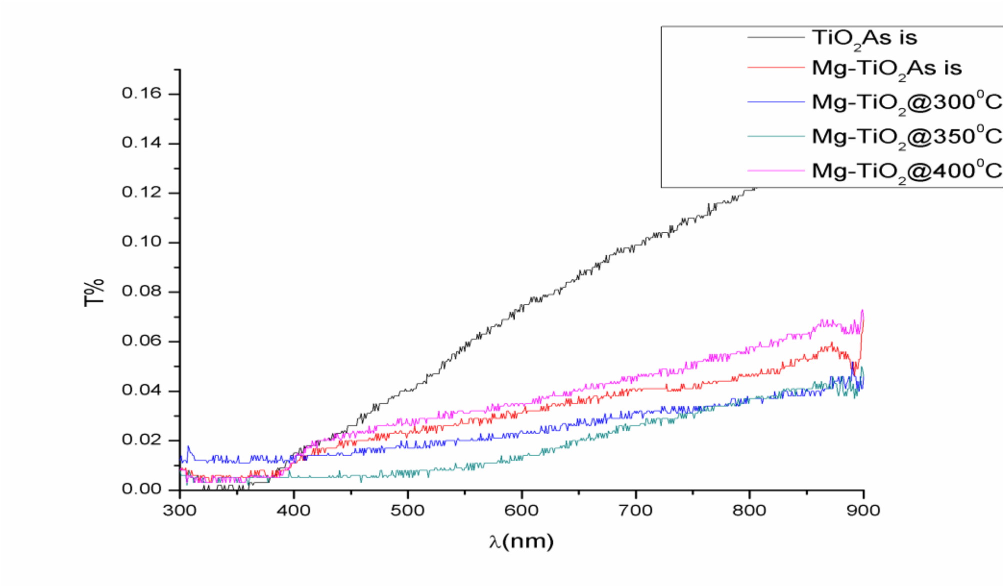

Figure 2 Transmitted spectra of TiO_2 and $Mg_{0.01}Ti_{0.99}O_2$ thin film annealed at different temperatures.

The optical parameters were calculated from the optical absorption spectra measured by Shimadzu-2540 UV–Vis photo spectrometer in 300–900 nm wavelength range. Usually light of energy greater than the band-gap value of the material excites the electrons to jump from the valence band to the conduction band. UV light is required to excite electron from valence band to conduction band creating a hole in anatase TiO_2 as band gap is 3.2eV. But, UV light only constitutes 5% of solar radiation so maximum part of solar radiation is unused. But, in $Mg_{0.01}Ti_{0.99}O_2$ thin film the absorption % increases compared to pure TiO_2 thin film. So it is can be said that $Mg_{0.01}Ti_{0.99}O_2$ is a visible light active TiO_2 nano thin films which will be able to use extra % of solar-radiation. The absorbance of both the films are compared and found that, absorption of the Mg-doped TiO_2 thin film is more after the wavelength range 422nm i.e. the Mg doping enhances the absorbance of TiO_2 thin film in the visible light range. The extended absorbance of Mg doped sample can be explained as excitation of electron of dopant to the conduction band of TiO_2. The metal dopant used here has different valence state than Ti^{4+} and hence may induce the oxygen deficiencies during synthesis. So the generation of new energy levels due to the injection of impurities within the band-gap coupled with generation of oxygen vacancies by metal ion doping may contribute to the observed visible light absorption of Mg doped TiO_2 thin film. The comparative absorption spectra are represented in Figure-3. As seen in the fig.3, the absorption % suddenly falls in pure TiO_2 thin film, but in case of Mg doped TiO_2 thin films the absorption % is consistent and uniform in the visible light range and that it is temperature dependent. For the sample which is annealed at 350℃ it is maximum and uniform from 400 to 500 nm and there after the absorption % decreases slowly in the visible range. Whereas for all other samples it is almost the same in the visible range. However, in the wavelength range 300 to 400 nm, there is a lot of longitudinal vibration in the higher orbital and transfer of charge particles is ultrafast giving rise to an anomalous behaviour, which is very clearly seen in TiO_2 as-is and other samples too.

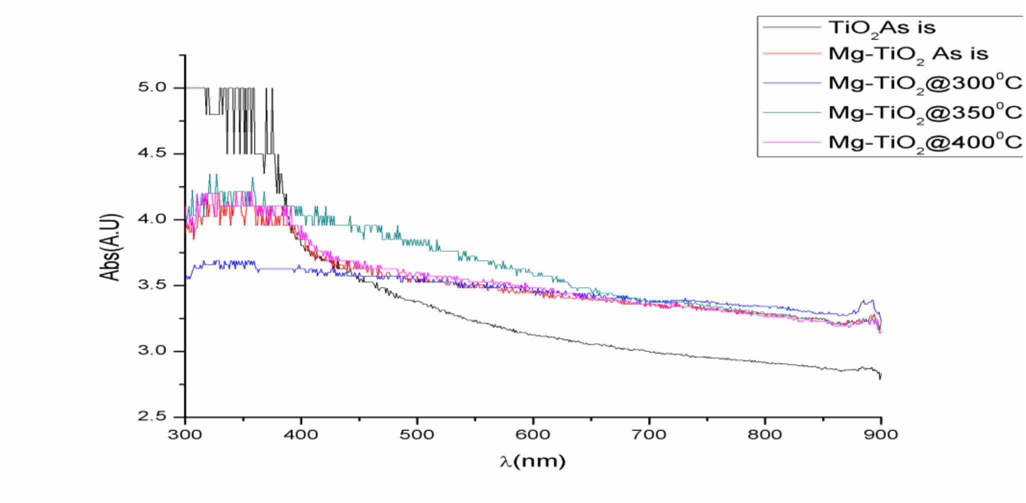

Figure 3 Absorption spectra of TiO_2 and $Mg_{0.01}Ti_{0.99}O_2$ thin film annealed at different temperatures.

The band-gap of all the films are calculated from Tauc plot that is a plot between $(\alpha h\nu)^n$ and hν, where hν is the incident photon energy [26-27]. Here α represents the absorption co-efficient and power coefficient n can have different values depending on the type of electronic transition. n=2 for allowed direct and n=1/2 for allowed indirect transition. The extrapolation of linear region of the graph to α=0 gave the band-gap value [28-29]. The band gap of both the pure and Mg-doped TiO_2 thin films are calculated by considering the direct transition since it is more favorable for anatase TiO_2 according to Reddy's paper [30]. The comparative band-gap calculation for both the films is shown in figure 4.

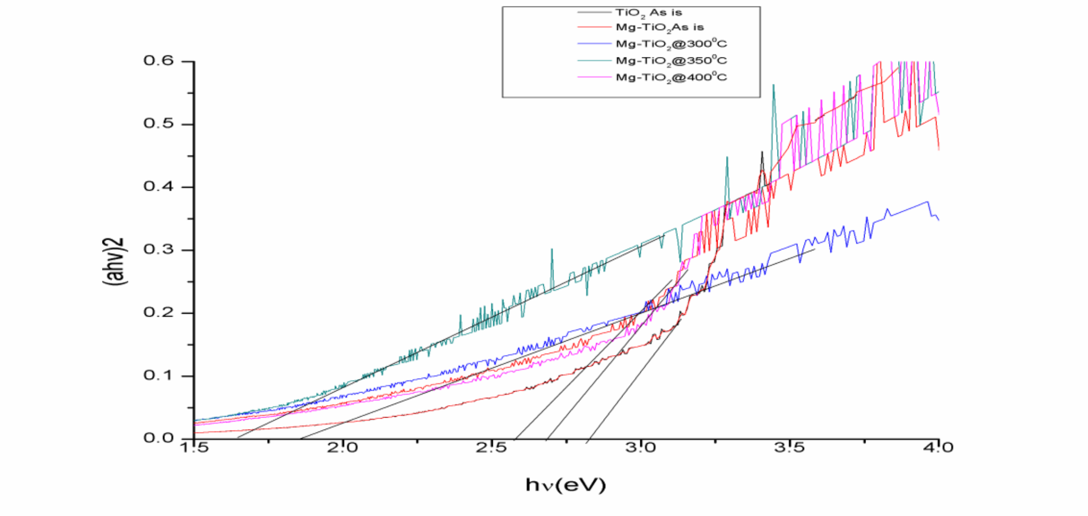

Figure 4 Band gaps of TiO_2 and $Mg_{0.01}Ti_{0.99}O_2$ thin film annealed at different temperatures.

The band-gap of TiO_2 thin film is found to reduce from 2.66 eV to 1.64 eV with Mg doping. This reduction in band-gap may be due to the four different interactions (i) the exchange interactions [31] (ii) carrier impurity interaction which affect the majority carrier band [32] (iii) carrier-carrier or electron–hole interaction [33] and (iv) Carrier impurity interaction which affect the minority carrier band [34-36]**.** Band gap values for different samples are presented in table-1. It is seen that though band gap decreases with Mg doping, from 2.82 to 2.56, it still further decreases when annealed with certain temperatures. In this case it is observed that at annealing temperature 350℃ the band gap value is minimize to 1.64 eV, but on further annealing to 400℃ the band gap value increases. In the studied range $Mg_{0.01}Ti_{0.99}O_2$ annealed at 350℃ is most suitable for photo voltaic applications.

The observed effects can be explained based on the electronic band structure of $Mg_{0.01}Ti_{0.99}O_2$. The band structure of $Mg_{0.01}Ti_{0.99}O_2$ has been studied several times. In general, the conduction band in $Mg_{0.01}Ti_{0.99}O_2$ is formed by magnesium modified titanium 3d bands and the valence band by 2p bands of oxygen [37–40]. In crystalline magnesium modified titanium, the fundamental absorption is mainly due to transitions from the oxygen p-type wave function to the 3d-type magnesium modified titanium wave functions. Therefore, the band gap corresponds to the energy gap between the top of the Oxygen 2p band and bottom of the magnesium modified titanium 3d band. The band gap widening in the films with relatively low grain size is mainly due to quantum size effects.

Fig.5 shows the variation of ln (resistivity) versus temperature of $Mg_{0.01}Ti_{0.99}O_2$ thin film annealed at different temperatures. Here, it is seen that, the resistivity jumps to a very high value when it is annealed at 300℃, but the resistivity drops when annealed with a further higher temperature at 350℃. On further annealing the sample the resistivity increases once again to half the value that decreases as we go from 300 to 350℃. Similar is the nature of Fig.6 which speaks about the variation of resistivity with annealing temperature. It is seen that, the sample annealed at 350 C has minimum resistivity and low band gap (≈1.64 eV). This is the beauty of this material at this particular temperature. Absorption % of this particular sample is almost linear in the wavelength range 350 to 500(nm) where as if one look into the transmitted spectra of all the annealed samples, it seen that for sample annealed at 350 C it has the minimum transmittance and linear within the wavelength range 350 to 500(nm). From Table-1 it is seen that at annealed temperature 350 C, the sample has minimum band gap (eV), maximum carrier conc. and mobility and minimum resistivity. Similarly, table-2 explain about the optical properties of the sample that, it has a thickness of 0.9018 um, maximum refractive index, and minimum coefficient of absorption ($\approx 3.74\text{x}10^4$ cm^{-1}) with 99.21% GOF. Table-2 presented the optical properties of different samples in terms of thickness, refractive index, absorption co-efficient and goodness of fit.

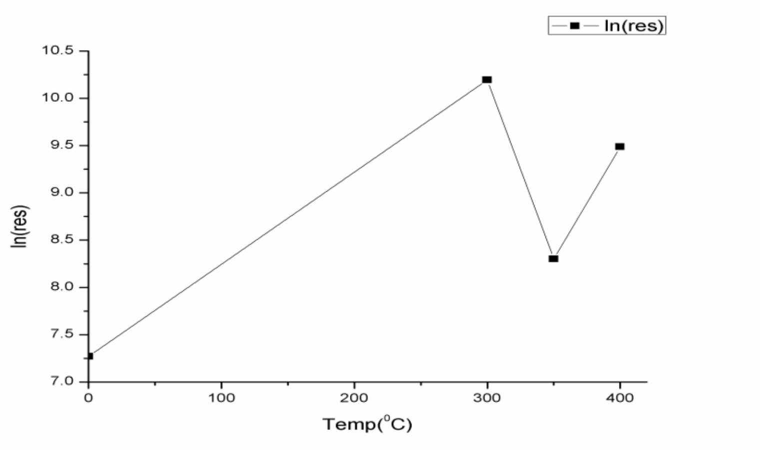

Figure 5 Tem. (℃) Vs. ln(Res.) of TiO_2 and $Mg_{0.01}Ti_{0.99}O_2$ thin film annealed at different temperatures.

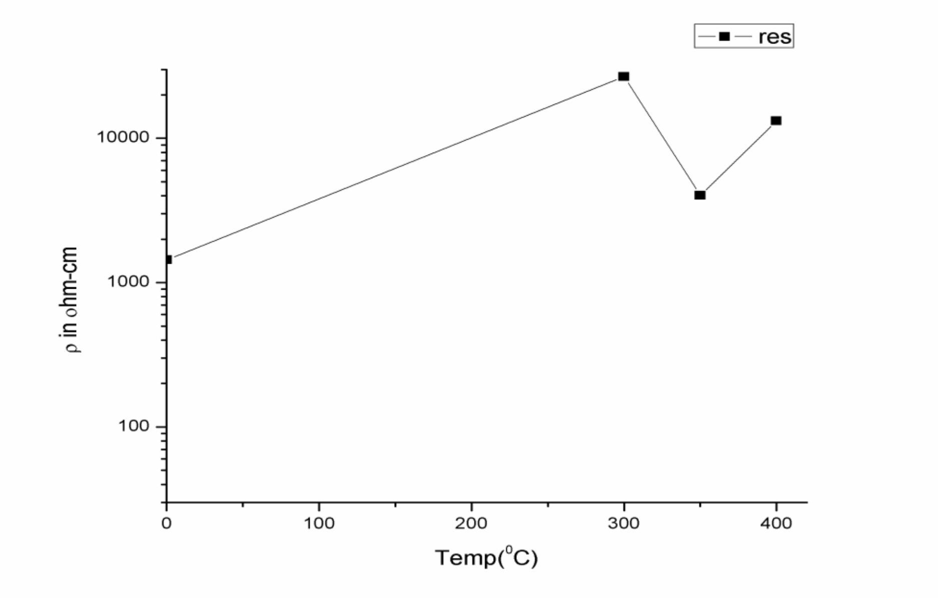

Figure 6 Tem. (℃) Vs. Resistivity of TiO_2 and $Mg_{0.01}Ti_{0.99}O_2$ thin film annealed at different temperatures.

Tables 2 Optical parameters of TiO_2 and $Mg_{0.01}Ti_{0.99}O_2$ thin film annealed at different temperatures.

Sample name	**Thickness in µm**	**n**	**α x(10^4) cm^{-1}**	**GOF**
TiO_2As is	0.9899	1.36	3.81	0.9888
Mg-TiO_2As is	0.9018	1.1765	4.18	0.9817
Mg-TiO_2@300°C	0.9018	1.2988	3.93	0.9954
Mg-TiO_2 @350°C	0.9018	1.3422	3.74	0.9921
Mg-TiO_2@400°C	0.9018	1.1752	4.18	0.9848

Fig.7 gives the very dense, uniform and euhedral micrographs of TiO_2 and Mg doped TiO_2 annealed at different temperatures in the studied range. It is seen that, the grain size is almost same and without much porosity. But, Mg doped TiO_2 annealed at 400 °C the grain size appears to be little bigger and may attributed to the fact that, the coalesce of nano size particle at a higher temperature.

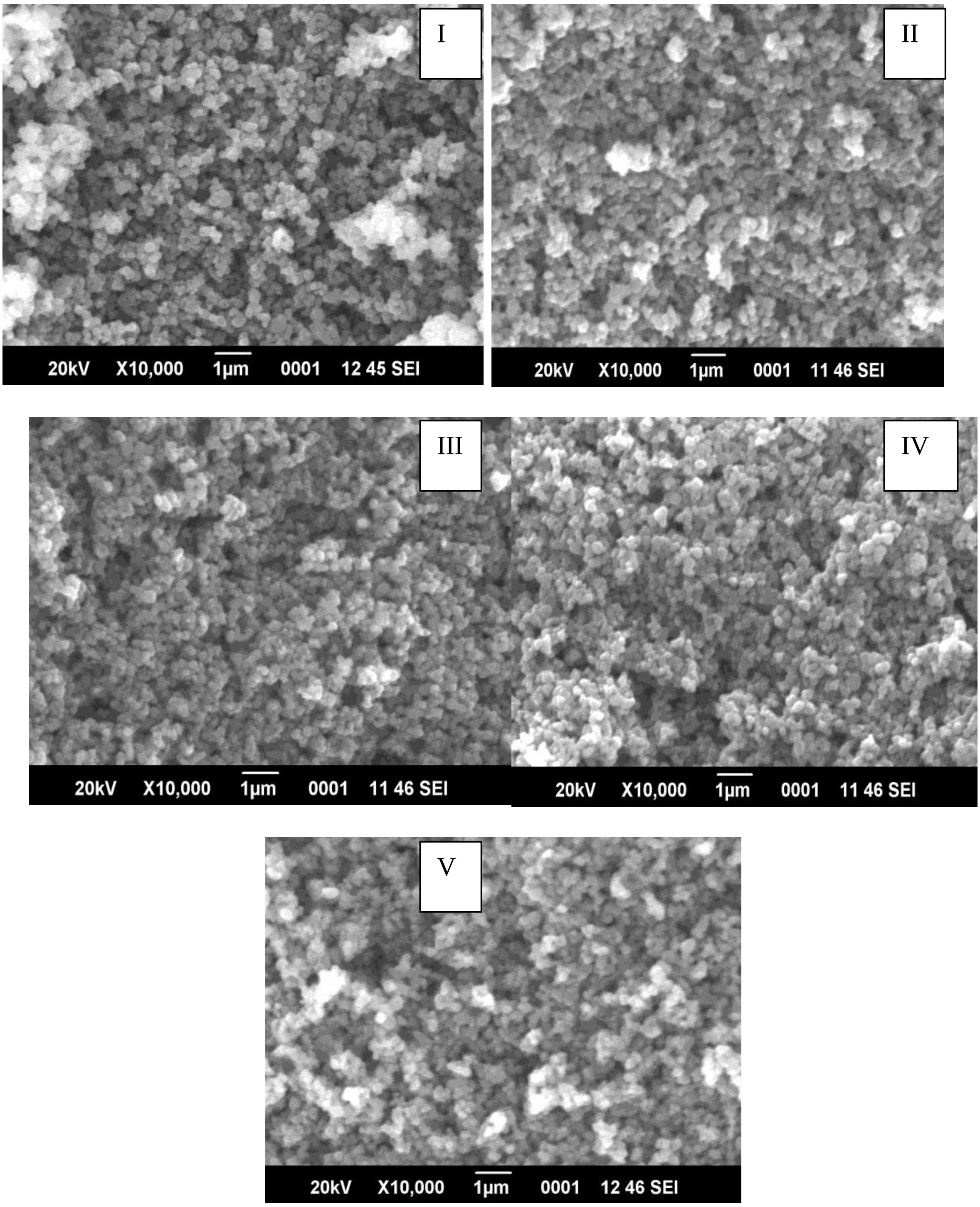

Figure 7 SEM micrographs of (I) TiO_2 As-Is,(II) Mg doped TiO_2 As-Is,(III) Mg doped TiO_2 annealed at 300 ℃, (IV) Mg doped TiO_2 annealed at 350 ℃, and (V) Mg doped TiO_2 annealed at 400 ℃.

5. Conclusion

Mg doped TiO2 thin films were synthesized by sol gel technique from powder reagent and annealed at different temperatures at 300 to 400℃. Structural, electrical and optical properties of these thin films were analysed. In this study it is observed that, Mg drops the band gap in $Mg_{0.01}Ti_{0.99}O_2$ from 2.82 to 1.62 eV in Mg doped TiO_2 thin film annealed at 350 ℃. Band gap of all the Mg doped TiO_2 thin films reduces in comparison to pure TiO_2 thin film. However, $Mg_{0.01}Ti_{0.99}O_2$ thin film annealed at 350℃ shows low band gap, high absorption %age, high mobility, low resistivity and large carrier conc. and hence may be suitable for different photovoltaic applications. The random distribution of the grains makes the film surface rough and results in the increased light scattering losses at the interface. Further, an increase in the scattering coefficient would decrease the optical transmittance in the UV region. This feature clearly observed in the transmittance curves as shown in Fig. 2 supports the idea of scattering losses due to random distribution of grains. The decrease in the band gap and changes in the spectral characteristics are attributed to random grain distribution, and structural modification of the material in the films. These observations could be useful while considering the $Mg_{0.01}Ti_{0.99}O_2$ thin films for electronic and optical applications.

Acknowledgement: SAIF KOCHI is sincerely acknowledged for providing SEM facilities.

References

[1] M.R. Hoffmann, S.T. Martin, W. Choi, D. W. Bahnemanns, Chem. Rev **95** (1995) 69
[2] M. A. Fox and M. T. Dulay, Chem. Rev **93** (1993) 341
[3] A. J. Maira, K. L. Yeung, C. Y. Lee, P. L. Yue, C. K. Chan, Catalysts J. Catal **192** (2000) 185
[4] B. O' Regan and M. Gratzel, Nature, **353** (1991) 737
[5] A.V. Emeline, V. N. Kuznetsov, V. K. Rybchuk, N. Serpone, International Journal of Photo energy **258394** (2008) 258394
[6] T. Umebayashi, T. Yamaki, H. Itoh, K. Asai, Appl. Phys. Lett **81** (2002) 454
[7] E. Borgarello, J. Kiwi, M. Gratzel, E. Pelizzetti, V. M. Visca, J. Am. Chem. Soc **2996** (1982) 14104
[8] K. L. Choy, Prog. Mater. Sci. **48** (2003) 164
[9] A. Goossens, J. Schoonman, J. Electrochem. Soc. **144** (1997) 1723
[10] R. W. Seigel, E. H. Hu and M. C. Roco, WTEC panel Report on R & D Status and Trend in nanoparticales Nanostructured Material, Nanodevices, Workshop, (1997).
[11] D. Szezuko, J. Werner, S. Oswald, G. Behr K. Wetzing, Appl. Surf Sci **179** (2001) 301
[12] Y. Cao, W .Yang, W. Zhang, G. Liub, New. J. Chem **2** (2004) 218
[13] W. Choi, A. Termin, M. R. Hoffmann, J. Phys. Chem. B **98** (1994) 13669
[14] A. J. Gjazai, H. A. Hassan, Z. Hassan and A. SH. Hussein, Int. J. Nanoelectronics and Materials **6** (2013) 113
[15] T. Nikolay, L. Larina, O. Shevaleevskiyb, B. Tae Ahn, Energy Environ. Sci **4** (2011) 1480
[16] J. Wang, M. Qin, H. Tao, W. Ke, Z. Chen, J. Wan, P. Qin, L. Xiong, H. Lei, H. Yu and G. Fang, Applied Physics Letters **106** (2015) 121104
[17] K.Manseki, I.Ikeya, A.Tamura, T.Ban, T.Suqiura and T.Yoshida, RSC Advances **4** (2014) 9652
[18] M. A. Behnajady, B.Alizade and N. Modirshahla, Photochemistry and Photobiology 87 (2011) 1308
[19] T. Siva Rao, T. Abdo Segne, T. Susmitha, A. BalaramKiran, and C. Subrahmanyam, Advances in Materials Science and Engineering **168780** (2012) 168780
[20] G. Ruani, C. Ancora, F. Corticeilli and C. Dionigi, Solar Energy Materials and Solar Cells **92** (2008) 537
[21] A. S. Kontos, A. G. Kontos, D. S. Tsoukleris etal., J. Mater. Process. and Tech. **196** (2008) 243

[22] S. Chen, J. H. Yang, X. G. Gong, Y. Yan, S. H. Wei, Appl. Phys. Lett **96** (2010) 221901

[23] T. Van Nam, N. T. Trang and B. T. Cong, VNU Journal of Science, Mathematics - Physics **28** (2012) 84

[24] J. G. Ma, Cai-Rong Zhang , Ji-Jun Gong and You-Zhi Wu etal., Materials, **8** (2015) 5508

[25]L. Zhang, D. Ouyang, and C. Mo, Nanostr. Mat. **8** (1997) 1991

[26] M. F. Alias, E. M. N. Al-Fawade and S. K. J. Ali-Ani, Int. J. Nanoelectronics and Materials **4** (2011) 101

[27] S. Kausar, S. Joshi and A. Srivastava, Int. J. Nanoelectronics and Materials **7** (2014) 77

[28] M. Sreemany, A. Bose, S. Sen, Physica B **405** (2010) 85

[29] H. Yang, X. Zhang, Q. Tao, A. Tang, J. Optoelectr. Advanc. Mater. **9** (2007) 2493

[30] K. Reddy, S. Manorama, A. Reddy, Mater. Chem. Phys **78** (2002) 239

[31] C. H. Kwon, H. Shin, J. H. Kim, W. Schoi and K. H. Moon, Mater. Chem. Phys. **84** (2004) 78

[32] C. S. Kim, B. K. Moon, J. H. Park and S. T. Chung, J. Cryst. Growth **254** (2003) 405

[33] Y. U. Kolenko, A. A. Burukhin and B. R. Cheraglove, Mater. Lett. **57** (2003) 1124

[34] S. C. Jain, D. J. Roulston, Solid-State Electron **34** (1991) 453

[35] G. Mahan, J. Appl. Phys. 51 (1980) 2634

[36] M. Devi, M. R. Panigrahi, U.P.Singh, J. Mater Sci: Mater Electron **26** (2015) 1186

[37] C. G. Granqvist, Handbook of Inorganic Electrochromic Materials, Elsevier (1995)

[38] C. V. Ramana, O. M. Hussain, B. S. Naidu, and P. J. Reddy, Thin Solid Films **219** (1997) 305

[39] A. Talledo and C. G. Granqvist, J. Appl. Phys. **77** (1995) 4655

[40] C.V. Ramana, R.J. Smith, O.M. Hussian, Phys. Stat. Sol. (A) **1** (2003) 199

Exp. Theo. NANOTECHNOLOGY 2 **(2017)** 81 – 96

Experimental and Theoretical
NANOTECHNOLOGY
http://etn.siats.co.uk/

Solid phase microextraction based micro-device for extraction of PCR amplifiable DNA

G. Samla[1], K. B. Gan[1,*], S. M. Then[2]

[1] *Department of Electrical, Electronic& Systems Engineering, Universiti Kebangsaan Malaysia, Selangor, Malaysia*
[2] *Faculty of Medicine & Health Sciences, University of Nottingham Malaysia Campus, Selangor, Malaysia*
*) E-mail: sam2011sj@yahoo.com

Received 30 Jan 2016; Revised 13 Feb. 2016; Accepted 2 March 2016

Deoxyribonucleic acid (DNA) extraction or sample preparation from biological sample (whole blood) for downstream process on microfluidic platform has been widely studied due to its crucial role in clinical diagnostic and genetic analysis. Sample preparation can be complicated since blood comprises complex matrices and repeated blood pricking from patients can be affected their health. Thus, introduction of solid-phase microextraction (SPME) method would be suitable to isolate, fractionate and concentrate the analyte from complex sample matrices and implemented on microfluidic device with small amount of sample. SPME is an effective sample preparation method by chemical lysis followed by purification mostly by using silica-based platform developed based on direct absorption into silica resins and desorption of analyte from silica resins.

Keywords: Extraction; Whole blood; Micro-device.
PACS: 88.20.jp; 87.19.um; 85.40.-e.

1. Introduction

Micro total analytical system (μTAS) is an integration of multiple chemical analytical systems in single micro-device [1] which breakthrough in analytical methodology and instrumentation. This micro-device is highly in demand for sample preparation in molecular diagnostics, clinical analysis, polymerase chain reaction (PCR) analysis and so on. Fundamentally, traditional bioanalytical methods involving complex matrices especially biological fluids are time consuming and difficult to perform. For example, convention DNA assay consisted of DNA purification from complex sample, PCR amplification and electrophoretic size separation of the DNA fragment [2, 3]. DNA purification is necessary and most important sample preparation step for effective PCR and other genetic or clinical analysis. Basically, efficient DNA extraction from µl of blood requires filtering out tens of µg of other organic compounds as well as contaminant from sample. Previous studies reviewed that bioanalytical sample preparation method particularly solid-phase extraction (SPE) are effective for DNA extraction and purification. The insoluble particulate material in SPE with high affinity for protein and low affinity for nucleic acids enable the effective extraction of DNA [4]. However, this technique needed spacious extraction phase and large amount of sample volume, buffer solution or solvent plus time consuming [5]. Even some modern analytical techniques such as liquid chromatography coupled with mass spectrometry is best known for rapid plus sensitivity in quantitative and qualitative analysis but it is limited by selectivity of analytes. The biological sample such as blood and urine contains varieties of organic compounds hence sensitivity for extraction or preparation of analyte of interest might be reduced. In contrast solid-phase microextraction (SPME) needed only small volume extraction phase to isolate, fractionate and concentrate the analyte from complex sample matrices [6-8]. This method has been widely implementing in various applications including micro-device with minimum number of handling steps and reproducible methodology. The high potential of SPME for rapid, solvent-free and simple study has continuously fascinating researchers in biochemical and clinical analysis [5,9].

2. Theory of Solid Phase Microextraction (SPME)

Analyte of interest preparation or separation from sample is vital for molecular or clinical analysis. This is difficult by traditional method as the sample consists of complex matrices and it consumes high purity and toxic solvent which hazardous to environment. Hence, SPME was introduced in the early 1990s, is a new and effective sampling and sample preparation method by chemical lysis followed by purification mostly by using silica-based resins [4]. SPME can be eco-friendly and fulfill the requirement for green analytical chemistry during the entire sample preparation stage as the utilization of solvent or buffer is reduced; the sample preparation steps are simple and fast; and cost effective analysis by removing pumps or power supply [10]. The initial idea was based on fibers and coated capillary tubes to extract analyte [11]. Rapid sample preparation can be achieved by SPME technique either in laboratory or on-site experimentation without complicated apparatus [11]. While, the latest commercial used SPME fibers are coated with liquid polymer or porous solid sorbent through immobilization of fused silica fibers. Some of these coated fibers are compatible with in-vivo SPME sampling method with gas chromatography (GC) or gas chromatography-mass spectrometry (GC-MS) device [12]. Fundamentally, SPME method was developed based on adsorption or absorption of analyte directly from sample onto micropillars, porous silica or immobilized magnetic silica beads which can be used in device directly. Thus, there are several types of methods can be used to extract analyte of interest by SPME using micropillar structure, porous solid phase or immobilized magnetic beads.

Microextraction by micropillar structure

Analyte of interest in a complex sample with varieties of composition can be extracted by using SPME method in micro-device. Sample preparation using SPME is typically performed in fiber coated surface. It is based on absorption of analyte into surface of the fiber and then removal of the absorbed analyte by several washing steps. The first microchip based SPME method using pillars to extract analyte on interest was demonstrated by [13]. The method started with filtration of particle based on size-exclusion principle using microfilter silica pillars and then extraction onto silica pillar surface. Then analyte will bind to designed microbinder surface in presence of buffer solution while other interferences and other molecules will be washed out through repeated washing steps. It follows by desorption or elution stage of analyte that bound to silica pillars surface using appropriate solvent (Fig.1).

According to Christel et al. [13], the micro-fabricated silica pillar structures are able to eliminate some centrifugation and mixing steps which requires for conventional sample preparation method**.**

Microextraction by porous solid phase

SPME method also can be done using porous silica solid phase or surface as microchannel of device. This porous silica surface in micro-device can be successfully fabricated by electrochemical etching technology. The selection of porous silicon for SPME is based on its huge specific surface area that will increase the interface area significantly; the availability or obtainability of porous silicon by electrochemical etching technology; porous silicon in SPME can be controlled well due to its pore geometry, surface morphology and the absorbency by electrochemical etching conditions [14, 15]. In past few years, numerous studies have been conducted to discover the application of porous silicon in scientific fields. Nano porous structures thin films was also developed by photo-electrochemical etching technique and can be used for detection of DNA as well by using photoluminescence method [16]. Besides, chemical disruption would be suitable in microfluidic platform for porous silicon phase. The technique started with cell lysis by solvent and the targeted analyte will bind to porous silicon surface while the other impurities can be removed by several washing steps. It follows by elution of analyte that bound onto porous silica surface and collected at outlet microchamber (Fig.2).

Microextraction by immobilized magnetic beads

Another method of SPME is by using immobilized silica particles or beads in micro-device. It involves the typical steps of SPME method as well which comprising binding of analyte to silica surface followed by several washing steps to desorb the analyte. This method was enhanced by Wolfe et al. [17] and Breadmore et al. [18] by modify immobilized bare-silica magnetic beads matrix in micro-device using sol-gel technology. Magnetic beads have been using in diversities of application due to their features especially in molecular biology. Magnetic beads that coated by silica resin can be used to capture particles in liquid by attaching and detaching simply by super-paramagnetic properties (controlling another magnet from the outer wall). The manipulation of magnetic beads is based on magtration technology (developed by Precision system science). Magtration was created from magnetic filtration process where particle can be separated and bound then released by magnetic field. Silica coated beads (magnetic silica microsphere) usually have large surface area thus the targeted analyte will bind onto surface and the particle will hold by assistance of magnet on the outer wall. The magnetic particles can be effectively separated and captured on the inner wall by magnet that comes into contact with outer wall of device (Fig.3). These magnetic silica beads have been used to extract DNA/RNA cell screening and others by some chemical modification [19, 20].

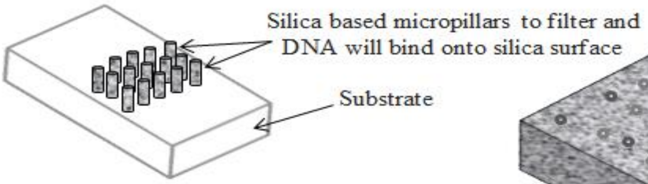

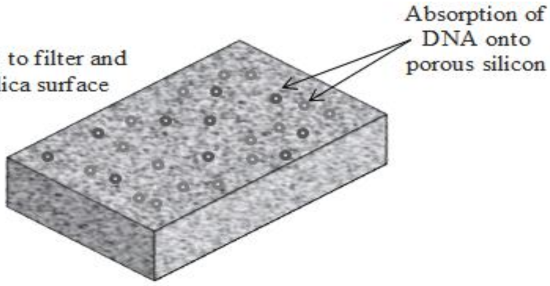

Fig. 1 Micropillars structure. **Fig. 2** Porous silicon layer.

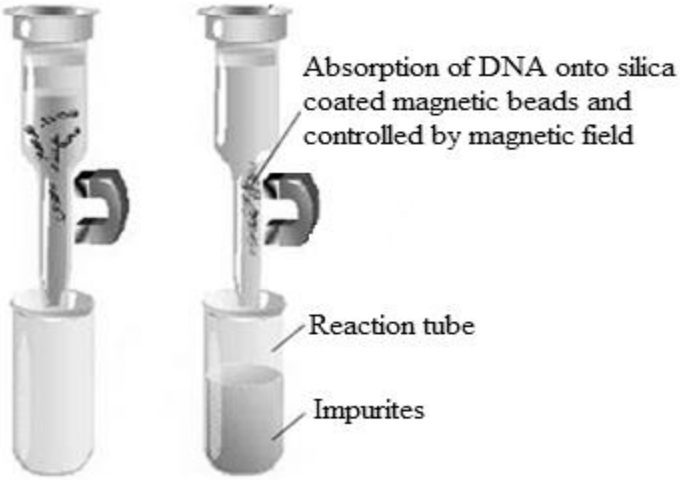

Figure. 3 Silica coated magnetic beads (modified from www.gibthai.com).

The simplicity (solvent-free) and easy accessibility of this method are main reasons for the enhancement of the SPME application in device (typically in syringe alike). Since SPME needed small space, coated fiber can be used to extract analytes in analytical chemistry application involving limited sample amount. Only a small dimension extracting phase is needed in contact with sample matrix and the extraction consider completed once analyte concentration has reached distribution equilibrium condition among sample matrix as well as fused silica fiber coating. The entire process begins with adsorption then diffusion of analyte and this can be described as Eq. (1) [11,21]:

$$n = \frac{K_{fs}V_f V_s C_0}{K_{fs}V_f + V_s} \tag{1}$$

Where n is the extracted analyte, K_{fs} is fiber coating sample matrix distribution constant, V_f is the fiber coating volume, V_s is the sample volume and C_0 is initial analyte concentration in sample. Besides that, the coated fiber enables extraction of analyte from small amount of sample such as single cell [22]. However, one of the limitations of SPME is poor sensitivity in extraction capacity. This can be solved by optimization of thicker and selective fiber coating [23]. Rapid and complete extraction is also possible for thick coating with small sample volume thus prevention of errors regarding analyte losses through decomposition or adsorption is promising. This can be applied to develop portable devices based on SPME technique. Conversely, in some cases, coating need to be modified especially when there is need for longer extraction, thus possibilities to form analyte with lower affinities are also high. Hence, modification of coating property is necessary with extraction time is less than the equilibrium time [24]. Also, analyte extraction is easier with high concentration of sample (as proven from equation 1). Additionally, there are two types of mode in SPME which includes the dynamic when the analyte pass through the tube and the static when the analyte being transferred to sorbent by diffusion process. In dynamic mode, the introduced sample transfers with linear velocity through the fused-silica capillary coated with thin film of extracting phase. The extraction is proportional to capillary length and inversely proportional to fluid flow rate [11, 25]. Whereas extraction of static mode occurs when the sample does not directly exposed to extracting phase (e.g contained protective tubing). Thus analyte transferred to the extracting phase based on diffusion principle of Fick's first law as Eq. (2) [26, 27]:

$$dn = AD_g \frac{dc}{dz} dt = AD_g \frac{\Delta C(t)}{Z} dt \tag{2}$$

where D_g is diffusion coefficients, A is extracting phase, Z is the position of extracting phase $C(t)$ is time dependent analyte concentration in the sample.

Based on equation 2, it can be concluded that, rate and amount of extracted analyte is proportional to sample concentration over the diffusion coefficient of analyte. A part from extracting modes, there are few other factors or parameters might be affected the extraction of distribution constant (K_{fs}) such as temperature, pH value, salting and quantity of solvent. For instance, when temperature increases, the extraction rate increases too but K_{fs}decreases concurrently. Also, SPME only can extract neutral non-ionic from water thus pH adjustment is crucial [11]. Based on considerable amount of literature reviews, the equilibrium method of SPME seems practical way to prepare specific analyte of interest (Kfs) in DNA extraction. It also provides efficient and sensitive sample clean-up (in-vitro bioanalysis) which can be applied to complex matrices such as whole blood, tissue, etc. without pretreatment of sample [8]. This analytical technique, however, also has some limitations when involving different analytes and sample matrices. Each sample matrices requires different SPME method to prepare or extract targeted analytes under specific consistent conditions. In addition, SPME method needs to be optimized with thicker and selective coating to overcome sensitivity issues caused by limited sample volume. Another limitation of SPME is matrix effect in complex sample put emphasis on usage of matrix matched standards, isotropic labeled internal standard and standard addition method for analysis or calibration [28].

3. Development of SPME: in-tube device to microfluidic device

SPME for sample preparation is mostly conducted using fiber coated and capillary tubes coated with an applicable stationary phase. In-tube SPME devices were developed in order to make it automated instrumentation performed using fused-silica capillary with stationary phase coating as miniaturization and automation system. The development of this technique by absorption then desorption of analytes initially designed in microsyringe (in-needle SMPE) and pipette tip (in-tip SPME). These were few examples which cost effective, pollution free and automated SPME in-tube devices [29, 30]. The fiber coated needle or fiber-packed needle successfully used for microextraction in a packed syringe. This microsyringe technique for sample preparation has been applied in analysis of anesthetics in human plasma [31]. A part from that, micropipette technique has been used in isolation and purification of proteins and peptides in genomic studies. In needle SPME method provides faster and easier plus uses disposable material which makes the entire development comparable to automated sample preparation machines. This was modified to fiber packed capillary for SPME-HPLC for continuous sampling process. However this method requires pure samples due to easy blockage of capillary plus extraction is low due to higher capacity of capillary. The in-tube method has been applied in multiplicities of field such as food, pharmaceutical, biomedical analysis, forensic, and clinical analysis for sample preparation plus extraction of analytes [8, 32]. Continuously, in-vivo SPME device discovered easy way especially to solve biomedical analysis process [8, 24]. As presented by Lord et al. [33] and Zhang et al. [34] in-vivo sampling for biogenic volatile organic compounds (human skin and breath) were successfully extracted to diagnose several diseases. In detail, direct SPME approach was done in sealed glass globe for skin emissions whereas collected human breath in Tedlar bag undergone direct exposure of SPME fiber into the bag. Different types of substances such as ketones, amines, aldehydes and others are synthesized by metabolism and release from human breath and skin. These organic compounds can be used to identify diseases, monitoring drug concentration and screening for toxicological exposure [35]. In-vivo SPME used to analyze concentration of aldehydes from collected breath exhalation (from patients who smoke and healthy control) and provides information regarding lung cancer and tumor specific composition [36, 37]. Direct SPME approach to extract organic compound from skin were used to study the features about skin cancer, wound healing and infection. Besides, in a recent study SPME sampling method were used to detect biomarkers named dimethylsulfide and dimethyltrisulfide for breast cancer in breath exhalation and skin emission correspondingly [38, 39]. A part from that, amount of protein binding of drugs in blood sample also can be extracted by SPME [8, 29]. Followed by this, the automated fiber SPME method was implemented for commercial usage. For instance, Combi-PAL auto sample (CTC analytics, Zwingen, Switzerland and other suppliers) was designed to perform various sample preparation stages such as dilution, agitation and extraction. Following by this, TriPlus (Thermo Fisher Scientific, Milan, Italy) auto sample was introduced with temperature control and stirring process [8]. Another advanced finding was the concept of multi-fiber SPME configuration with 96 robotic systems for automated high-throughput analysis (Professional Analytical System Technology, Magdala, Germany). Based on in-tip SPME micropipette method, automated sample preparation analysis of 96-tip arrays was developed researchers. Few extraction tips commercially available in market are including ZipTip (Milipore, Bedford, MA), Omix (Varian, Palo Alto, CA), NuTip and MonoTip C18 (GLScience, Tokyo, Japan). The tip also can be coupled with LC-MS/MS especially for drug analysis. This device can be connected to HPLC for further analysis and utilized mostly in drug protein binding studies [39, 40]. Based on this idea, 96-well plate technology was developed which able to hold 96 SPME fibers for multiple extraction with high precision [41]. The high efficient multi-well plate system then well modified with orbital shakers, arm robotic system and LC-MS/MS analysis for simultaneous high output usage. This has been validated by the accurate and sensitive analysis of benzodiazepines in human blood with preparation of 96 samples simultaneously within 100 minutes [42]. Accordingly, the developing technology caused progression of micro-device due to the ability to integrate multiple analyses in single μTAS and reduce time, cost and consumptions of reagents. Integrated microfluidic system for total analysis promises easy automation plus high throughput analysis for purification of biological molecules including DNA, protein to define genetic transformation and others. The silica based used for microfluidic device can be fabricated by electrochemical etching technology since it is compatible with latest microelectronic technology. The process in micro-device started with DNA absorption into silica surface in the presence of chaotropic solution and then removal of PCR inhibitors with appropriate solvent. Essentially, DNA carries negative charge per base pair over a wide range of pH condition. Likewise, silica surface able to exist as negatively charged at basic or neutral condition. The intermolecular forces of DNA in silica surface enable electrostatic repulsion of DNA and dissolved out from silica adsorption. Several previous studies emphasized that SPME micro-device system for nucleic acid purification, PCR amplification, and electrophoretic separation has been developed as automated and high sensitive device [35]. The latest commercial used SPME fibers are coated with liquid polymer or porous solid sorbent through immobilization of fused silica fibers in micro-device. For example polar polydimethylsiloxane (PDMS) which has high affinity extraction of non-polar compounds and blended coating with porous solid particle such as divinylbenzene (DVB) and template resin (TPR) which has larger surface area. Some of these coated fibers are compatible with in-vivo SPME sampling method with gas chromatography (GC) or gas chromatography-mass spectrometry (GC-MS) device [30]. Some papers stated PDMS fibers can be used to extract licit drugs (cocaine) opioids (morphine and acetyl morphine) and cannabinoids from plasma, hair also urine. Subsequently analyze them in GC-MS and this method was widely used in forensic, clinical toxicology particularly for detection of drug abuse [43, 44, 45]. The entire development of SPME from in-tube to micro-device is summarized as visual in Fig. 4.

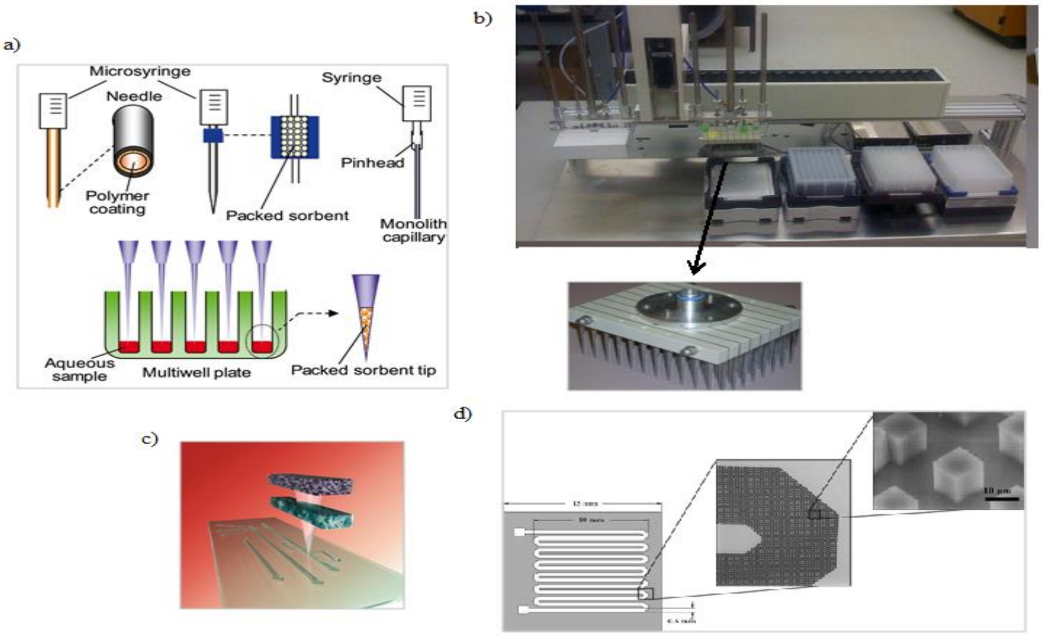

Figure. 4 Development of SPME method to from in-tube to microfluidic device to extract biological compounds; a) microsyringe and micropipette in silica packed sorbent; b) auto-sampler station based on in-tip method for 96 simultaneous extractions from PAS technology, Maglada Germany; c) microfabricated device with porous silicon layer to extract and bind DNA; d) microfabricated silica pillars to filter cells based on size-exclusion and the remaining biological compound will trap into silica micropillar structure [Adapted from 12, 35, 46, 47].

4. Solid Phase Microextraction for DNA extraction in Micro-device

There is a consensus among researchers that DNA-PCR microchips have wide applications in clinical diagnostics and genetic analysis. However, only limited amount of paper has been published regarding this parallel DNA-PCR microchip. In other word, integration of sample (analyte of interest) preparation step from biological compound follows by PCR and detection on single micro-device is very limited [48, 49, 50, 51]. Human blood is a superb source of DNA. Fundamentally DNA is present in white blood cell which has nuclei and approximately 51 µl is sufficient to extract enough DNA for PCR analysis. Thus far, a number of studies highlighted factors that are associated with features of the integrated device such as sample preparing and handling method in microfluidic, selection material plus design and fabrication of device, temperature control system for thermal cycling and also detection module for real time analysis [51, 52]. Generally, DNA preparation or extraction from blood sample in micro-device can be effectively done in the silica based solid phase microextraction

(SPME) either in the form of micropillars, porous silicon surface or immobilized silica beads [9, 46, 51]. Over the past decade, most research in chemical and molecular analysis has emphasized the use of silica surface for successful DNA extraction. Silica solid surface could be implemented in microchannel either as microfilters, porous silicon surface or silica coated magnetic particles. The basic steps in SPME for DNA begins with injection of sample into silica based microchannel in presence of high concentration of chaotropic salts plus organic solvents and follows by injection of buffer solution for cell lysis process. Then, double-stranded linear DNA will bind or absorb to silica surface and other molecules will wash out to the outlet by several washing steps. Finally the elution buffer with high pH and low ionic strength will remove the absorbed DNA and collect at the outlet. The DNA absorption and desorption from silica surface is generally based on few driving forces such as electrostatic screening effect, dehydration effect and the presence of intermolecular hydrogen bonds [53]. Under most experimental conditions, silica surface and DNA are negatively charged particles. Silica surface can be hydrolyzed and added with silanol groups by acid treatment and silica's negative surface charge density can be decreased by lowering the solution pH. As a consequence, electrostatic repulsion between DNA and silica can be reduced. Another driving force for DNA absorption is hydrogen bond between silica surfaces and DNA molecules. When DNA absorbed to silica surface, it increases in entropy indirectly then water molecules will solvate and release the DNA. Basically, the amount of DNA bind onto silica surface depends on solution pH, ionic strength, electrolyte type and this can be studied using quartz crystal microbalance with dissipation monitoring (QCM-D). For thin, rigid, and uniform films, the adsorbed mass can be calculated using the Sauerbrey equation Eq. (3):

$$\Delta m = \frac{-C\Delta F_n}{n} \tag{3}$$

whereΔm the change in mass is, $\Delta F_n$is the change in the frequency of oscillation (Hz) at an overtone n, and $C$is a constant. QCM-D experiments suggest that increasing the ionic strength of monovalent electrolytes results in DNA adsorbing to silica in a more rigid and compact conformation [54-56].

Integration of multiple analysis steps is the major advantages of development of SPME DNA extraction micro-device. In molecular diagnostic, DNA isolation micro-device was initially studied by Tian et al. [57,58] based on electrophoretic separation and then chip-based PCR. Consequently, considerable amount of research has been published on SPE for DNA purification. Fundamentally, DNA purification involves DNA adsorption onto a solid surface through hydrogen bond or electrostatic interactions. This technique was demonstrated first by Tian et al. [57, 58] by capillary packed silica-based resin SPME and then developed the real DNA purification from whole blood cell for PCR ready analysis. The demand for this method was increased as the achievable efficiency of extraction was about 70 % with 80% of intracellular protein removal. Besides, this method only used small amount of solvents as well as sample and reduces time consuming of entire analysis. However this method required pretreatment of sample before the purification step. In the following study, Christel et al. [13] reported first suitable approach for micro-chip based DNA purification using pillars to increase the silica surface area for adsorption. The prospective of this method was limited by the complex fabrication, cost required for each microchip and sample clogging problem could not be completely solved. Several studies have attempted to integrate rapid DNA extraction and PCR amplification in single micro-device [59, 60]. Nevertheless, this study required pure DNA with free of contamination. Meanwhile, in another study, Wolfe at al. [17] have stated silica-based solid phase extraction system would be suitable for integrate with μTAS. Wolfe et al. [17] and Breadmore et al. [18] modified immobilized bare-silica beads matrix in microchannel by sol-gel technology for DNA purification in less than 30 minutes. One of the limitations with this micro-device is back pressure and clogging of crude sample due to larger surface area of packing density. Although the method was a success, but it required complex design of packing matrix plus hard to control in microchip. Schilling et al. [61] reported continuous lysis of bacteria cells were possible using β-galactosidase in simple T-type microfluidic device. Likewise Sethu et al., [62] demonstrated continuous flow microfluidic device based on SPME for erythrocyte lysis. Accordingly, solid phase matrix made of porous silicon has developed based on advanced technology to extract DNA due to better performance and the fabrication steps were compatible to the modern microelectronic and MEMS technology for micro-device [63, 64].There were numerous studies concerning application of porous silicon in scientific fields. Usage of porous silicon recognized in solar cells, biochemical, sensor technology, enzyme micro reactor to absorb enzyme and protein, antibody micro-assay and just to list a few [65, 66, 67, 68, 69, 70]. Previous studies revealed the usage of porous silicon in SPME device for DNA purification has great advantages compared to conventional technique. Typically DNA extraction can be done by either cells disrupting and cell lysis step by enzymes, chemical lytic agents and mechanical forces in SPE technique. However chemical disruption is more suitable than cell lysis method in microfluidic platform. Furthermore, the fabrication process for chemical disruption in SPME device is simpler and compatible. In 2006, Chen et al. [63] designed SPE microfluidic chip with silicon-PDMS glass structure for DNA extraction. Porous oxidized silicon was used as solid phase matrix (coiled channel) for DNA purification while PDMS glass cover (withstand of continuous fluxion of buffers) was fabricated on substrate by optimal pressing method. The chip was extracted 23.5ng of PCR amplifiable DNA from 1µl of hole blood sample within 40-50 min. typically, the process of SPE microfluidic based on adsorption of DNA onto solid surface, then washing and elution steps. Theoretically, the solid phase matrix surface reduces electrostatic repulsion among negative DNA, and then both the matrix surface and DNA was dehydrated by high concentrated binding salt by forming hydrogen bond. Then breaking of hydrogen bonds happens in high pH (6.4~6.7) and low (4~6 M) concentrated binding salt condition. DNA desorbs from matrix when repulsion force among surface and DNA increases. The pure DNA can be achieved by continuous fluxion of the binding, washing and elution buffers [64]. As silicon based microfluidic chip to extract DNA from white bold cell needed complex structure with multiple layers of silicon, Ji et al. [71] has demonstrated micro-machined silicon chip for DNA purification from bold sample. The micro-device which consisted of micromixer, microfilter, microbinder and microvalve in single layer, functioned based on high chaotropic salt agent to isolate DNA from the sample [72]. The method started with mixing of solvent to sample then filtration of white blood cell (WBC) by pillar structure filter. As the size of WBC larger than red blood cell (RBC) and RBC was able to align by its own to pass through narrow spacing, WBC was trapped based on size-exclusion principle using microfilter pillars [73]. Besides, microvalve with solid plug paraffin for one time used has been designed to isolate waste from extracted DNA. The solid plug of paraffin will activate thermally (change from solid to liquid) and block off the normal flow to redirect the flow of waste or sample to another channel. Finally the extracted DNA will bound to designed microbinder surface in high salt concentration solution [71, 74]. In another study, silicon or glass microfluidic chip integrated with mixer, paraffin valves, filter and binder was fabricated and designed with automation system for DNA extraction from white blood cell (WBC) by Hui et al. [76]. This method started with separation of WBC using filter of 3µm gap and lyse using high salt solution to release DNA. Then DNA was captured reversibly by binder and purified with solvent. Based on this experiment, average 1ng of DNA was extracted from 1µl of sample. In order to justify the obtained results, PCR amplification was performed through gel electrophoresis and proven the method was a success as positive PCR results were shown [76]. After few attempt, Zhang and his group successfully overcome the sample clogging problem for extraction of DNA using magnetic beads by modifying the design of microfluidic platform with control of microvalves plus micropump. They introduced DNA extraction by superparamagnetic particles based SPE to perform cell lysis, DNA binding, washing and PCR on single microfluidic platform [51, 77]. Moreover, the PCR analysis in executed in droplet oil manner where the oil injected will encapsulate PCR reagent and prevent from evaporating plus contamination. Thus there is no need for chamber sealing for the PCR analysis. This research group has effectively demonstrated the capability of the main application of this microfluidic platform to analyze Rsf-1 gene. More recently, MEMS based micro-device based online cell lysis by continuous chemical disruption and genomic DNA purification by SPME was presented by Chen et al [5]. Porous silicon matrix was fabricated by electrochemical etching technology and average 39.7ng of DNA was extracted from 1µl whole blood (small sample volume) within less than 20 minutes [5]. Besides, Cao et al. [78] has developed microfluidic chip integrates with SPE for sample preparation which is nuclei acid extraction followed by reverse transcription polymerase chain reaction (RT-PCR) for molecular amplification. The aim of this chip was mainly to detect influenza virus in human nasopharyngeal aspirate (NPA) and nasopharyngeal swab (NPS) specimens. The entire process from sample extraction and amplification of influenza specimen was done within 3 hours or less and then product was sent for detection (off chip) through capillary electrophoresis. SPE based filtration using monolithic aluminum oxide membrane (AOM) for DNA extraction from saliva and real time polymerase chain reaction for amplification was developed by Oblath et al. [79]. They have reported effective identification *Streptococcus mutans*in a saliva sample with amplification of 300 fg (100–125 copies) of both methicillin-susceptible *Staphylococcus aureus* (MSSA) andmethicillin-resistant *S. aureus* (MRSA) genomic DNA (gDNA) in less than 2.5 hours. On the other hand, instead of using chaotropic-based sample loading and washing, Nakagawa et al. [80] proved another method where DNA can be purified by ion exchange capture phase using amine groups in microchannel. Sample of blood could be loaded at pH 6 and eluted at pH 7.5 for microchannel coated by amine groups (e.g. 3-aminopropyltriethoxysilane) thus usage of chaotropic salts and organic solution can be avoided. Although the analysis steps were towards greener technology, yet it only extracted 27-40% of efficient DNA [81]. Following by this, a novel method where DNA captured by pH-induced and bind by chitosan coated was proposed by Cao et al. [75] Chitosan is categorized in amino group, linear polysaccharide produced from deacetylation of chitin (crab and lobster shells). Chitosan coated channels responsible to bind DNA at pH 5 and release them at pH 9. Besides, protein binding can be reduced by the hydrophilic surface of chitosan as well [81]. This method has reported high efficiency of DNA extraction (~75%) with low protein binding to microchannel using small elution volume of 1.5µl. the summary of DNA extraction based on SPME was listed in Table 1.

Table 1 Summary of DNA extraction method based on SPME.

Phase	Sample	Remark	Ref.
SPME chip based on micro-pillars	Blood cells	Complex fabrication, costly, sample clogging problem	[13]
Capillary packed silica-based resin	Blood cells	Achieved 70 %efficiency of extraction but required pretreatment of sample before the purification step	[57, 58]
Immobilized bare-silica beads matrix in microchannel by sol-gel technology	Blood cells	DNA purification in less than 30 minutes but back pressure and clogging of crude sample problem	[17, 18]

Lysis of bacteria cells using β-galactosidase in simple T-type microfluidic device.	Bacteria cells		[61]
Purification by ion exchange capture phase using amine groups coated microchannel.	Blood cells	Avoiding chaotropic salts and organic solution, towards greener technology, yet it only extracted 27-40% of efficient DNA	[80]
Microfluidic chip with silicon-PDMS glass	1µl of whole blood cells	Extracted 23.5ng of DNA within 40-50 min.	[64]
Micro-machined silicon chip with micromixer, microfilter, microbinder and microvalve in single layer	Blood cells		[71]
Silicon microfluidic chip with mixer, paraffin valves, filter and binder	1µl white blood cell	1ng of DNA was extracted	[76]
DNA captured by pH-induced and bind by chitosan coated microchannel	Blood cells	Achieved ~75% efficiency of DNA extraction using small elution volume of 1.5µl.	[78]
20-30 nm Porous microfluidic channels in silicon via anodization in an HF electrolyte.	Blood cells	Achieved ~80% efficiency of DNA extraction	[63]
DNA extraction by superparamagetic particles based SPE and PCR on single microfluidic platform. PCR analysis in executed in droplet oil manner where the oil injected will encapsulate PCR reagent and prevent from evaporating plus contamination.	Blood cells	Successfully overcome the sample clogging problem for extraction of DNA using magnetic beads and analyze Rsf-1 gene	[19]
SPE for sample preparation (nuclei acid extraction) followed by reverse transcription polymerase chain reaction (RT-PCR). The aim of this chip was mainly to detect influenza virus.	Human nasopharyngeal aspirate (NPA) and nasopharyngeal swab (NPS) specimens	The entire process from sample extraction and amplification of influenza specimen was done within 3 hours or less and then product was sent for detection (off chip) through capillary electrophoresis.	[78]
Micro-device based online cell lysis by continuous chemical disruption	1µl whole blood	39.7ng of DNA was extracted within less than 20 minutes	[5]
SPE based filtration using monolithic aluminum oxide membrane (AOM) for DNA extraction from saliva and real	Saliva	Effective identification *Streptococcus mutans*in a saliva sample with amplification of 300 fg (100–125 copies) of both	[79]

time polymerase chain reaction for amplification.		methicillin-susceptible *Staphylococcus aureus*(MSSA) andmethicillin-resistant *S. aureus*(MRSA) genomic DNA (gDNA) in less than 2.5 hours.

5. Conclusion

Selecting an appropriate method for sample preparation is essential for further analysis and it's greatly influences the accuracy of yield. Extraction of pure sample is the key factor for success of further downstream process especially in clinical analysis to diagnosis dieses. Separation of analyte from most of biological sample is complicated thus, specific analyte extraction and purification method or micro-device would be suitable for rapid analysis. SPME can be used for effective sample preparation from whole blood with minimal error and high accuracy.

Acknowledgement

We would like to thank Malaysia Ministry of Science, Technology and Innovation for funding this project (Science Fund: 02-02-12-SF0234) and Mr. Murrali for providing assistance needed for this research.

References

[1] A. Manz, N. Graber, H. M. Widmers, Miniaturized total chemical analysis systems: A novel concept for chemical sensing, Sensors and Actuators B: Chemical, **1** (1990) 244
[2] Y. Shi, P. C. Simpson, J. Scherer, D. Wexler, C. Skibola, M. Smith, A. Mathies, Radial Capillary Array Electrophoresis Microplate and Scanner for High-Performance Nucleic Acid Analysis, Anal. Chem. **71** (1999) 5354
[3] A. G Hadd, S. C. Jacobson, J. M Ramsey, Microfluidic Assays of Acetylcholinesterase Inhibitors, Analytical Chemistry, **71** (1999) 5206
[4] C. L. Arthur, J. Pawliszyn, Solid phase microextraction with thermal desorption using fused silica optical fibers, Anal. Chem. **62** (1990) 2145
[5] X. Chen, D Cui, H. Cai, H. Li, J. Sun, L. Zhang, MEMS-Based Micro-device for Cell Lysis and DNA Extraction, Microelectro-mechanical Systems and Devices, InTech, (2012)
[6] P. L. Kole, G. Venkatesh, J. Kotecha, R. Sheshala, Recent advances in sample preparation techniques for effective bioanalytical methods, Biomedical Chromatography, **25** (2011) 199
[7] H. Gika, G. Theodoridis, Bioanalysis **3** (2011) 1647
[8] H. Kataoka, K. Saito, Recent advances in SPME techniques in biomedical analysis, J. Pharm. & Biomed. Anal. **54** (2011) 926
[9] J. P. Landers, M. C. Breadmore, K.A. Wolfe, I. G. Arcibal, W. K. Leung, D. Dickson, B. C. Giordano, M.E. Power, J. P. Ferrance, S. H. Feldman, P. M. Norris, Microchip-based Purification of DNA from Biological Samples, Anal. Chem. **75** (2003)1880

[10] A. Spietelun, L. Marcinkowski, M. de la Guardia, J. Namiesnik, T. Marcinkowski, Recent developments and future trends in solid phase microextraction techniques towards green analytical chemistry, J. Chrom. A **1321** (2013)1

[11] J. Pawliszyn, Theory of Solid-Phase Microextraction, Journal of Chromatographic Science **38** (2000) 270

[12] D. Vuckovic, X. Zhang, E. Cudjoe, J. Pawliszyn, Solid-phase microextraction inbioanalysis: new devices and directions. J. Chrom. A. **1217** (2010) 4041

[13] L. A. Christel, K. Petersen, W. McMillan, M. A. Northrup, Rapid Automated Nucleic Acid Probe Assays Using Silicon Microstructures for Nucleic Acid Concentration, Transactions of the ASME **121** (1999) 22

[14] O. Bisi, S. Ossicini, P. Pavesi, Porous Silicon: a Quantum Sponge Structure for Silicon based Optoelectronics, Surface Science Reports **38** (2000) 1

[15] P. Schmuki, U. Schlierf, T. Herrmann, G. Champion, Pore Initiation and Growth on porous, Electrochimica Acta **48** (2003) 1301

[16] H. A. Saleh, Z. Hassan, F. K. Yam, Physical properties of porous $In_{0.08}Ga_{0.92}N$, Int. J. Nanoelectronics and Materials **8** (2015) 33

[17] K. A. Wolfe, M. C. Breadmore, J. P. Ferrance, M. E. Power, J. F. Conroy, P. M. Norris, J. P. Landers, Toward a Microchip-based Solid-Phase Extraction Method for Isolation of Nucleic Acids, Electrophoresis **23** (2002) 727

[18] M. C. Breadmore, Wolfe Ka, I. G. Arcibal, W. K. Leung, D. Dickson, B. C. Giordano, J. Landers, Microchip-based purification of DNA from biological samples, Analytical Chemistry **75** (2003) 1880

[19] C. Zhang, D. Xing, Single-Molecule DNA Amplification and Analysis Using Microfluidics, Chem. Rev. **110** (2010) 4910

[20] F. Wang, M. Burns, Performance of nanoliter-sized droplet-based microfluidic PCR, Biomedical Micro-devices **11** (2009) 1071

[21] J. Pawliszyn, Solid Phase Microextraction Theory and Practice, Wiley, New York, NY, (1997)

[22] J. Pawliszyn, Kinetic model of Supercritical fluid extraction, J. Chromatogr. Sci. **31** (1993) 31

[23] M. J. Bogusz, Forensic Science. Handbook of Analytical Separations **6** (2008) 63

[24] Z. Mester and J. Pawliszyn, Rapid Commun. Mass Spectrom. **13** (1999) 1999

[25] R. Eisert and J. Pawliszyn, Automated in-tube solid-phase microextraction coupled to high performance liquid chromatography, Anal. Chem. **69** (1997) 3140

[26] Martos and J. Pawliszyn, Calibration of solid phase microextraction for an analyses based on physical chemical properties of the coating, Anal. Chem. **69** (1997) 206

[27] J. Crank, Mathematics of Diffusion, Clarendon Press, Oxford, 1989

[28] S. Risticevic, H. Lord, T. Gorecki, C. L. Arthur, J. Pawliszyn, Protocol for solid-phase microextraction method development, Nat. Protoc. **5** (2010) 122

[29] D. Vuckovic, E. Cudjoe, D. Hein, J. Pawliszyn, Automation of solid-phase microextraction in high-throughput format and applications to drug analysis, Anal. Chem. **80** (2008) 6870

[30] D. Vuckovic, E. Cudjoe, F. M. Musteata, J. Pawliszyn, Automated solid-phase microextraction and thin-film microextraction for high-throughput analysis of biological fluids and ligand-receptor binding studies, Nat. Protoc. **5** (2010) 140

[31] Z. Altun, M. Abdel-Rehim, L.G BlombergJ. Chromatogr. B: Anal. Technol. Biomed Life Sci. **813** (2004) 129

[32] C. Dietz, J. Sanz, C. Camara, Recent developments in solid-phase microextraction coatings and related techniques, J. Chromatogr. A. **1103** (2006) 183

[33] H.L. Lord, R.P. Grant, M. Walles, B. Incledon, B. Fahie, J. Pawliszyn, Development and evaluation of a solid-phase microextraction probe for in vivopharmacokineticstudies. Anal Chem **75** (2003) 5103

[34] X. Zhang, A. Es-Haghi, J. Cai, J. Pawliszyn, Simplified kinetic calibration of solid-phase microextraction for in vivo pharmacokinetics, J. Chromatogr. A. **1216** (2009) 7649

[35] H. Kataoka, Current Developments and Future Trends in Solid-phase Microextraction Techniques for Pharmaceutical and Biomedical Analyses, Analytical Sciences : The International Journal of the Japan Society for Analytical Chemistry **27** (2011) 57

[36] M. Ligor, T. Ligor, A. Bajtarevic, C. Ager, M. Pienz, M. Klieber, H. Denz, Fiegl, W. Hilbe, W. Weiss, P. Lukas, H. Jamnig, M. Hackl, B. Buszewski, W. Miekisch, J. Schubert, A. Amann, Clin. Chem. Lab Med. **47** (2009) 550

[37] D. Vuckovic, I. Lannoy, B. Gien, Y. Yang, F. M. Musteat, R. Shirey, L. Sidisky, J. Pawliszyn, J. Chromatogr. A **1218** (2011) 3367

[38] C. Bicchi, C. Cordero, E. Liberto, P. Rubiolo, B. Sgorbini, P. Sandra, J. Chromatogr. A **1148** (2007) 137

[39] S. Riazanskaia, G. Blackburn, M. Harker, D. Taylor, C.L.P. Thomas, Analyst **133** (2008) 1020

[40] C. Hasegawa, T. Kumazawa, X.P. Lee, A. Marumo, N. Shinmen, H. Seno, K. Sato, Anal. Bioanal. Chem. **389** (2007) 563

[41] X. P. Lee, C. Hasegawa, T. Kumazawa, N. Shinmen, Y. Shoj, H. Seno, K. Sato, J. Sep. Sci. **31** (2008) 2265

[42] L.G. Blomberg, Two new techniques for sample preparation in bioanalysis: microextraction in packed sorbent (MEPS) and use of a bonded monolith absorbent for sample preparation in polypropylene tips for 96-well plates, Anal. Bioanal. Chem. **393** (2009) 797

[43] D. Vuckovic, J. Pawliszyn, Automated study of ligand–receptor binding using solid-phase microextraction, J. Pharm. Biomed. Anal. **50** (2009) 550

[44] G. Merola, S. Gentili, F. Tagliaro, T. Macchia, Anal Bioanal. Chem. **397** (2010) 2987

[45] M. Moller, K. Aleksa, P. Walasek, T. Karaskov, G. Koren, Forensic Sci. Int. **196** (2010) 64

[46] C. Dizioli Rodrigues de Oliveira, M. Yonamine, M. Lucia de Moraea Moreau, J. Sep. Sci. **30** (2007) 128

[47] N. C. Cady, S. Stelick, C. A. Batt, Nucleic acid purification using microfabricated silicon structures, Biosensors and Bioelectronics, **19** (2003) 59

[48] J. Wen, L. A. Legendre, Purification of nucleic acids inmicrofluidic devices.Anal. Chem. **80** (2008) 6472

[49] Q. Xiang, B. Xu, Miniature real time PCR on chip with multichannel fiber optical fluorescence detection module, Biomed. Micro-devices **9** (2007) 443

[50] J. Pipper, M. Inoue, Catching bird flu in a droplet, Nat. Med. **13** (2007) 1259

[51] J. Pipper, Y. Zhang, Clockwork PCR including sample preparation, Angew. Chem. Int. Ed. **47** (2008) 3900

[52] Z. Yi, P. Seungkyung, Y. Samuel, W. Tza-Huei, An all-in-one microfluidic device for parallel DNA extraction and gene analysis, Biomed. Micro-devices **12** (2010) 1043

[53] C. S. Zhang, J. L. Xu, PCR microfluidic devices for DNA amplification. Biotechnol. Adv. **24** (2006) 243

[54] L. Xu, Z. Jixi, G. Hongchen, Study on the Adsorption Mechanism of DNA with Mesoporous Silica Nanoparticles in Aqueous Solution, Langmuir, **28** (2012) 2827

[55] P. Tyson, L. Santiago, A. Oveta Fullerb, J. Michael, J. Solomona, G. L. Ronald, Adsorption and elution characteristics of nucleic acids on silica surfaces and their use in designing a miniaturized purification unit, Anal. Biochem. **373** (2008) 253

[56] E. Peter, D. Van, S. Jessica, Lin, J. Theodore, Zwang, N. Ali, S. Malkiat, Johal, N. Angelika, Multiphasic DNA Adsorption to Silica Surfaces under Varying Buffer, pH, and Ionic Strength Conditions, J. Phys. Chem. B. **116** (2012) 5661

[57] H. Tian, A. Jaquins-Gerstl, N. Munro, M. Trucco, L.C Brody, J.P. Landers, Single-strand conformation polymorphism analysis by capillary and microchip electrophoresis: a fast, simple method for detection of common mutations in BRCA1 and BRCA2. Genomics **63** (2000) 25

[58] H. Tian, A. F Hühmer, J. P Landers, Evaluation of silica resins for direct and efficient extraction of DNA from complex biological matrices in a miniaturized format, Analytical Biochemistry **283** (2000) 175

[59] J. Khandurina, T. E. McKnight, S. C. Jacobson, L. C. Waters, R. S. Foote, J. M. Ramsey, Integrated System for Rapid PCR-Based DNA Analysis in Microfluidic Devices, Analytical Chemistry, **72** (2000) 2995

[60] E. T. Lagally, P. C. Simpson, R. A. Mathies, Monolithic integrated microfluidic DNA amplification and capillary electrophoresis analysis system, Sensors and Actuators, B: Chemical **63** (2000) 138

[61] E. A. Schilling, A. E .Kamholz, P. Yager, Cell Lysis and Protein Extraction in a Microfluidic Device with Detection by a Fluorogenic Enzyme Assay, Anal. Chem. **74** (2002) 1798

[62] P. Sethu, M. Anahtar, L. L. Moldawer, R. G. Tompkins, M. Toner, Continuous Flow Microfluidic Device for Rapid Erythrecyte Lysis, Anal. Chem. **76** (2004)6247

[63] X. Chen, D. F. Cui, C. C. Liu, H Li, Microfabrication and Characterization of Porous Channels for DNA Purification, J. Micromech. Microeng. **17** (2007) 68

[64] X. Chen, D. F. Cui, C. C. Liu, H. Y. Cai, Fabrication of Solid Phase Extraction DNA Chips based on Bio-Micro-electro-Mechanical System Technology, Chin J. Anal. Chem. **34** (2006) 433

[65] R. Bilyalo, L. Stalmans, G. Beaucarn, R. Loo, M. Caymax M, J. Poortmans, J. Nijs, Porous Silicon as an Intermediate Layer for Thin-Film Solar Cell, Solar Energy Materials and Solar Cells **65** (2001) 477

[66] M. Björkqvist, J. Salonen, J. Paski, E. Laine, Characterization of Thermally Carbonized Porous Silicon Humidity Sensor, Sensors and Actuators A **112** (2004) 244

[67] E. Massera, I. Nasti, L. Quercia,I. Rea, G. Di-Francia, Improvement of Stability and Recovery Time in Porous-Silicon-based NO2, Sensor Sensors and Actuators B **102** (2004) 195

[68] C. Melander, M. Bengtsson, H. Schagerlöf, F. Tjerneld, T. Laurell, L. Gorton, Investigation of Micro-Immobilised Enzyme Reactors Containing Endo-glucanases for Efficient Hydrolysis of Cellodextrins and Cellulose Derivative, Anal. Chimica Acta **550** (2005) 182

[69] J. Y. Park, J. H. Lee, Characterization of 10 µm Thick Porous Silicon Dioxide Obtained by Complex Oxidation Process for RF Application, Materials Chemistry and Physics **82** (2003) 134

[70] C. Steinhauer, A. Ressine, G. Marko-Varga, T. Laurell, C. A. K. Borrebaeck, C. Wingren, Biocompatibility of Surfaces for Antibody Microarrays: Design of Macroporous Silicon Substrates, Analytical Biochemistry **341** (2005) 204

[71] H. M. Ji, V. Samper, Y. Chen, W.C. Hui, H. J. Lye, F. Mustafa, A. C. Lee, L. Cong, C. K. Heng, T.M Lim, Sensors and Actuators A **139** (2007) 139

[72] J. H. Kim, B. G. Kim, H. Nam, D. E. Park, K. S. Yun, L. B. Yoon, J. You, E. Yoon, A disposable DNA sample preparation microfluidic chip for nucleic acid probe assay, IEEE, Micro Electro Mech. **55** (2002) 133

[73] H. M. Ji, V. Samper, L. Yobas, Y. Chen, C. K. Heng, T. M. Lim Silicon-based microfilters for whole blood cell separation, in: µTAS 2006, Tokyo, Japan, 323–325

[74] C. L. Arthur, J. Pawliszyn, Protocol for solid-phase microextraction method development, Heather Lord, Nature protocols **5** (2010) 122

[75] F. M. Musteata, J. Pawliszyn, In vivo sampling with solid phase microextraction, J. Biochem. Biophys.Met. **70** (2007) 181

[76] W. C. Hui, L. Yobas, V. Samper, C. K. Heng, S. Liwa, JiHongmiao, Y. Chena, L. Cong, J. Li, T. Meng, Sensors and Actuators A **133** (2007) 335

[77] J. Vasudev, Bailey, Z. Yi, Brian, Keeley, Y. Chao, L. Kristen, Pelosky, B. Malcolm, B. Stephen, Baylin, G. James, Herman, W. Tza-Huei, Single-Tube Analysis of DNA Methylation with Silica Superparamagnetic Beads, Clinical Chemistry, **56** (2010) 1022

[78] Q. Cao, M. Mahalanabis, J. Chang, B. Carey, C. Hsieh, Microfluidic Chip for Molecular Amplification of Influenza A RNA in Human Respiratory Specimens, PLoS ONE **7** (2012) 33176

[79] A. Emily, W. Oblath, H. Hampton, P.A. Jean, R. Michael, A microfluidic chip integrating DNA extraction and real-time PCR for the detection of bacteria in saliva, Lab Chip. **13** (2013) 1325

[80] T. Nakagawa, J. Biotechnol. **116** (2005) 105

[81] S. Agata, M. Łukasz, G. Miguel de la, N. Jacek, Recent developments and future trends in solid phase microextraction techniques towards green analytical, chemistry, Journal of Chromatography A **1321** (2013) 1

Exp. Theo. NANOTECHNOLOGY 2 **(2017)** 97 – 101

Experimental and Theoretical NANOTECHNOLOGY
http://etn.siats.co.uk/

Study of non-ohmic electrical behavior and microstructure of ZnO-V_2O_5 varistor

Mehdi Mirzayi [1]

Department of science, Miyaneh Branch, Islamic Azad University, Miyaneh, Iran
[1]E-mail: m_mirzayi2003@yahoo.com

Received 28 Dec. 2015; Revised 14 May 2016; Accepted 30 May 2016

Electronic ceramics based on ZnO with 1,2,3,4 and 5 mol% of V_2O_5 were prepared by conventional powder processing route and sintered at 1000 °C for 2 hour. Microstructure of samples was investigated by X-Ray and SEM. It was observed that the microstructure of the samples consists of ZnO grains as main phase, and the density of samples was increased with increase in V_2O_5 content. All of the prepared ceramics showed characteristic of non-ohmic current – voltage behavior. Non-linear coefficient increased with increase in V_2O_5 content. The non-linear electrical behavior was explained by considering formation of the potential barriers at grain boundaries.

Keywords: Varistor; ZnO grain; Break down voltage.
PACS: 84.32.Ff; 77.55.hf; 77.22.Jp.

1. Introduction

Today, electronic equipment contain small and fast semiconductor devices, which could be damaged by low transient voltage surges and therefore by reducing transient voltage surges, most high voltage substations and distribution equipment can be made less costly and more reliable. Varistors are available to protect circuits over a very wide range of voltages, from a few volts for low-voltage varistors in semiconductor circuits to tens of kilovolts for electrical power distribution networks [1-3]. The combination of high nonlinearity and high-energy absorption capability coupled with low power loss has made the ZnO varistor extremely attractive for high power applications [4].

Matsuoka1et al. [5] in the early 1970s reported that polycrystalline ZnO ceramics incorporated with several transition metal oxides showed a highly non-ohmic conduction. Since then many researches and studies have been performed on the fabrication and the physicochemical properties of this material. Zinc Oxide is an n-type semiconductor with direct band gap and multi-junction grain boundary with an electrostatic potential barrier between grains in the sintered body, compared with back-to-back Zener diode using single pn-junction for Si. This possesses a much higher energy handling capability than the Zener diode. Non-linear current–voltage characteristic of ZnO varistors are directly related to their microstructure, specifically the ZnO grain size that affects the varistor breakdown voltage. To achieve a given breakdown voltage, one can change either the varistor thickness or the grain size. Also the method of sintering process is critical for producing good varistor materials [6-7]. The advantage of vanadium-doped ZnO varistors is that the ceramic can be sintered at a relatively low temperature of about 900 ◦C. This is important for multilayer components because such ceramics can be co-fired with a silver inner-electrode having a melting point of around 960◦C. V_2O_5 is also a better sintering aid compared to Bi_2O_3 since it has been found that V_2O_5-doped ZnO materials can be densified to the same density at a lower temperature compared to Bi_2O_3-doped ZnO materials[8,9].

In this work, the effect of V_2O_5 concentration (1, 2, 3, 4 and 5 mol%) on the microstructure (grain size and shape) and electrical properties (breakdown point and non-linear coefficient) of ZnO ceramics were investigated. Furthermore, the mechanism of potential barrier formation between grain-boundary are discussed and clarified.

2. Experimental procedure

Samples according to general formula; $ZnO_{(100-x)\%}$-$V_2O_{5(x)\%}$ where x=1,2,3,4,5 mol% were prepared by the conventional ceramic fabrication route. Vanadate pentoxide was mixed in proper ratios according to the formula with Zinc Oxide powder by ball-milling with zirconia balls for 4 h. After milling, the obtained powder were pressed into disks of about 12mm in diameter and 1mm in thickness without binder. The disks were sintered at 1000 °C in air for 2 h and cooled to room temperature. Electrodes formed by silver paste onto the sample surfaces, were used for the electrical measurements. Phase analysis of the samples was carried out by X-ray diffractometry (XRD; PW1710, Philips) using Cu Kα radiation. The microstructures of the sintered specimens were examined using a scanning electron microscope (SEM, Cam scan MV2300). Electrical current-voltage behaviour was measured with an electrometer (Model 617, Keithley, USA) and in direct current mode.

3. Results and discussion

It is widely observed that the change of dopant concentration always indicates significant influence in the properties and performance of the electronic ceramics products. In the prepared electro-ceramics, SEM images and X-Ray diffraction pattern proved the presence of the vanadium intergranular phase. Figs. 1 show SEM micrograph of the samples. They showed large grains with oblong shape dispersed in a matrix composed of small grains. It was found that, grain size increases with increase in V_2O_5 content. In other word, addition of V2O5 has the tendency to promote grain growth of ZnO. The high reactivity of the V-rich liquid phase during sintering caused such a grain growth. V-rich liquid phase accelerated the solution and precipitation process of grains, and effectively helped the grains to diffuse easily. As a result, small grains near V-rich grain boundaries dissolved more easily than big grains. The dissolved grains moved through the liquid phase and precipitated in the surface of big grains with low surface energy, where the big grains grow bigger and bigger. Finally, the exaggerated grains formed [10].

Density of the samples was measured at room temperature using the Archimedes method. It was found that density lie in the range of 5.2-6.3 gr/cm3 which increase with increase in V_2O_5 content. In order to examine whether any additional phases are formed during sintering process, we carried out the structural investigation using the X-ray powder diffraction technique. Powder XRD pattern of the sample with 5 mol% of V_2O_5 is given in Fig. 2. X-Ray pattern of other samples were similar to this figure. According to references, pronounced diffraction peaks of hexagonal ZnO are observable which has been shown with Z. In addition, peaks of $Zn_3(VO_4)_2$ secondary phase were found [11,9,16].

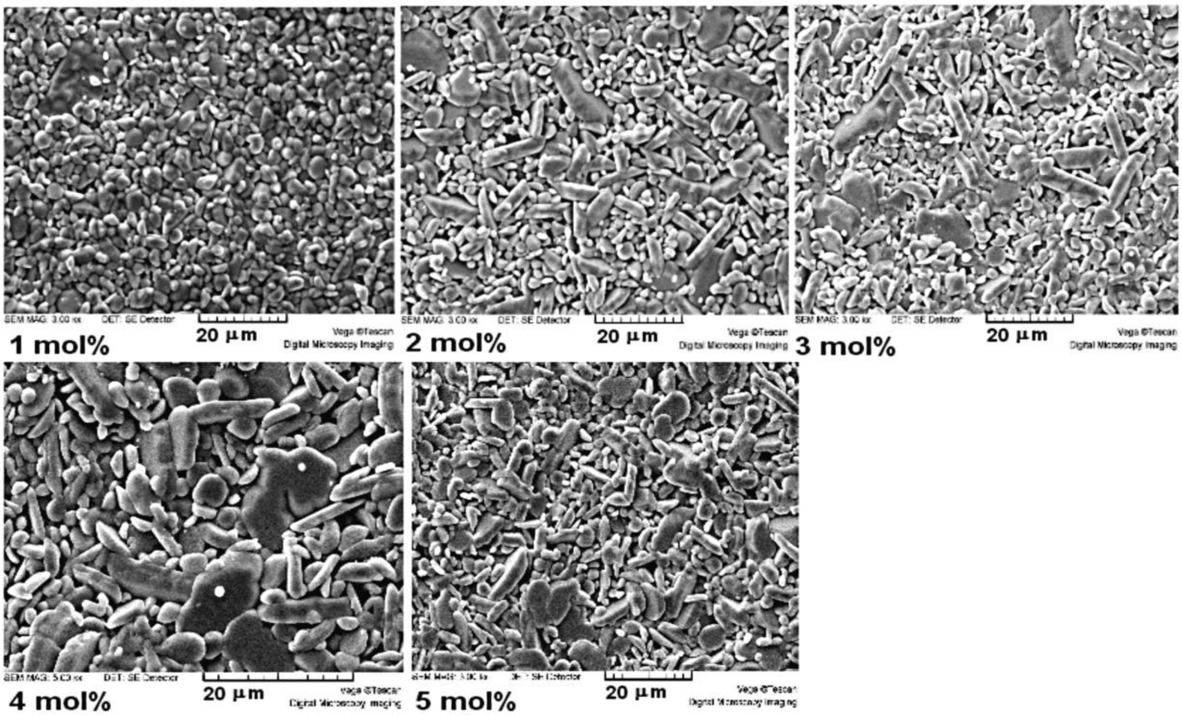

Figure 1 SEM micrograph of the samples.

I-V characteristic (current-voltage) of Zinc oxide varistors with V_2O_5 dopant is very sensitive to the microstructure due to abnormal grain growth of ZnO grains in the presence of V_2O_5. Fig.3 shows I-V characteristic of the samples at room temperature. It is clearly shown that the conduction is non-ohmic and the curves are divided into ohmic regions, which are of high resistance and very low resistance or non-ohmic region. In the non-ohmic region the current increases much more quickly than the voltage. It is clear that, in the prepared ceramics, the knee gradually becomes more pronounced in accordance with increasing V_2O_5 content. In other word, with the increase in V_2O_5 content, the non-linear property increases. Also, breakdown point (the point at which non-linearity begins) decreases with increasing of V_2O_5 content. The non-linear coefficient values (α) were obtained by linear regression of the logarithm scale plot of current density versus applied electrical field; $\alpha = d(\log I)/d(\log V)$ [12]. The value of α lies in the range of 3.79-5.4 . It was found that, α value increases with increase in V_2O_5 content and the sample with 5 mol% V_2O_5 exhibits the highest nonlinearity coefficient. It should be mentioned that, in the V_2O_5-doped system, much lower temperature can be used for sintering. Electrical characteristic of the prepared samples has been summarized in Tab 1.

The non-linear property of the varistors is explained by the existence of potential barrier at the grain boundaries [13]. In practice, there are a variety of inter-grain conduction paths that operate in parallel in varistors. These can be through the grain boundary region or through the bulk inter-granular material. In fact transition metal oxides, are involved in the formation of interfacial states and deep bulk traps at grain boundaries, providing large potential barriers to give better nonlinear characteristics [14]. This barrier is Schottky-type in which conduction in linear region dominated by thermionic emission over this Schottky barrier. Also, the conduction in non-linear region is dominated by Folower–Nordheim field emission through the Schottky barrier [13].

Table 1 Electrical properties of the samples.

Sample	ZnO (mol%)	V_2O_5 (mol%)	Density (gr/cm3)	Non-linear coefficient (α)	Break down Voltage (Volt)
C1	99	1	5.2	3.79	15.6
C2	98	2	5.39	3.95	13.5
C3	97	3	5.8	4.5	13
C4	96	4	6.05	5.22	12.2
C5	95	5	6.3	5.4	10.8

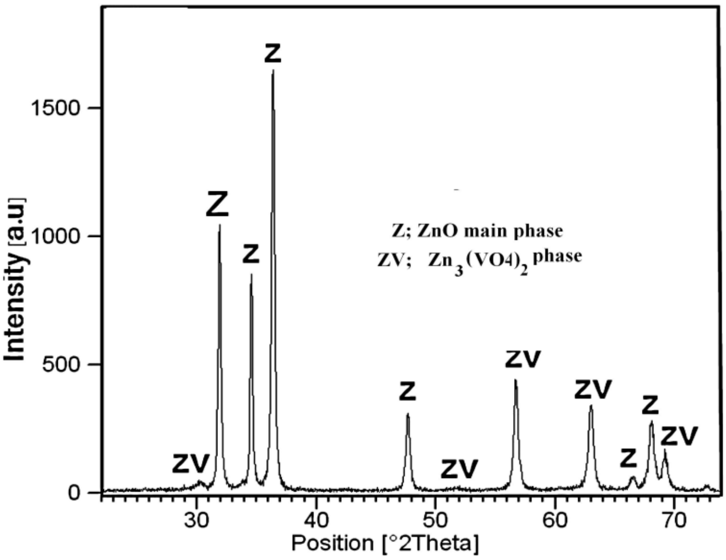

Figure 2 X-Ray diffraction pattern of C5.

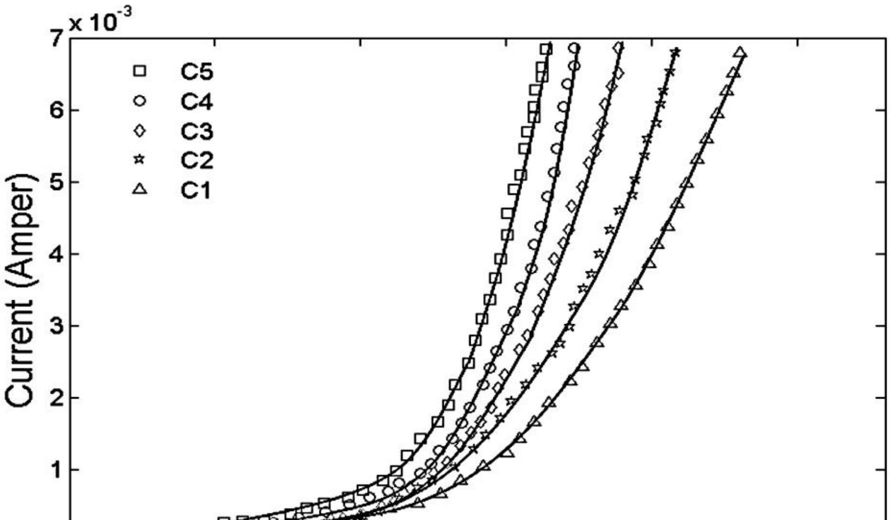

Figure 3 I-V characteristic of the samples.

In other words, the I-V characteristic of the electro-ceramic is controlled by the existence of potential barrier at the grain boundaries. The grain-boundary is treated as a junction in which the Fermi level of the bulk or grains are different from that of the layer between two grains. When the junction is formed and equilibrium is reached, the Fermi level is the same along the junction so that the binding energy gained by an electron occupying a trap state is equal to the electrostatic energy spent in moving an electron from the interior of the grains to the boundary. The result of this equilibrium is that the interface trapped electrons act as a sheet of negative charge at the boundary, leaving behind a layer of positively charged donor sites on either side of boundary, and creating an electrostatic field with a barrier at the boundary [5]. Thus we can attribute this behavior (increase in nonlinear coefficient with increase in V_2O_5 content) to a lowering of the grain boundary barrier height [15].

4. Conclusion

The effect of small amount of V_2O_5 (1-5 mol%) content on the microstructure and electrical properties of the ZnO ceramic were investigated. The grain growth of ZnO are strongly influenced by doping with V_2O_5. It was found that ZnO doped with V_2O_5 resulted in a vanadium-rich intergranular phase formed between the ZnO grains. The abnormal grain growth of ZnO grains was observed in the presence of V_2O_5 in which the grains size increase with increasing of V_2O_5 content. Similary the non-linear coefficient increased with increasing of V_2O_5 content. The non-linear electrical behavior is inferred to be due to the existence of potential barrier at the grain boundaries.

References

[1] B.H. Lee, S.M. Kang, Curre. App. Phys **6** (2006) 844
[2] C.Kim, J.H.Kim, J. Europ. Ceram. Soc **24** (2004) 2537
[3] M.Mirzayi, M.H.Hekmatshoar, A.Azimi, Key. Engin. Mater **495** (2012) 190
[4] M.M. Oliveira, P.C. Soares Jr, P.R. Bueno, E.R. Leite, E. Longo, J.A. Varelac, J. Eur.Ceram. Soc. **23** (2003) 1875
[5] P.R.Bueno, J.A.Varela, E. Longo: J. Eur.Ceram. Soc **28** (2008) 505
[6] N.Che Ani, Sharul A.Kamaruddin1, N.Nayani, S.N.Mohd Tawil, M.Z.Sahdan, Int. J. Nanoelectronics and Materials **8** (2015) 15
[7] Ch.W.Nahm, Mater Lett **60** (2006) 3311
[8] H.Hng , P.L.Chan, Mater Chem Phys **75** (2002) 61
[9] J.K. Tsai, T.B. Wu, J. Appl. Phys. **76** (1994) 4817
[10] X. Liu, F. Gao, L. Zhao, M. Zhao, Ch. Tian, J Electroceram.**18** (2007) 103
[11] R. Slama, F. Ghiribi, A. Houas, C. Barthou, L.El Mir, Int. J. Nanoelectronics and materials **3** (2010) 133
[12] P. N. Santhosh, D.K. Kharat, S.K.Date , Mater Lett **28** (1996) 37
[13] S. Pianaro, P. Bueno, P. Olivi, E. Longo, J. Mater. Sci.: Mater. Electron. **9** (1998) 159
[14] H.H. Hng, P.L. Chan, Mater. Chem. Phys. **75** (2002) 61
[15] Dong.Xu, Liyi Shi, Z.Wu, X.Wu: J Euro Ceram Soc, **29** (2009) 1789
[16] R. Singh1, I. S. Hudiara, S. Panday, P.Kumar4, S.B.Rana, Int. J. Nanoelectronics and Materials **9** (2016) 1

Exp. Theo. NANOTECHNOLOGY 2 **(2017)** 103 – 121

Experimental and Theoretical
NANOTECHNOLOGY
http://etn.siats.co.uk/

Optical properties of gelatin/TGS composites

A.M.Shehap[1], Kh.H.Mahmoud[1], M.F.H.Abdelkader[2], Tarek M.El-Basheer[3]

[1]*Department of Physics, Faculty of Science, Cairo University, Giza, Egypt*

[2]*Department of Biophysics, Faculty of Science, Cairo University, Giza, Egypt*

[3]*Department of Acoustics, Mass and Force Metrology Division, National institute for standards (NIS), Giza, Egypt*
3)tarek31.uv@gmail.com

Received 19 march. 2016; Revised 22 march 2016; Accepted 1 May 2017

Films of pure Gelatin and five Gelatin samples doped with the ferroelectric material triglycine sulphate (TGS) at various concentrations of 2, 4, 6, 8 and 10 wt. %TGS by weight have been prepared using the solvent-casting technique.Ultraviolet-visible (UV-vis) absorption spectra were measured in the range 190-900nm. The UV-Visible spectra show some shift in the absorption edge indicating change in optical band gap energy. The optical transitions were found mainly to be indirect allowed transitions and the optical band gaps (Eopt) were determined. Measuring the absorbance, transmittance and reflectance of Gelatin, TGS and their composites permitted the calculation of the refractive index (n). The refractive index dispersion curve of composite films obeys the single-effective oscillator model (Wemple-DiDomenico model).

Keywords:TGS; Absorption edge; Band tail.
PACS*:* 77.84.Fa; 78.70.Dm; 81.05.Ni.

1. Introduction

Recent studies have shown that Gelatin-based films with various additives have good potential for applications in a number of optoelectronic devices [1]. Gelatin containing ammonium dichromate is a well-known holographic recording material and is used in some holographic recording systems [2,3]. Gelatin-based films have been used in grating couplers [4], multiplexed gratings [5] and optical interconnections[6]. Poled Gelatin-nitro phenol compositions have shown good electro optical properties [7]. Pyroelectric and dielectric properties of Synthetic polypeptide triglycerol-Gelatin films were investigated [8-10]. Gelatin is a relatively low cost protein, industrially produced all over the world and that have excellent film forming properties. Mainly because of that, this protein is being extensively explored in edible and/or biodegradable films production and characterization studies, pure [11-15], or blended with other biopolymers [16, 17]. However, those Gelatin-based films present the typical characteristics of biopolymer-based films made with hygroscopic plasticizers are highly affected by room conditions, mainly relative humidity. Due to hygroscopic character of this material, relative humidity changes may lead to alteration of it moisture content affecting consequently the film properties, as water has a strong plasticizing effect on polymeric systems [18, 19]. Gelatin is nutritionally rich in glycine, proline, hydroxyproline, but lacking tryptophan and containing small amounts of other important amino acids, Fig. 1 shows the structure of Gelatin. It has a primary structure based on a repeating sequence (glycine/proline/hydroxyproline) [20].Triglycine sulphate [(NH2CH2-COOH)3 H2SO4] is one of the most extensively studied material as it possess excellent pyroelectric and ferroelectric properties. It exhibits strong absorption in most of the infrared region. At room temperature, its pyroelectric coefficient value is very large [21]. This crystal is suitable to make speed broad band infrared pyroelectric detectors and vidicon. Also, it is a technologically important material for carbon dioxide laser (10.6μm) and hydrogen cyanide laser (337μm). Triglycine sulphate (TGS) finds wide applications as IR detectors, storage devices and laser devices [22-24], owing to its excellent ferroelectric properties. Triglycine sulphate (TGS) is an important material used in the fabrication of high sensitivity infrared detectors at room temperature [25-27]. Ferro electricity in most of these compounds is related to the ordering of protons in their structure. The crystal structure of TGS was reported by Hoshino et al.[28] and the curie temperature was reported a typical second-order ferroelectric phase transition at the Curie point $Tc=49^oC$ [29,30]. TGS family crystals belong to the monoclinic system with the polar point symmetry group P21 in the Ferroelectric phase, spontaneous polarization Ps arises along the b-axis and P2m in the Para electric phase [31,32]. The ferroelectric properties of the TGS Family crystals have been extensively studied with doping it with various amino acids [33, 34]. TGS crystal has some disadvantages over doped TGS crystal such as i) the ferroelectric domain possess high mobility at room temperature therefore it is necessary to stabilize domains, ii) easy depolarization by electrical , mechanical and thermal means and iii) microbial contamination with time during the growth. In order to overcome these disadvantages and to improve the ferroelectric properties of TGS, variety of dopants such as amino acids, Organic and inorganic compounds have been introduced in TGS crystal. Scientific and technical developments are closely linked with the implementation of new materials. One of the most important advances is the composite material or hetero phase material. The composites have steadily gained growing importance during the last decade[35]. One class of these polymer composites has high modulus, high strength and low cost that makes it useful instead of fiber-reinforced composites that are relatively expensive and are intended for demanding structural application. On the other hand, a special class of composites based on polymers and ferroelectrics has been proved to have extraordinary properties. Therefore, polymer/ferroelectric composites would a good replacement for either class alone and would have the desirable properties of both materials [35]. Accordingly, the composite of Gelatin and TGS is expected to be a good candidate for new material with enhanced physical properties. UV-visible (UV-vis) spectra and particularly the absorption edge, band tail and optical constants are used to provide a good idea about structural changes of the composite films(gelatin/TGS). In the present work, gelatin/TGS films with different additive (TGS) percentage have been prepared by casting technique. The objective is to study the effect of the dopant throughout all the samples towards the optical properties.

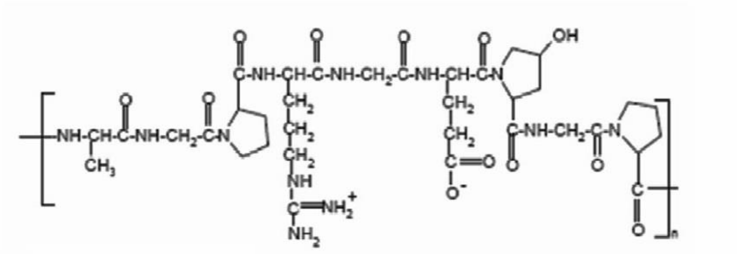

Figure.1 Structure of gelatin.

2. Materials used

The macromolecule used for film production was: Gelatin (Type B, and Bloom=190-200) was supplied by E.Merck(Darmstadt, Germany), and the average molecular-weight ≈100.000 gm/mol. From the specifications, Gelatin was composed of glycine (27%), proline and hydroxyproline (25%), glutamic acid (10%), arginine (8%), alanine (9%), aspartic acid (6%) and other amino acids (15%).

The ferroelectric material triglycine sulphate (TGS) was purchased from Acros Organic. Its molecular weight is 170. TGS crystals in the ferro- and paraelectric phase, 3-4 cm long.

2.1 Sample preparation

In order to obtain a film of pure Gelatin, Gelatin was dissolved in distilled water and in water bath at temperature of 37°C with continuous stirring for 30 min. until completely dissolved, then pour it into Petri dishes and cooled down at room temperature. Polymer/ ferroelectric composite samples were prepared by weighed amount of Gelatin and TGS in powder form with different concentrations 2, 4, 6, 8 and 10 wt. % TGS then dissolved them in distilled water at room temperature using magnetic stirrer. Thickness of films was measured using digital micrometer with sensitivity 0.01mm. Five to ten thickness measurements were taken on each film and took the average. Thus, thin films of appropriate thickness (≈0.05 mm) were cast on to Petri dishes and then dried at room temperature for about two or three days until the solvent completely evaporated. Films were cut into slab pieces and prepared to fit the cell of measuring techniques. All Films were conditioned in a desiccators with saturated solutions of NaBr(58% relative humidity) at 25°C until used.

2.2 Measuring techniques

The ultraviolet/visible absorption spectra of the samples under investigation were recorded on a Perkin Elmer 4B spectrophotometer over the range 190-1100 nm.

3. Results and discussion

3.1 Optical properties

Ultraviolet – visible spectra

The study of optical absorption spectra has proved to be very useful for elucidation and understanding the electronic structure of material through the determination of the optical band gaps. The data of transmittance can be analysed to determine optical constants such as refractive index, extinction coefficient and dielectric constants which are of considerable importance for application in integrated optical devices such as switches and filters modulators, etc…. .Figure 2 shows the electronic absorption spectra (UV-visible spectra) of Gelatin, TGS and their composites (2, 4, 6, 8 and 10 wt. % TGS) at wavelength within the Uv-vis. range of 190 – 900nm. One can see that two essential maximum peaks at 230 and 275nm for the Gelatin absorption spectra. These two peaks may be attributed to the electronic transition $\pi\rightarrow\pi^*$ at 230nm, and the second due to $n\rightarrow\pi^*$ at 275nm. The strong absorption at 230nm that can be attributed to the non-aromatic amino acids while the observed band at the longest wavelength interval(≈275nm) may be due to the presence of aromatic amino acids[37,38].

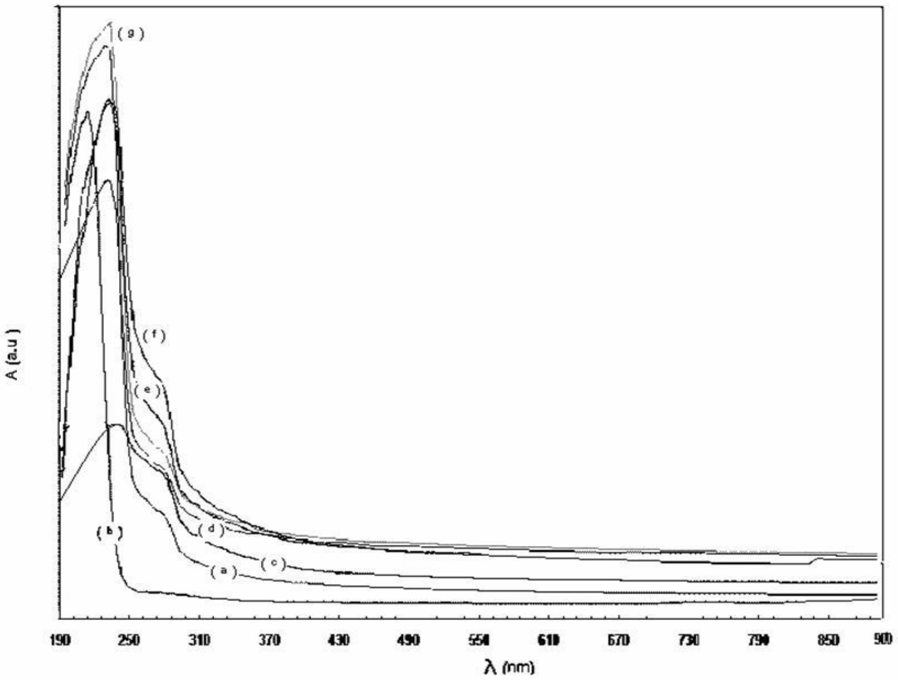

Figure.2 Absorption spectra for (a) pure gelatin (b) pure TGS (c) 2 (d) 4 (e) 6 (f) 8 and (g) 10 wt.%TGS.

The absorption spectra of TGS shows an essential maximum peak at 215nm that may be attributed to π→π* transition which is characteristic of the crystalline state [39, 40]. The absorption spectra of the composite samples give two maximum transition peaks; one is sharp while the other is shoulder-like band. There is small shifting in their wavelength assignment that depending upon the TGS concentration. It is clear that the sample (2wt%TGS) has the lower absorbance than the two pure samples and the other composites. Various optical transitions between these energy levels and the conduction or valence bands are found, together with transition between these impurity levels. Electron states can also be delocalized by increasing the impurity concentration and this is because the large spatial extension of the impurity states- the overlap of impurity wave function and thus delocalization occurs at low impurity concentration. For small impurity concentrations, transitions from the valence band to the impurity levels, or from these levels to the continuum of states, are possible leading to sharp absorption lines, together with transition between states. The type and degree of absorption depend on the type of impurity present and its concentration [41]. On the other hand there is little absorbance is detected through the visible spectral range for all the investigated samples (i.e the all samples are transparency in the visible region).

Optical Parameters:

The absorption coefficient α(λ) is calculated from the experimental optical absorption spectra using the relation [42]

$$\alpha(\lambda) = \frac{1}{d} \ln \frac{1}{T} \tag{1}$$

where d is the film thickness and T is the transmittance. The absorption coefficient was obtained with an error ±4%. The values of α(λ) for TGS sample are in good agreement with that previously reported[43-45].

The fundamental absorption edge is an important feature of absorption spectra of crystalline and amorphous materials. The absorption process involves the transition of electrons from valence band to conduction band [47]. At the point where there is an abrupt rise in absorption called fundamental absorption edge.

Figure 3 shows the dependence of the absorption coefficient on the photon energy for pure Gelatin and TGS as well as their composite samples.

The absorption edge in many disordered materials follows the Urbach rule [47] given by $\alpha(\upsilon) = \beta \exp(h\upsilon / \Delta E)$ (2)

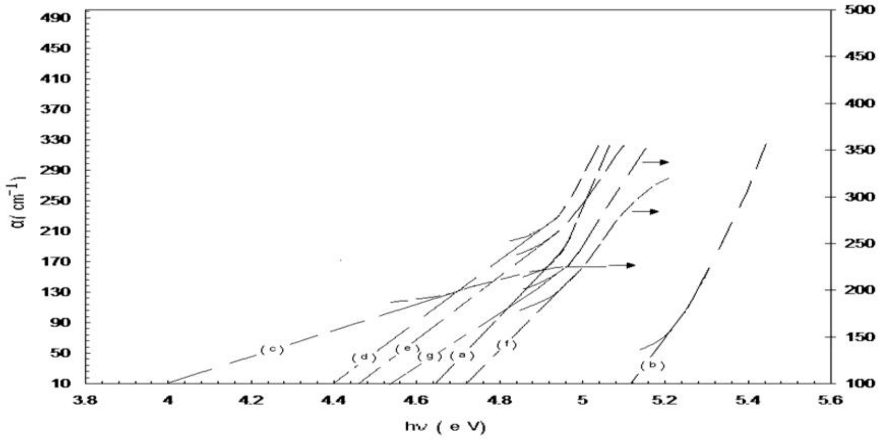

Figure.3 The absorption coefficient α as a function of photon energy hν for (a) pure gelatin (b) pure TGS (c) 2 (d) 4 (e) 6 (f) 8 and (g) 10 wt.%TGS.

From Fig. 3, it is clear that α(hν) exhibits a steep rise near the absorption edge and then rapidly increases in a straight line relationship in the relatively high α-region. This rapid increase of α is attributed to inter band transitions. The intercept of extrapolation to zero absorption with photon energy axis was taken as the value of the absorption edge. These values are listed in Table 1. The values of the absorption edge for composite samples are less than the two pure samples. The reduction of absorption edge of the composite samples compared to pure Gelatin can be attributed to the changes of the crystallinity induced by TGS, which is consistent with earlier X-ray diffraction data. In addition, this may reflect the induced changes in the number of available final states according to composite composition.

The origin of the exponential dependence of absorption coefficient on photon energy (hν) has been suggested by Tauc[48]that it arises from electron transitions between localized states where the density of localized states is exponentially dependent on energy.

Table1 Values of absorption edges of Gelatin, TGS and their composite samples

.

Sample	**Absorption edge(eV)**
Gelatin	4.64
TGS	5.12
2wt.% TGS	4.00
4wt.% TGS	4.40
6wt.% TGS	4.48
8wt.% TGS	4.72
10wt.% TGS	4.56

For the samples investigated in the present work, the exponential behaviour is observed obeying Urbach relation [47]. The absorption tails in amorphous and semi-crystalline materials can be interpreted in terms of the Dow-Redfiled effect [48] or the Urbach's[46] relation. The band tailing behavior may be caused by many kinds of structure disorder such as point defect, alloying disorder, inhomogeneous strain, exciton absorption and impurity levels in the middle of band gap [50].

Figure 4 shows the relation between lnα and hν for Gelatin, TGS and their composite samples. The straight lines obtained suggest that the absorption follows the quadratic relation for inter-band transitions [51] and the Urbach rule is obeyed. The values of band tail ΔE were calculated from the slopes of these lines and are listed in Table 2. The values of band tails ΔE for the composites are higher than both of pure materials (Gelatin and TGS) and it is worth to pay an attention for the composite sample 2wt.%TGS that has the largest value of the band tail among the other composites. It has been assumed that the amorphous state is a perturbed crystalline-state (i.e a modified band picture could be considered for non-crystalline system [52]. The formations of composite samples probably induce tails in the density of states by perturbing the band edge via a deformation potential, coulomb interaction and by forming localized band states [51].

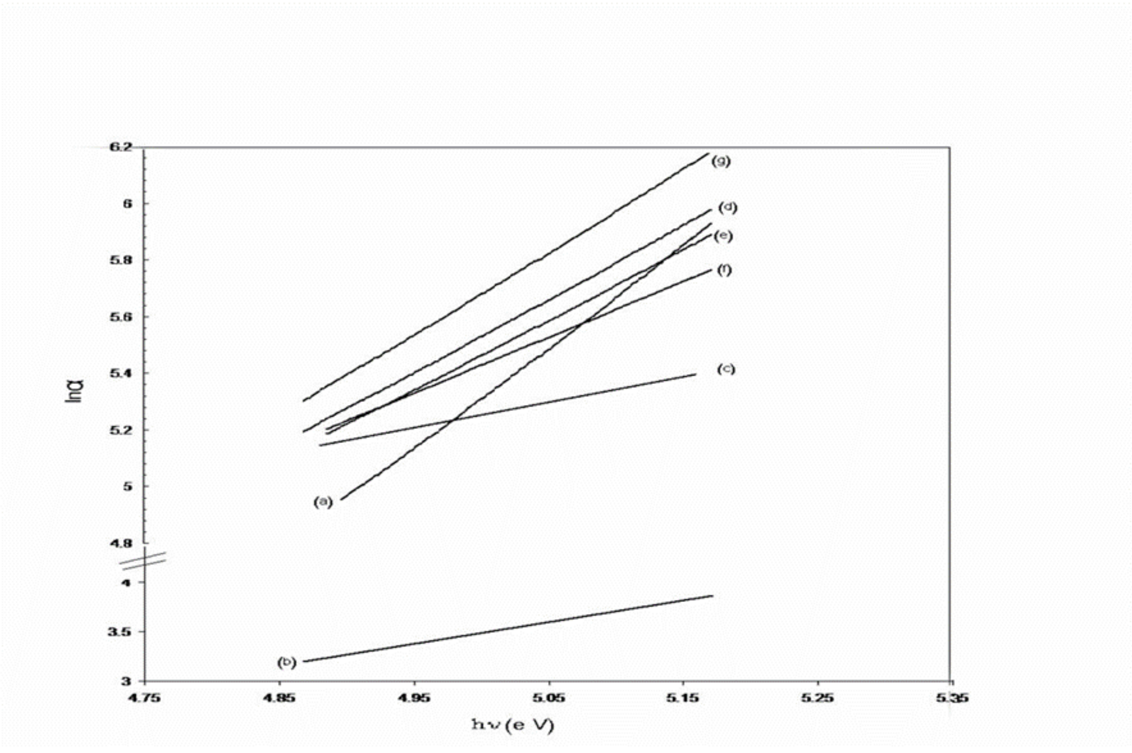

Figure4 Relation between ln(α) and (hν) for (a) pure gelatin (b) pure TGS (c) 2 (d) 4 (e) 6 (f) 8 and (g) 10 wt.%TGS.

Table 2 Values of band tails of Gelatin, TGS and their composite samples.

Sample	Band tail(e V)
Gelatin	0.40
TGS	0.35
2wt.% TGS	0.95
4wt.% TGS	0.55
6wt.% TGS	0.53
8wt.% TGS	0.65
10wt.% TGS	0.51

Thus, the model [52] based on electronic transition between localized states in the band edge tails and the density state of which is assumed to fall exponentially with energy, is preferable. In the high energy side, for the inter band transitions near the fundamental edge, the absorption coefficient α is given by the following relationship [47]

$$\alpha = \frac{B}{h\upsilon}(h\upsilon - E_g)^n \tag{3}$$

Where hν is the photon energy, Eg is the optical energy gap and (n) is an exponent characterizing the optical absorption process. For direct allowed transition n=1/2, for direct forbidden transition n=3/2, for indirect allowed transition n=2, for indirect forbidden transitions n=3.

The simplest way to deduce the type of transition is to examine the value of n which relates (hν) to (αhν) with a straight line relationship. The values of n=2 showed the linear most fit of equation(3).

So, the optical absorption data for Gelatin, TGS and their composite samples show an indirect allowed transition.

The absorption coefficient for indirect allowed transition αi can be expressed as

$$\alpha_i = \alpha_a + \alpha_e \tag{4}$$

$\alpha_a and \alpha_e$ Being respectively, the contribution due to absorption and emission of phonons and they take the forms.

$$\alpha_a = \frac{B(T)(h\nu - E_{gi} + E_p)^2}{h\nu} \tag{5}$$

$$\alpha_e = \frac{B^{/}(T)(h\nu - E_{gi} - E_p)^2}{h\nu} \tag{6}$$

whereE$_{gi}$ is the indirect energy gap, Ep the phonon energy, B(T) and B/(T) are constants nearly independent of photon energy and known as disorder parameters.

The spectral distribution of (αhν)1/2 for Gelatin, TGS and their composites are shown in Fig. 5. It is clear from the figure that the total absorption exhibits a long varying tail at low energies. Values of the optical energy gap for pure and composite samples obtained by extrapolating the linear regions to (αhν)1/2=0. These values are listed in Table 3.

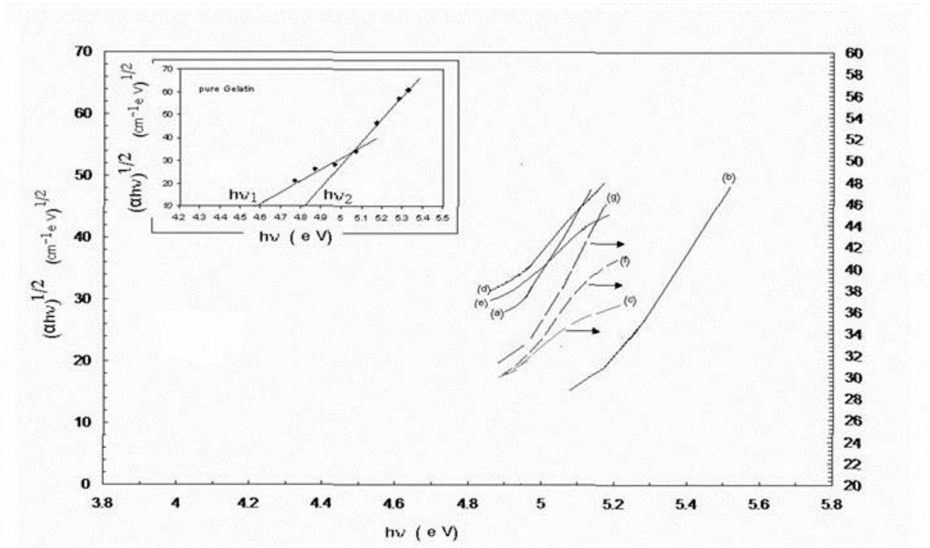

Figure5 The plots of variations (αhν)1/2 against photon energy (hν) for (a) pure gelatin (b) pure TGS (c) 2 (d) 4 (e) 6 (f) 8 and (g) 10 wt.%TGS.

Table 3 Values of optical energy gaps and phonon energies of Gelatin, TGS and their composite samples.

Sample	**Optical energy gap(e V)**	**Phonon energy (e V)**
Gelatin	4.70	0.20
TGS	5.00	0.28
2wt.% TGS	4.10	0.14
4wt.% TGS	4.45	0.18
6wt.% TGS	4.35	0.16
8wt.% TGS	4.19	0.15
10wt.% TGS	4.59	0.17

The graph(Fig.5) representing the relation between $(\alpha h\nu)^{1/2}$ and hν may be resolved into two straight lines. The straight line obtained at lower photon energy corresponding to phonon absorption processes and cut photon energy axis at $h\nu_1$= (Egi – Ep). The other line corresponding to the phonon emission and cut the x-axis at $h\nu_2$= (Egi+Ep).

The study of the optical constant in the vicinity of the absorption edge has yielded significant information on the role of various atoms or molecules in the composite system. It is known that, if a multiple reflections are neglected, the reflectance R of the samples can be calculated from the experimental measured values of the transmittance T and absorbance using the following equation[54],

$$R = [1 - (T \exp A)]^{1/2} \tag{7}$$

Also, the extinction coefficient (k) is given as

$$k = (\frac{\alpha\lambda}{4\pi}) \tag{8}$$

Using the values of k and R , the refractive index can be determined from the following equation[54]

$$n = [(1+R)/(1-R)] \pm \{[(R+1)/(R-1)]^2 - (1+k^2)\}^{1/2} \tag{9}$$

Reasonable values form may be evaluated by considering the plus sign of the last equation.

Figure 6 shows the n(λ) spectra from 350 to 850nm for all investigated samples. It is clear from the figure that the refractive index decreases slightly with increasing wavelength, and the changes become larger at shorter wavelengths showing the typical shape of a dispersion curve. The values of n is reached at longer wavelength to constant value n_0. The values of n_0 for different investigated sample are given in Table 4. The values of refractive index no for the composite samples are higher than both gelatin and TGS.

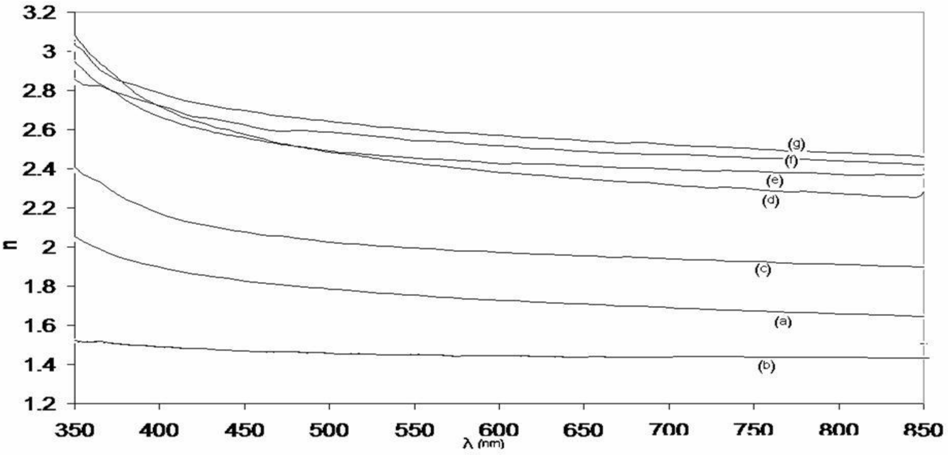

Fig 6 Variation in refractive index (n) with wavelength (λ nm) for (a) pure gelatin (b) pure TGS (c) 2 (d) 4 (e) 6 (f) 8 and (g) 10 wt.%TGS.

Table 4 Values of refractive index of Gelatin, TGS and their composite samples.

Sample	**Refractive index n_0**
Gelatin	1.64
TGS	1.50
2wt.% TGS	1.89
4wt.% TGS	2.40
6wt.% TGS	2.43
8wt.% TGS	2.45
10wt.% TGS	2.52

The refractive index is one of the fundamental properties of a material and is closely related to the electronic polarizability of ions and the local field inside the material. Perhaps the polarization direction of doping molecules of TGS associated with gelatin molecules in the composite samples plays a much more important role in improving the bond polarizabilities [55]. It is worth to mention that the production of high refractive index, transparent composite film is essential for development of many photonic applications such as Ultra-low-loss optical waveguides and more efficient gain or non-linear optical devices.

Figure 7 shows the extinction coefficient k as a function of wavelength for both pure materials and their composite samples. The dependence preserves that behavior of the absorption coefficient for all samples near the absorption edges.

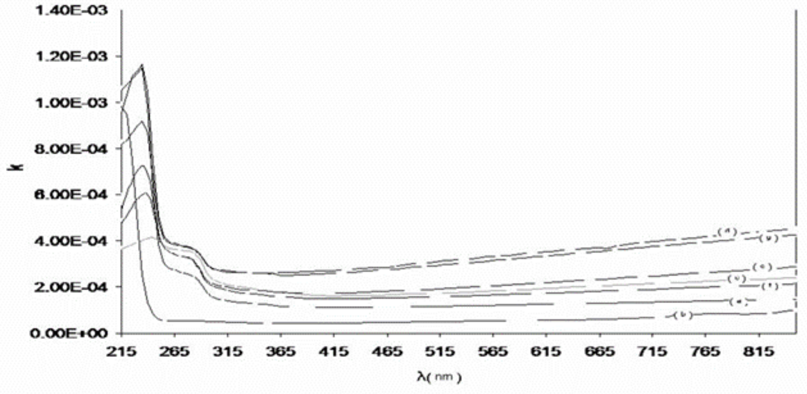

Figure 7 Variation in extection coefficient (k) with wave length(λ) for (a) pure gelatin (b) pure TGS (c) 2 (d) 4 (e) 6 (f) 8 and (g) 10 wt.%TGS.

Parameters of the single-effective-oscillator model:

The imaginary dielectric constant ε_i is the optical constant accessible to physical interpretation using result of refractive index dispersion below the inter-band absorption edge corresponding to the fundamental electronic excitation spectrum.

Wemple and Domenico[56] have analysed more than 100 widely different solids and liquids using single-effective-oscillator fit of the form

$$\varepsilon_r(E) = 1 + \frac{F}{(E_0{}^2 - E^2)} \tag{10}$$

Where the single oscillator energy (E_o) having a straight forward relation with dipole strength(F) and the corresponding transition frequencies of all oscillators. By a special combination of parameters Wemple and Domenico[56] have defined a parameter E_d such that it is a measure of the strength of intra-band optical transitions:

$$E_d = \frac{F}{E_0} \tag{11}$$

In the transparent region, equation (10) together with equations (11)

$$\varepsilon_r = n^2 - k^2 \text{and} \, \varepsilon_i = 2nk \tag{12}$$

Neglecting values of k in the transparent region we can have

$$\varepsilon_r(E) = n^2(E) = 1 + \frac{E_d E_0}{E_0{}^2 - E^2} \tag{13}$$

$$(n^2 - 1) = \frac{E_d E_0}{E_0^2 - E^2} \tag{14}$$

$$(n^2 - 1)^{-1} = \frac{E_0^2}{E_d E_0} - \frac{E^2}{E_d E_0} = (-\frac{1}{E_d E_0})E^2 + \frac{E_0}{E_d} \tag{15}$$

By plotting (n2-1)$^{-1}$ versus E_2 (eV). The result would be a straight line with negative slope (1/$E_d E_0$) and intersection (E0/Ed). The data was fitted to the best straight line as shown in Fig. 8. The estimated values of E_0 and Ed for pure materials Gelatin and TGS and their composite samples are given in Table5.

Table 5 Single-Oscillator parameters of Gelatin, TGS and their composite sample

Sample	**E_0 , (eV)**	**E_d , (eV)**	**F**	**λ_0 , (nm)**	**n_∞**	**S_0 , (nm^{-2})**	ε'_∞
Gelatin	6.91	23.06	135.1	213.36	1.7	$4.15*10^{-5}$	2.89
TGS	6.9	7.25	49.68	179.34	1.54	$4.06*10^{-5}$	2.37
2wt.%TGS	6.15	43.93	269.99	203.87	1.9	$6.27*10^{-5}$	3.61
4wt.%TGS	5.58	45.41	253.38	221.77	2	$6.09*10^{-5}$	4
6wt.%TGS	5.45	47.015	256.4	227.06	2.35	$8.70*10^{-5}$	5.52
8wt.%TGS	5.19	48.52	251.81	238.43	2.4	$8.37*10^{-5}$	5.76
10wt.%TGS	5.04	57.16	294.08	247.5	2.55	$8.98*10^{-5}$	6.5

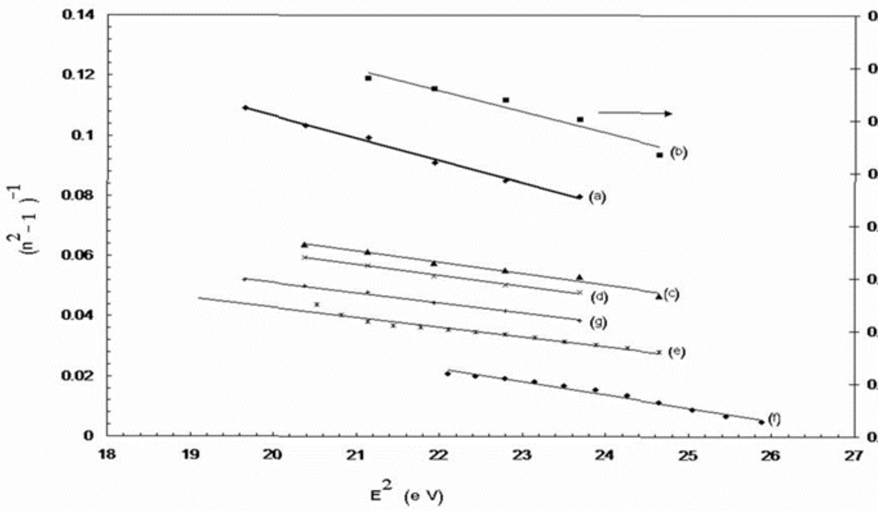

Figure 8 A plots of $(n^2\text{-}1)^{-1}$ as a function of photon energy (hν) for (a) pure gelatin (b) pure TGS (c) 2 (d) 4 (e) 6 (f) 8 and (g) 10 wt.%TGS.

On the other hand, the parameters of single-oscillator model E_0 and E_d are connected to M_{-1} and M_{-3} moments of the ε(E) optical spectrum, through the two relations[56]:

$$E_0{}^2 = \frac{M_{-1}}{M_{-3}} \quad (16)$$

$$E_d{}^2 = \frac{M_{-1}}{M_{-3}} \quad (17)$$

whererth moment of the optical spectrum is given by

$$M_r = \frac{2}{\pi}\int_{E_t}^{\infty} E_{\varepsilon_i}{}^r(E)dE \quad (18)$$

and E_t is the absorption threshold energy.The two moments M_{-1} and M_{-3} were calculated from the data on E_0 and E_d, and their values for pure gelatin and TGS and their composite samples are listed in Table 6.

Table 6 The two moments M_{-1} and M_{-3} of Gelatin, TGS and their composite sample

Sample	**M_{-1}** (eV)$^{-2}$	**M_{-3}** (eV)$^{-2}$
Gelatin	3.94	0.11
TGS	1.04	0.02
2wt.%TGS	7.2	0.19
4wt.%TGS	8.13	0.26
6wt.%TGS	8.63	0.29
8wt.%TGS	8.65	0.32
10wt.%TGS	11.76	0.47

The single-oscillator model enables us to calculate the refractive index at infinite wavelength (n_∞), average oscillator wavelength (λ_0), and oscillator strength (S_0) through the relation[57].

$$\frac{n_\infty{}^2 - 1}{n^2 - 1} = 1 - \frac{\lambda_0{}^2}{\lambda^2} \quad (19)$$

Rearranging this equation yields

$$n^2 - 1 = \frac{S_0{}^2 \lambda_0{}^2}{(1 - \lambda_0{}^2)/\lambda^2} \quad (20)$$

where $S_0 = (n_\infty{}^2 - 1)/\lambda_0{}^2$. The values of n_∞ and S_0 are derived from a linear plot of $(n^2\text{-}1)^{-1}$ versus $1/\lambda^2$as seen in Fig. 9 and presented in Table 5.

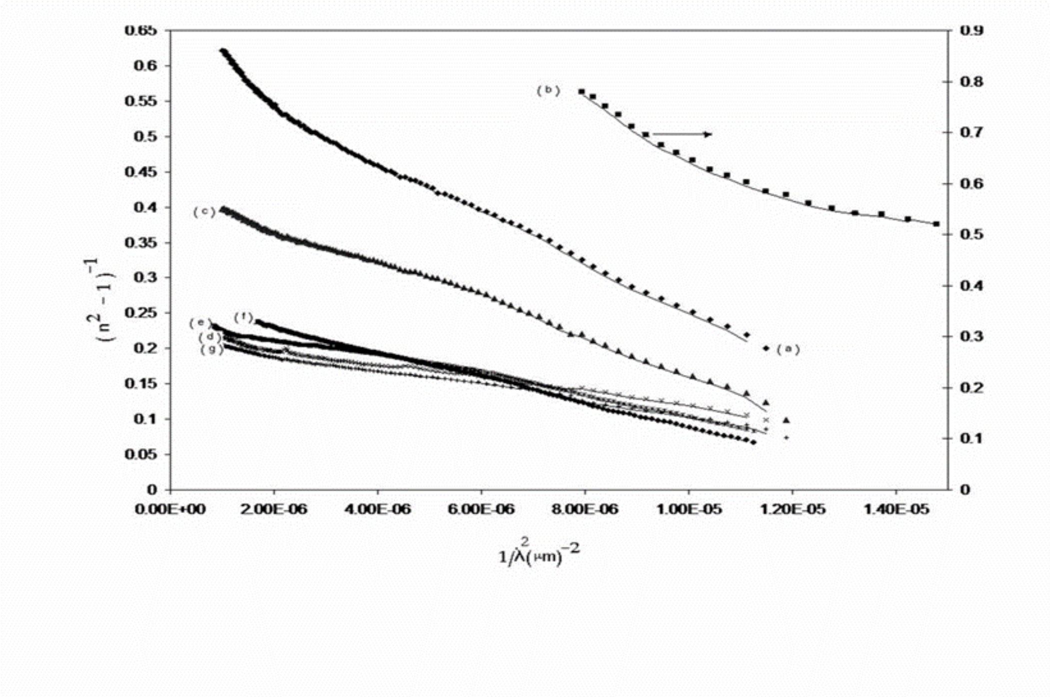

Figure 9 Relation between $(n^2-1)^{-1}$ and $1/\lambda^2$ for (a) pure gelatin (b) pure TGS (c) 2 (d) 4 (e) 6 (f) 8 and (g) 10 wt.%TGS.

4. Conclusions

From UV-visible studies, it is recognized that polymer/ferroelectric compositions ratio highly affect the electronic structure and molecular configuration of the composite matrix as seen from the pronounced changes in absorption spectra and confirmed by the calculated optical parameters.

The allowed indirect transition is the most probable type of transition near the fundamental absorption edge of TGS/Gelatin composites.

The sample 2wt.%TGS has the highest band tail and the lowest optical energy gap while the other composite samples are less band tails and highest optical energy gap.

The compositional dependence of the refractive index can be caused by the interference phenomena due to domain structure, molecular orientation and processing conditions.

The relatively high increase of the refractive index of the composition samples may be attributed to an increase in the valence density of charge carriers.

The single oscillator parameters E_d, E_0, n_∞, λ_0 and S_0 have compositional dependence where the dipole strength F and the strength of the intra band optical transition are enhanced by increasing the concentration of the ferroelectric material TGS into Gelatin.

References

[1] V. E. Khutorsky and Sidney B. Lang J. Appl. Phys. 82(1997) 25

[2] J. R. Magarin˜os and D. J. Coleman Opt. Eng. 24 (1985) 769

[3] B. J. Chang, Opt. Eng.19(1980) 642

[4] R. T. Chen,W. Phillips, T. Jannson, and D. Pelka, Opt. Lett. 14 (1989) 892

[5] R. T. Chen, M. R. Wang, and T. Jannson, Appl. Phys. Lett.57 (1990)2071

[6] R. T. Chen, M. R. Wang, G. J. Sonek, and T. Jannson, Opt. Eng. 30 (1991) 622

[7] Z. Z. Ho, R. T. Chen, and R. Shih, Appl. Phys. Lett. 61 (1992) 4

[8] D. Damjanovic, A. S. Bhalla, and L. E. Cross, Ferroelectr. Lett. Sect. 11 (1990)117

[9] D. Damjanovic, A. S. Bhalla, and L. E. Cross, Ferroelectrics 109 (1990)333

[10] D. Damjanovic, A. S. Bhalla, and L. E. Cross, IEEE Trans. Ultrason. Ferroelectr. Freq. Control 38 (1991) 630

[11] P.J.A. Sobral, F.C. Menegalli, M.D. Hubinger, M.A. Roques, J.Food Hydrocolloids 15 (2001)423

[12] R.A. Carvalho, C.R.F. Grosso,J. Food Hydrocolloids 18 (2004)717

[13] M. Thomazine, R.A. Carvalho, P.J.A. Sobral, J. Food Science 70 (2005) 172

[14] F.M. Vanin, P.J.A. Sobral, F.C. Menegalli, R.A. Carvalho, A.M.Q.B. Habitante, J.FoodHydrocolloids19 (2005) 899

[15] P.V.A. Bergo, R.A. Carvalho, P.J.A. Sobral, F.R.S. Bevilacqua, J.K.C. Pinto, J.P. Souza, J.Measurement Science and Technology17 (2006)3261

[16] I. Arvanitoyannis, E. Psomiadou, A. Nakayama, S. Aiba, N. Yamamoto, J. FoodChemistry 60(1997)593

[17] Y. Pranoto, C.M. Lee, H.J. Park, Lebensmittel-WissenschaftundTechnologie,40 (2007)766

[18] L.T. Lim, Y. Mine, A. Tung, J. Food Science64 (1999) 616

[19] N. Gontard, S. Guilbert, J.-L. Cuq, J. Agricultural and Food Chemistry58 (1993) 206

[20] Rose PJ, Mark HF, Bikales NM, Overberger CG, MengesG,Kroschwitz JI, editors. Encyclopedia of polymer science and engineering, vol. 7, 2nded. New York, USA: Wiley, 1989:488-513.

[21] R.B.Lal and A.K.Batra,Ferroelect.142 (1993)51

[22] N.Nakatani,Jpn.J.Appl.Phys.29 (1990)2774

[23] N.Nakatani,Jpn.J.Appl.Phys.32 (1993)4268

[24] R.W.Whatmore,Rep.Prog.Phys.49 (1986)1335

[25] A.K. Batra, PadmajaGuggilla, Dewanna Cunningham, M.D.Aggarwal, R.B. Lal,Physica B 371 (2006) 210

[26] J. Novotny, J. Zelinka, F. Moravec, J.Sensor Actuator A 119 (2005)300

[27] Jiann-Min Chang, A.K. Batra, R.B. Lal, J.Cryst. Growth Desn.2 (2002) 431

[28] S.Hoshino,Y.Okaya,andR.Pepinsky,J.Phys.Rev.115(1959)323

[29] R.LeBihan and G.Grandet,J.Ferroelect.39 (1981)117

[30] D. Sun, X. Yu, Q. Gu, J. Cryst. Res. Technol.34 (1999)1255

[31] Landolt-Bornstein, Crystal and Solid State Physics, New series,GroupIII, vol. 16b, Springer, New York, 1969, p. 223.

[32] H.V. Alexandru, C. Berbecaru, F. Stanculescu, L. Pintilie, I. Matei, M. Lisca, J.Sensor.Actuators A 113 (2004)387

[33] J.Novotny, L.Prokopova, and Z.Micka, J.Cryst.Growth 226 (2001)333

[34] K.Meera, R.Muralidharan , P.Santhanaraghaven, R,Gopalakrishnan, and P.Ramasamy, J.Cryst. Growth 226 (2001)303

[35] A.ArockiaLinson, AnbarasuPaulthurai, BalamuruganDamaraj, Int.J.Nanoelectronics and Materials 7(2014)93

[36] W.Sakamoto, S.Kagesawa, D.K andaD.Das-Gupta, J. Mater .Sci.33(1998)3325

[37] C. Abrusci, A. Mart´ın-González, A. Del Amo, F. Catalina, , P. Bosch, T. Corrales J. Photochemistry and Photobiology A: Chemistry163 (2004)537

[38] Diogo F. Vieira, C´esar O. Avellaneda, AgnieszkaPawlicka, J. ElectrochimicaActa 53(2007) 1404

[39] K. Meera, A. Claude, R. Muralidharan, C.K. Choi, P. RamasamyJ. Crystal Growth285 (2005) 358

[40] T. Balu, T.R. Rajasekaran, P. Murugakoothan, J.Current Applied Physics, 9 (2009)435

[41] M.A. Omar , Elementary solid state physics principles and applications, Addison Wesley Publishing Inc., (1975).

[42] J. Rodriguez, M. Gómez, J. Ederth, G.A. Niklasson, C.G. Granqvist, Thin Solid Films, 365 (2000)119

[43] A.Abass and F.Al-Eithzn,J.Phys.Chem.Soilds47(1986) 933

[44] A.AbuEl.Fadl, J.Cryst.Res.Technol. 34(1999) 1047

[45] A.AbuEl.Fadl, J. Phys. and Chem. Solids60 (1999)1881

[46] A.Miller, ″Handbook of optics″, vol.1,McGrow Hill, New York, Chap. 9,(1994)

[47] F.Urbach, Phys.Rev.92 (1953)1324

[48] J. Tauc, in: F. Abeles (Ed.), Optical Properties of Solids, North Holland, (1969)

[49] J.D.Dow and D.Redfiled, Phys.Rev.B8 (1970) 3358

[50] X.Tang, F.Hossain,K.Wongchotigul and M.G.Spence, J. Appl.Phys.Lett. 72(1998) 1501

[51] N.F.Mott and E.A.Davis,″ Electronic processes in non-crystalline materials″, 2nd ed., Oxford university press, Oxford

[52] J.Tauc,″Optical properties of solids″,ed.S.Nuddelman and S.Mitra,New York: Plenum,(1969)

[53] J. Tauc, in: F. Abeles (Ed.), Optical Properties of Solids, North Holland, (1969)

[54] M. A Mahdi and S. K. J. Al-Ani, Int. J. Nanoelectronics and Materlials5 (2012) 11

[55] E.M.Vogel, M.J.Weber, D.M.Krol.J.Phys.Chem. Glasses 32(1991) 25

[56] S.H. Wemple, M. Di Domenico, Phys. Rev. B3 (1971)1338

[57] F.Yakuphanoglu, M.Durmus, M.Okutan,O.Koysal, and V.Ahsen, J. Phys. B 373(2006) 262

AUTHOR GUIDELINES FOR JOURNAL ARTICLE

Introduction

This document enables the user to have a better understanding of rules and regulations used for writing journals. However, each institute has its own template so it is advised that after writing any journal or publication, refer to your specific institute references for writing journals and publications.

Format

All files should be submitted as a Microsoft Word Document.

Article Length

Articles should usually be between **4000 and 10000 words** in length. This includes all text including references and appendices. Please allow roughly **280 words** for each figure or table.

Article Title

A title of not more than **16 words** is advised.

Article Title Page

An Article Title Page should be submitted alongside each individual article using the template provided.

This should include:

- Article Title
- Author Details (see below)
- Acknowledgements
- Author Biographies
- Structured Abstract (see below)
- Keywords (see below)
- Article Classification (see below)

Author Details

Details should be supplied on the Article Title Page including:

- Full name of each author
- Affiliation of each author, at time research was completed
- Where more than one author has contributed to the article, details of who should be contacted for correspondence
- E-mail address of the corresponding author

Structured Abstract

Authors should supply a structured abstract on the Article Title Page, set out under 4-7 sub-headings:

- Purpose (mandatory)
- Design/methodology/approach (mandatory)

- Findings (mandatory)
- Research limitations/implications (if applicable)
- Practical implications (if applicable)
- Social implications (if applicable)
- Originality/value (mandatory)

Maximum should roughly be **250** words in total (including keywords and article classification.

Keywords

You should provide up to **10 keywords** on the Article Title Page, which encapsulate the principal topics of the paper.

Article Classification

Categorize your paper on the Article Title Page, under one of these classifications:

- Research paper
- Viewpoint
- Technical paper
- Conceptual paper
- Case study
- Literature review
- General review.

Headings

Headings should be concise, with a clear indication of the distinction between the hierarchies of headings.

The preferred format is for first level headings to be presented in bold format and subsequent sub-headings to be presented in medium italics.

Notes/Endnotes

Notes or Endnotes should be used only if absolutely necessary and must be identified in the text by consecutive numbers, enclosed in square brackets and listed at the end of the article.

Research Funding

Authors must declare all sources of external research funding in their article and a statement to this effect should appear in the Acknowledgements section. Authors should describe the role of the funder or financial sponsor in the entire research process, from study design to submission.

Figures

All Figures (charts, diagrams, line drawings, web pages/screenshots, and photographic images) should be submitted in electronic form.
All Figures should be of high quality, legible and numbered consecutively Graphics may be supplied in color to facilitate their appearance on the online database.

- Figures created in Microsoft Word, Microsoft PowerPoint, Microsoft Excel and Illustrator should be supplied in their native formats. Electronic figures created in other applications should be copied from the origination software and pasted into a blank Microsoft Word document or saved and imported into an Microsoft Word document or alternatively create a .pdf file from the origination software.
- Figures which cannot be supplied in as the above are acceptable in the standard image formats which are: .pdf, .ai, and .eps. If you are unable to supply graphics in these formats then please ensure they are .tif, .jpeg, or .bmp at a resolution of at least 300dpi and at least 10cm wide.
- To prepare web pages/screenshots simultaneously press the "Alt" and "Print screen" keys on the keyboard, open a blank Microsoft Word document and simultaneously press "Ctrl" and "V" to paste the image. (Capture all the contents/windows on the computer screen to paste into Microsoft Word, by simultaneously pressing "Ctrl" and "Print screen".)

Photographic images should be submitted electronically and of high quality. They should be saved as .tif or .jpeg files at a resolution of at least 300dpi and at least 10cm wide. Digital camera settings should be set at the highest resolution/quality possible.

Tables

Tables should be typed and included in a separate file to the main body of the article. The position of each table should be clearly labelled in the body text of article with corresponding labels being clearly shown in the separate file.
Ensure that any superscripts or asterisks are shown next to the relevant items and have corresponding explanations displayed as footnotes to the table, figure or plate.

References

References to other publications must be in Harvard style and carefully checked for completeness, accuracy and consistency. This is very important in an electronic environment because it enables your readers to exploit the Reference Linking facility on the database and link back to the works you have cited through CrossRef.
You should cite publications in the text, for example: (Adams, 2006) using the first named author's name or (Adams and Brown, 2006) citing either names of two, or (Adams et al., 2006), when there are three or more authors. At the end of the paper a reference list in alphabetical order should be supplied:

References for Books

For books you should follow below template:
Surname, Initials (year), Title of Book, Publisher, Place of publication.

References for Book Chapters

For book chapters you should follow below template:
Surname, Initials (year), "Chapter title", Editor's Surname, Initials, Title of Book, Publisher, Place of publication, pages.
e.g. Calabrese, F.A. (2005), "The early pathways: theory to practice – a continuum", in Stankosky, M. (Ed.), Creating the Discipline of Knowledge Management, Elsevier, New York, NY, pp. 15-20

References for Journals

For journals you should follow below template:
Surname, Initials (year), "Title of article", Journal Name, volume, number, pages.
e.g. Capizzi, M.T. and Ferguson, R. (2005), "Loyalty trends for the twenty-first century", Journal of Consumer Marketing, Vol. 22 No. 2, pp. 72-80.

References for Published Conference Proceedings

For journals you should follow below template:
Surname, Initials (year of publication), "Title of paper", in Surname, Initials (Ed.), Title of published proceeding which may include place and date(s) held, Publisher, Place of publication, Page numbers.
e.g. Jakkilinki, R., Georgievski, M. and Sharda, N. (2007), "Connecting destinations with an ontology-based e-tourism planner", in Information and communication technologies in tourism 2007 proceedings of the international conference in Ljubljana, Slovenia, 2007, Springer-Verlag, Vienna, pp. 12-32.

References for Unpublished Conference Proceedings

For unpublished conference proceedings you should follow below template:
Surname, Initials (year), "Title of paper", paper presented at Name of Conference, date of conference, place of conference, available at: URL if freely available on the internet (accessed date).
e.g. Aumueller, D. (2005), "Semantic authoring and retrieval within a wiki", paper presented at the European Semantic Web Conference (ESWC), 29 May-1 June, Heraklion, Crete, available at:http://dbs.uni-leipzig.de/file/aumueller05wiksar.pdf (accessed 20 February 2007).

References for Working Papers

For Working Papers you should follow below template:

Surname, Initials (year), "Title of article", working paper [number if available], Institution or organization, Place of organization, date.

e.g. Moizer, P. (2003), "How published academic research can inform policy decisions: the case of mandatory rotation of audit appointments", working paper, Leeds University Business School, University of Leeds, Leeds, 28 March.

References for Encyclopedia Entries (no author or editor)

For encyclopedia entries you should follow below template:

Title of Encyclopedia (year) "Title of entry", volume, edition, Title of Encyclopedia, Publisher, Place of publication, pages.

e.g. Encyclopaedia Britannica (1926) "Psychology of culture contact", Vol. 1, 13th ed., Encyclopaedia Britannica, London and New York, NY, pp. 765-71.

References for Newspaper Articles (non-authored)

For Newspaper Articles you should follow below template:

Newspaper (year), "Article title", date, pages.

e.g. Daily News (2008), "Small change", 2 February, p. 7.

References for Electronic Sources

If it is available online, the full URL should be supplied at the end of the reference, as well as a date that the resource was accessed.

e.g. Castle, B. (2005), "Introduction to web services for remote portlets", available at: http://www-128.ibm.com/developerworks/library/ws-wsrp/ (accessed 12 November 2007).

Standalone URLs, i.e. without an author or date, should be included either within parentheses within the main text, or preferably set as a note (Roman numeral within square brackets within text followed by the full URL address at the end of the paper).

==

For more information

Contact us:

The Scientific Institute for Advanced Training and Studies
Email: publisher@siays.co.uk
Phone: (0060) 11 113 331 80
WhatsApp & viber
Facebook: https://www.facebook.com/siats.mutamd?ref=bookmarks
Experimental and Theoretical NANOTECHNOLOGY
http://etn.siats.co.uk
Guidelines link: http://www.siats.co.uk/author-guidelines-for-journal-article/

Content